ULTIMATE CAPACITY OF SUCTION CAISSON IN NORMALLY AND LIGHTLY OVERCONSOLIDATED CLAYS

A Thesis

by

PARTHA PRATIM SHARMA

Submitted to the Office of Graduate Studies of
Texas A&M University
in partial fulfillment of the requirements for the degree of

MASTER OF SCIENCE

May 2004

Major Subject: Civil Engineering

ULTIMATE CAPACITY OF SUCTION CAISSON IN NORMALLY AND LIGHTLY OVERCONSOLIDATED CLAYS

A Thesis

by

PARTHA PRATIM SHARMA

Submitted to Texas A&M University
in partial fulfillment of the requirements
for the degree of

MASTER OF SCIENCE

Approved as to style and content by:

Charles P. Aubeny (Chair of Committee)	James D. Murff (Member)
Jose Roesset (Member)	Junuthula N. Reddy (Member)

Paul N. Roschke
(Head of Department)

May 2004

Major Subject: Civil Engineering

ABSTRACT

Ultimate Capacity of Suction Caisson in

Normally and Lightly Overconsolidated Clays. (May 2004)

Partha Pratim Sharma, B.E.,

Visvesvaraya National Institute of Technology

Nagpur, India

Chair of Advisory Committee: Dr. Charles Aubeny

Petroleum exploration and production in recent years have moved into increasingly deeper water off the continental shelf. Some of these facilities are anchored in water depths in excess of 1000 meters. Exploration and production in deep water present new technological challenges where traditional fixed platforms have given way to floating structures. Today suction caissons are the most commonly used anchorage system for permanent offshore oil production facility. The objective of this study is to numerically predict the ultimate capacity of suction caissons in normally consolidated and lightly overconsolidated clays. Representative soil profile from the Gulf of Mexico and the North Sea are taken and analyzed for suction caissons with length over diameter ratios of 2, 4, 6 & 8. Normalized failure load interaction diagrams are generated for each of the cases. The location of optimum attachment point is also reported for each of the cases.

General purpose finite element computer program ABAQUS is used for the numerical prediction. The finite element study is carried out with three-dimensional models using hybrid elements. A simplified elastic perfectly plastic model with von-Mises yield criterion is used for the study. The saturated clay is treated as an incompressible material.

Results of the study compares well with existing simplified method for estimating load capacity of suction caisson anchors.

ACKNOWLEDGEMENTS

I would like to thank the Offshore Technology Research Center at Texas A&M University for sponsoring this research.

I would like to express my sincere gratitude to Dr. Charles Aubeny for his kind advice and guidance throughout my graduate studies. I would especially like to thank him for introducing me to the field of finite element analysis. It has been an absolute privilege to study under Dr. James D.Murff. His experience and knowledge has been a tremendous help in this study. I also wish to acknowledge the support and guidance of my committee members Dr. J.N.Reddy and Dr. Rosset. Special thanks to the staff of the supercomputing facility for their support. I wish to thank my colleagues in the department for a healthy and friendly atmosphere.

Finally, I would like to thank my parents and family for their unconditional support. I express my sincere thanks to my wife, Sangeeta for her love and care.

Lastly, I thank the Almighty for guiding me in every step of my life. Thank you, God !!

TABLE OF CONTENTS

Page

TABLE OF CONTENTS (continued)

TABLE OF CONTENTS (continued)

TABLE OF CONTENTS (continued)

LIST OF FIGURES

Page

LIST OF FIGURES (continued)

Page

LIST OF FIGURES (continued)

Page

LIST OF FIGURES (continued)

Page

LIST OF FIGURES (continued)

Page

LIST OF TABLES

Page

LIST OF TABLES (continued)

Page

LIST OF TABLES (continued)

Page

LIST OF TABLES (continued)

Page

CHAPTER I

INTRODUCTION

Petroleum exploration and production in recent years have moved into increasingly deeper water off the continental shelf. The transition from 3000 feet to 6000 feet of water has brought about many innovative designs in offshore structures. Traditional fixed platforms have given way to floating structures. Today some of these facilities are anchored in water depths in excess of 1000 meters. Unlike conventional structures, floating systems may require foundations to resist uplift forces. These anchors must also resist cyclic loading arising due to action of wind, current and ocean waves on the floating structure. Traditionally, piles have been used for anchoring permanent floating systems. The installation of these piles involves use of large underwater hammers and associated heavy equipment and is therefore a very time consuming and expensive process. The relative inefficiency of piles in resisting lateral forces has also led the offshore industry to consider alternative anchorage systems. Some of the anchors that are being considered are suction caissons, drag anchors and suction embedment plate anchors (Aubeny et al., 2001a).

Suction caissons are steel cylinders, which are driven into the seabed by self-weight and drawdown pressure developed by pumping out the water from the interior of the caisson. The differential pressure drives the caisson into the seabed.

This thesis follows the style and format of the *Journal of Geotechnical and Geoenvironmental Engineering.*

Suction caissons can be installed very quickly and precisely at the desired location with less heavy installation equipment and at lower cost. Suction caissons can be used as foundations for fixed structures as well as anchors for floating structures. The relative ease in installation and the applicability as a foundation system for a wide range of offshore structures has made suction caisson the most widely used anchorage system in deep water. Suction caissons have emerged as a viable anchorage system in a wide variety of soils ranging from soft clay to dense sands and overconsolidated clays and for a wide variety of structures ranging from floating exploration platforms to permanent production facilities. These caissons can be as big as 7m or more in diameter and up to 30 meters in length. Because of the large size of the caisson, there are no full-scale load test data are available. The absence of collapse load test data of suction caisson is one of the primary reasons for conducting this numerical study.

1.1 CURRENT TRENDS IN OFFSHORE EXPLORATION

As exploration and production has moved into deeper waters, the definition of "deep water" has constantly changed. Today the offshore industry defines it as the water depth that is too deep for conventional platforms such as the steel jackets in the Gulf of Mexico and the large concrete gravity structures in the North Sea. That depth is approximately 400 meters (1,300 feet) which is greater than the height of the Empire State Building (Exxon Mobil web site). This definition of deep water is likely to change again as exploration and production reaches water depths of 3,000 meters (10,000 feet) and more.

Exploration is now being carried out in ultra deep water of 3000 meters off the coast of Brazil. Deep water offshore production sites in Brazil, the Gulf of Mexico, the North Sea and the West African Gulf are some the most attractive regions for deepwater oil exploration today (Figure 1.1).

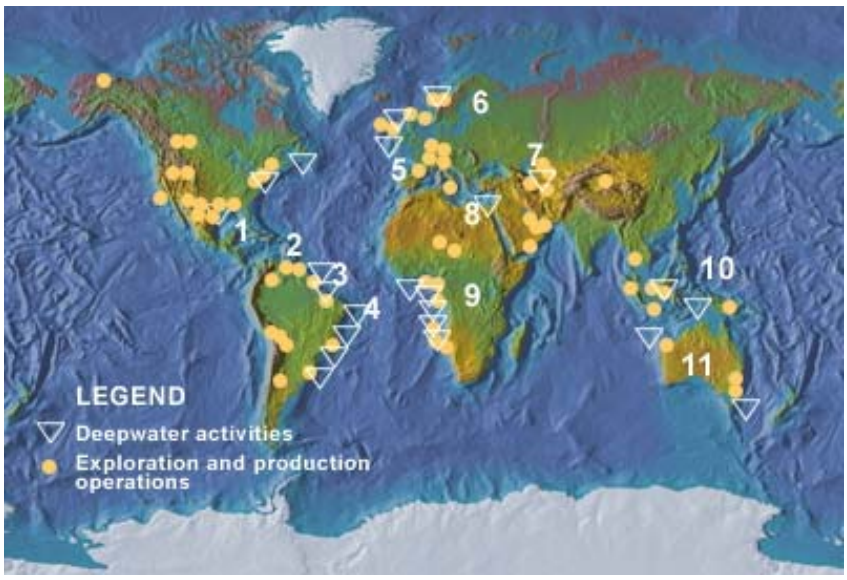

Figure 1.1 Deepwater activities worldwide (Exxon Mobil)

1.2 DEVELOPMENT OF OFFSHORE STRUCTURES

Developments in over 1500 ft of water have brought about many innovative designs in offshore structures. This is primarily because at this water depth, the natural period of the conventional fixed platforms approaches the dominant frequency of the waves creating a resonant condition. As a result, compliant structures are designed to have natural periods much grater than that of the ocean waves. Some of these are Compliant Piled Tower (CPT), Floating Production System (FPOS), Tension Leg

Platforms and Spars (Aubeny et al., 2001a).The latter three structures are anchored to the seabed by mooring lines.

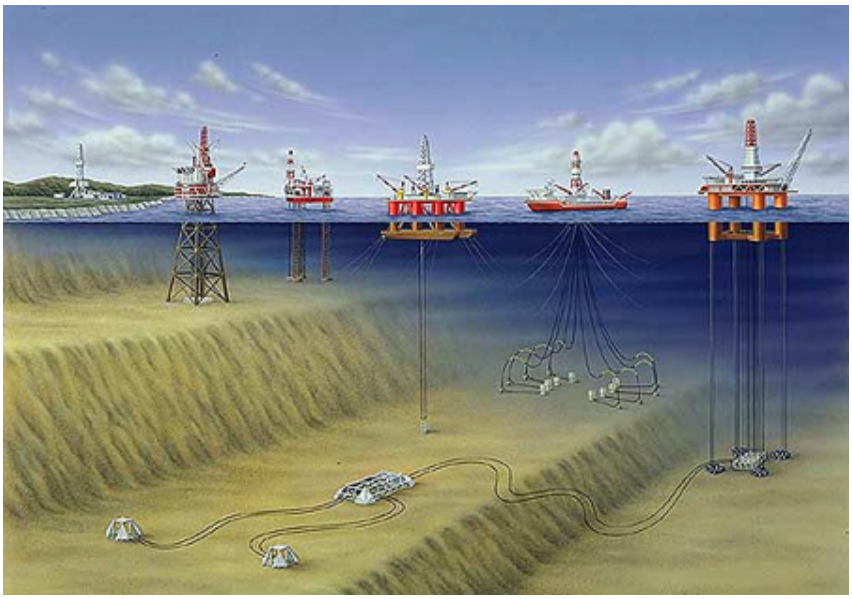

Figure 1.2 Example of offshore structures (MMS 2000)

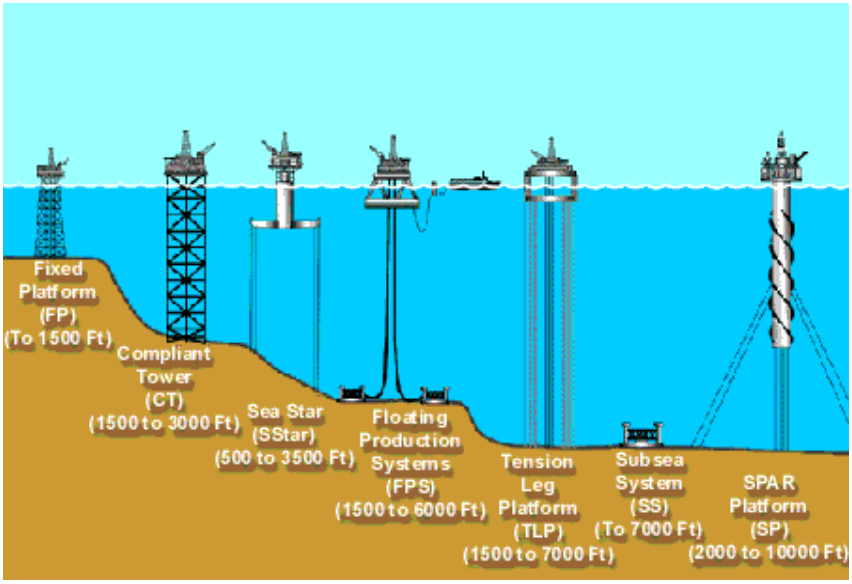

Figure 1.3 Development of offshore structures (MMS 2000)

1.2.1 COMPLIANT PILED TOWER (CPT)

The compliant piled tower (CPT) is a bottom-founded structure having a long slender steel substructure with an approximately constant cross sectional area. The CPT is very flexible in bending and as a result the natural period is quite long compared to conventional bottom founded structures like steel jackets. The CPT has been found to be a competitive option in moderately deep waters of 1500 to 2500 ft (Aubeny et al., 2001a).

1.2.2 FLOATING PRODUCTION SYSTEMS (FPS)

The semi- submersible FPS and the tanker based floating production storage and offloading system (FPOS) are large floating bodies which are anchored to the sea bed.

These systems have been used for quite some time but now they are being considered as viable for deep and ultra-deep water applications. FPS's are widely used in offshore Brazil. FPS are being used in water depths of about 1500 to 6000 ft (MMS 2000) but are also used in shallower waters.

1.2.3 TENSION LEG PLATFORM (TLP)

The tension leg platform employs a semi-submersible moored by taut vertical tendons. The buoyancy of the structure maintains the tension even during severe storm conditions. The loading in the foundation system in primarily vertical and lateral load is estimated to be less than 10% of the vertical loading (Aubeny et al., 2001a).Tension leg platforms are being considered for water depths ranging from 1,500 to 7,000 feet (MMS 2000).

1.2.4 SPAR

The spar platform has recently emerged as a very popular structure in water depths of 2,000 to 6000 feet (Aubeny et al., 2001a) and is currently being considered for ultra-deep water applications in water depths upto 10,000 ft (MMS 2000).The spar is essentially a deep-draft truncated cylinder which supports a platform by its buoyancy. The spar is tied to the seabed by catenary or taut mooring lines. The drilling and the production risers run down a centerwell shielding them from the action of ocean waves and currents. The spar is a very stable structure and like typical deep-water moored structures, it has a natural period much longer than that of the ocean waves.

1.3 DEVELOPMENT OF ANCHORAGE SYSTEMS

Trends to deepwater have led to the development of floating and semi-submersible systems, which are anchored to the seabed by mooring lines. These production facilities may cost in excess of a billion dollar with operational costs, excluding overheads being in the range of hundreds of thousands of dollars a day. Given the amount of investment involved, highly reliable, economical methods of anchorage are required. Unlike conventional structures, the new structures require foundation systems to resist uplift as well as lateral loads. These structures must also be designed to resist cyclic loading due to wave and wind action. The development of permanent deepwater anchors is fairly new and therefore very little performance data is available. Current design procedures for these anchors employ the use of large factors of safety relative to conventional pile founded structures. The offshore industry has been actively pursuing research and development of these anchors. Some of the anchor types that are being considered are suction caisson anchors, drag embedment plate anchors and suction embedded plate anchors (SEPLA).The following section presents a brief discussion on some of these anchors.

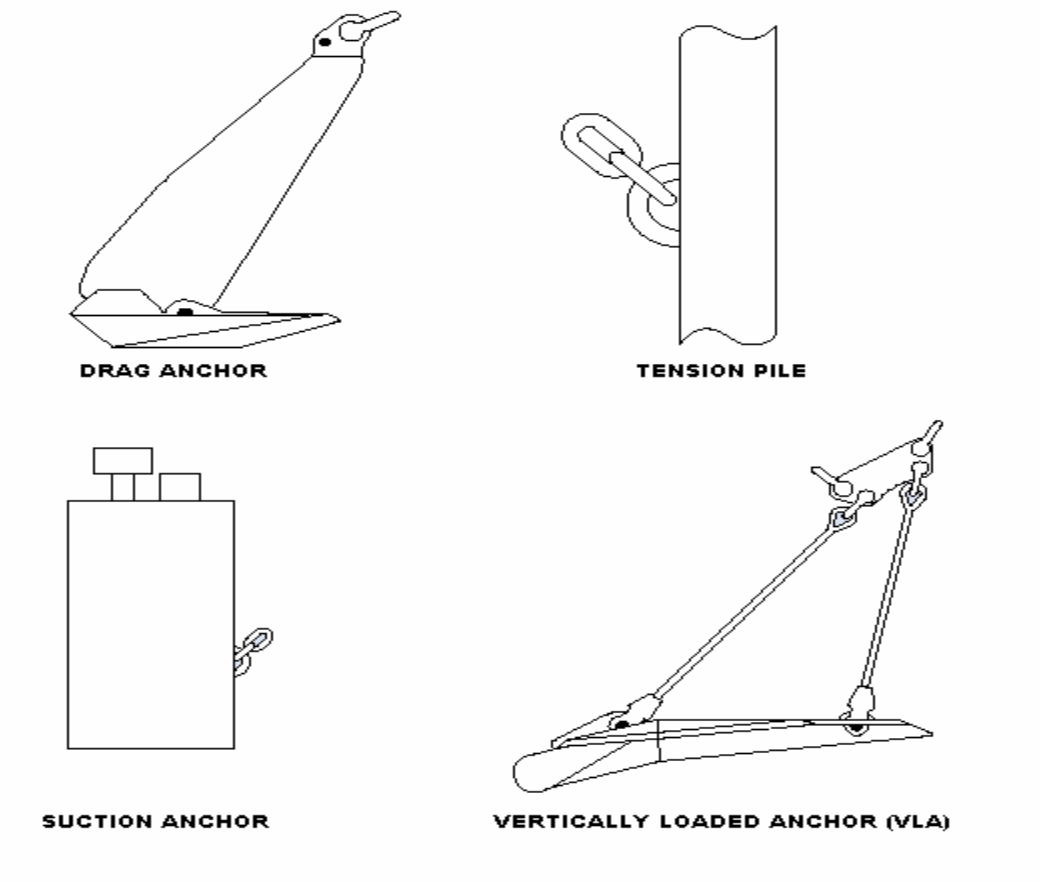

Figure 1.4 Types of anchors (Vryhof Anchor Manual)

1.3.1 SUCTION CAISSON

Suction Caissons are steel cylinders, which are driven into the seabed by self weight and subsequently drawdown pressure created by pumping out the water from the interior of the caisson. The differential pressure, which is developed due to drawdown, creates a huge driving force, which enables the caisson to penetrate the seabed. Suction caissons can be installed quickly with the use of lighter installation equipment.

Figure 1.5 Suction caissons (Delmer)

Suction caissons have been found to be successful in resisting vertical, horizontal and inclined loading conditions. Suction caissons have also been used for conventional jackets in the North Sea resisting both up left and compressive load. Suction caissons have been found to be a viable option in a wide variety of soil conditions ranging from soft clays of the Gulf of Mexico to overconsolidated clays in parts of the North Sea. Suction caissons have also been proven to be successful in dense sands and calcareous soils (Randolph et al., 1998) although the experience with the later is limited (Aubeny et al., 2001a).

1.3.2 DRAG EMBEDMENT ANCHORS

As the name suggests, a drag embedment anchor is a type of anchor, which is embedded into the seabed by dragging with an anchor line or chain. A drag anchor is primarily a bearing plate, which develops resistance by means of bearing directly on the soil. The resistance includes the bearing and friction along the embedded portion of the

soil. The resistance includes the bearing and friction along the embedded portion of the mooring line. (Aubeny et al., 2001a). Drag anchors have primarily been used for temporary mooring being very effective in resisting large horizontal load. They have typically not been employed to resist significant vertical load (Vryhof Anchor Manual 2000). However, recently drag embedment anchors have been developed to resist vertical loads

1.3.3 SUCTION EMBEDDED PLATE ANCHOR (SEPLA)

A suction embedded plate anchor is a new concept in which a vertically oriented plate is inserted into the seabed by attaching it to a suction caisson. The suction caisson is then withdrawn and the plate is rotated to an inclined position. These types of anchors have received attention because they can be cheaper than a suction caisson and can be accurately positioned at a desired depth.

1.3.4 TENSION PILES

Some of the earlier TLP's used tension piles as anchors. Tension piles are driven piles, which require large underwater hammers for installation. Pile driving in very deep water is expensive and presents significant complexities and is therefore not an ideal choice for deep-water applications. Tension piles are not very efficient in resisting lateral loads and are therefore being replaced by other types of anchors.

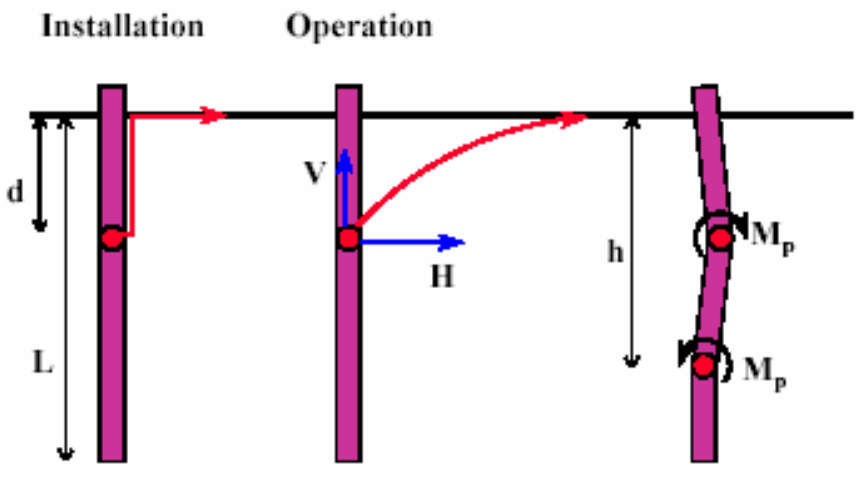

Figure 1.6 Failure mechanism of anchor piles (COFS)

1.4 SUCTION ANCHOR DESIGNS ISSUES

Several key issues regarding design of suction caissons need to be addressed for efficient ultra-deep water application as were highlighted in a recent OTRC report (Gilbert and Murff, 2001a).The following section discusses some of these issues.

Suction caissons have diameters of around 5 to 7 meters with lengths up to 30 meters. Some of the typical aspect ratios are 1.5 to 3.0 in stiff clay and up to 5 or more for soft clays (Aubeny et al., 2001a).Early suction caissons installed in stiff clays of the North Sea were very short and were designed for tensile loading. Due to low length to diameter ratios, end effects were important in these short stubby caissons. In the soft clays of the Gulf of Mexico, long caissons are required to obtain sufficient capacity. End effects in these cases are not as important but other key issues remain. Among these are the effects of rate of loading, load reversal and cyclic loading, anchor line attachment

point, inclination of loading (Bransby and Randolph, 1998), drained vs. undrained loading condition (Sukumaran and McCarron, 1999), reduced adhesion & formation of gap on the side of the caisson, and mobilization of reverse end bearing. The present study addresses some of these issues the details of which are outlined in the section titled "Scope of Study".

1.5 SUCTION CAISSON LOADING CONDITIONS

Suction caissons may be required to resist both uplift and lateral loading. The angle of loading can vary from zero degrees with respect to the horizontal to ninety degrees. For example, in case of tension leg platforms, the load is essentially 90 degrees even during the case of severe wind and wave loading. The type of loading on the caisson primarily depends on the type of mooring system. In case of a taut leg system, the loading can be typically vary between 30 and 60 degrees. For a catenary system, the angle of loading can range from zero to 20 degrees. The angle of loading significantly affects the ultimate mobilized capacity. The attachment point of the anchor line also plays a very significant role in the ultimate capacity. When the anchor line is attached near the seafloor and the load is applied laterally, a forward rotational failure mode is developed. As the attachment point of the anchor line becomes deeper, the tendency to rotate is reduced and a pure translation mechanism is ultimately developed which maximizes the capacity. If the attachment point is below the optimum point of attachment, the caisson tends to rotate backwards which results is reduction of capacity. This is one of the important design aspects, which are addressed in this study. The

ultimate capacity can also depend on the duration and rate of loading. For rapid loading, such as during severe wave loading, the undrained capacity is more important than the drained capacity. In the long term such as after consolidation, the drained behavior under sustained loading may be more significant. This study is restricted to undrained loading condition. The formation of a gap on the windward side of the caisson can significantly reduce the load carrying capacity. This issue is not addressed in this study.

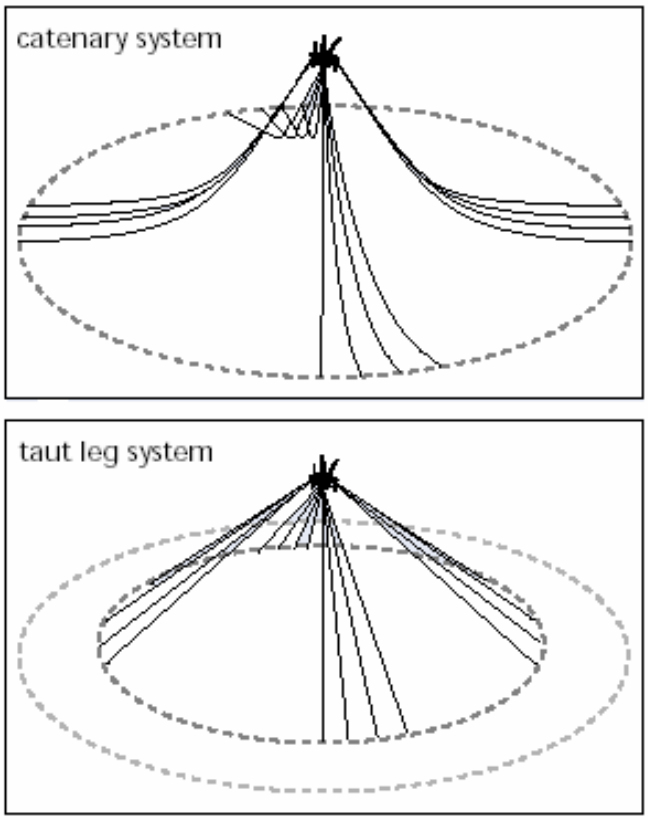

Figure 1.7 Types of mooring systems (Vryhof Anchor Manual)

1.6 SUCTION CAISSON INSTALLATION

A suction caisson is installed in two stages, in the first stage it is allowed to penetrate the seabed under its self-weight. In the second stage suction or drawdown pressure is applied to the inside of the caisson. Due to the large head of water above, the pressure difference creates a driving force and the caisson is driven into the seabed.

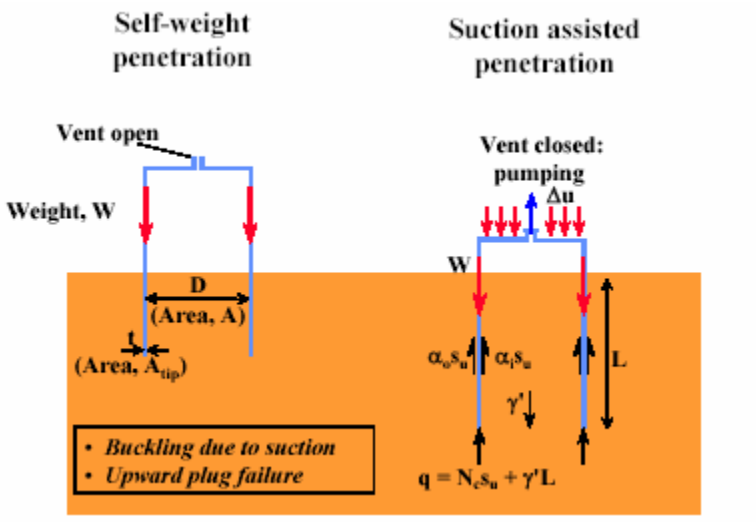

Figure 1.8 Suction caisson installation (COFS,2001)

The forces acting on the caisson during installation are the end-bearing resistance on the skirt tip, the external friction between the caisson wall and the surrounding soil and the internal friction between caisson and soil plug. Buckling of the caisson and upward failure of the soil plug are the two most critical modes of failure during installation (COFS, 2001). Internal stiffeners are provided to prevent buckling, and these add to the soil resistance to penetration of the caisson.

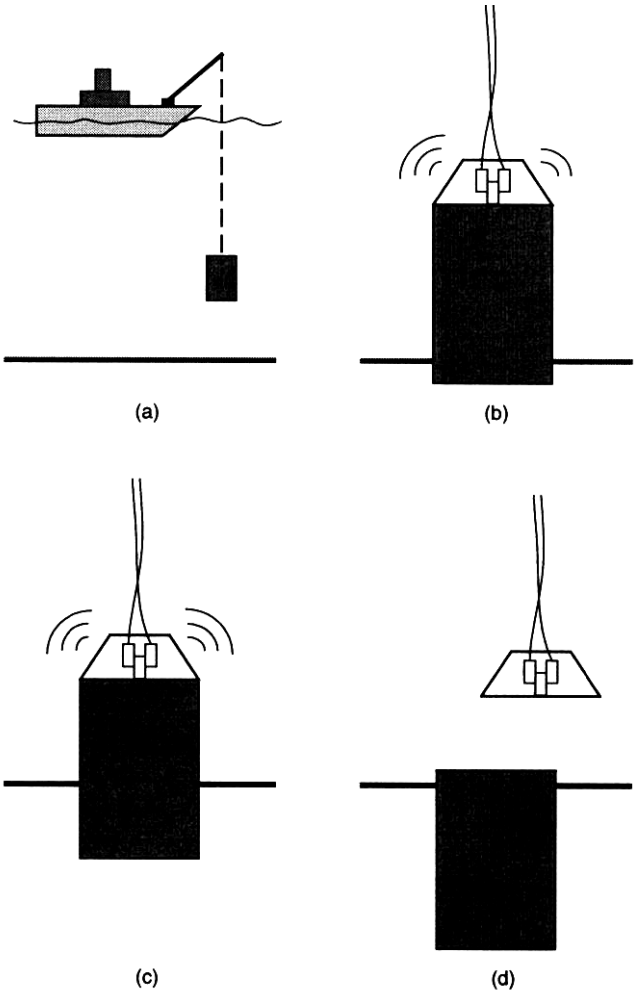

Figure 1.9 Suction caisson installation(Pavlicek,1992)

The steps in caisson installation are outlined as follows (Colliat et al., 1995)

- Bring the anchors and the mooring lines to expected site on a cargo base.
- Lifting anchor and lowering it to the seabed. Its contact area increases with penetration producing sufficient sliding resistance to facilitate positioning the anchor in its final location as the anchor chain reaches the seabed.

- Penetrate the anchor using its self weight.
- Complete the remainder of penetration using drawdown pressure inside the caisson by pumping out water using power supplied by ROV (remotely operated vehicle).
- Laying the mooring line on the seabed, and attaching the end of the buoy for later retrieval, connection to floating facility and tensioning.

1.7 SCOPE OF RESEARCH

The objective of this study is to determine the undrained ultimate capacity of Suction Caissons with length over diameter ratios of 2, 4, 6 & 8 in certain representative soil profiles from the Gulf of Mexico and the North Sea for various load inclinations. A suite of horizontal-vertical load interaction diagrams for varying soil profiles and caissons with different aspect ratios has been generated for this study. The optimum attachment point (loading depth at which capacity is a maximum) is also reported for each of these cases.

The study is restricted to undrained loading conditions and issues such as soil strength anisotropy (Murff, 1980) gap formation behind the caisson etc have not been included. The ultimate capacities for various inclined load cases are determined by the finite element method (FEM) and are also compared to results estimated using a simplified plasticity solution (Aubeny et al., 2003b). The objective is to verify the solutions and to study the limitations of the postulated failure mechanisms (Murff and

Hamilton, 1993) which are employed in the simplified upper bound plasticity calculations.

CHAPTER II

REVIEW OF STATE OF KNOWLEDGE

This chapter presents a summary of earlier research, which provides the background for the current finite element study. The plastic limit analysis method has been employed by Randolph and Houlsby (1984) and Murff and Hamilton (1993) in previous analytical studies for predicting the lateral resistance of piles under undrained loading condition. A discussion on fundamentals of plasticity theory and plastic limit analysis (Chen, 1975) is presented in this chapter. The chapter also discusses results from previous numerical studies predicting the capacity of suction caissons under lateral loading condition (Aubeny et al., 2001b) and general loading conditions (Aubeny et al., 2003a).

2.1 FUNDAMENTALS OF PLASTICITY THEORY

Ductile materials, when subjected to high levels of stress, show plastic behavior characterized by permanent deformation, i.e. when the stresses are removed, the material does not regain its original shape (Boresi and Schmidt, 2002). Mild steel and aluminum are perfect examples of material, which fails by plastic yielding. Soils, particularly normal consolidated soils, and lightly overconsolidated soils also fail by plastic yielding when subjected to compressive and shear stress. Different material exhibit different post yield behavior. After reaching the yield point, the slope of the stress strain curve could be less than, equal to, or greater than zero. Depending on the gradient of the post yield

curve, materials are classified as softening, perfectly plastic, or hardening material (Prager, 1959).

Ductile materials, when subjected to high levels of stress, show plastic behavior characterized by permanent deformation, i.e. when the stresses are removed, the material does not regain its original shape. Mild steel and aluminum are perfect examples of material, which fails by plastic yielding. Soils, particularly normal consolidated soils, and lightly overconsolidated soils also fail by plastic yielding when subjected to compressive and shear stress. Different material exhibit different post yield behavior. After reaching the yield point, the slope of the stress strain curve could be less than, equal to, or greater than zero. Depending on the gradient of the post yield curve, materials are classified as softening, perfectly plastic, or hardening material (Figure 2.1)

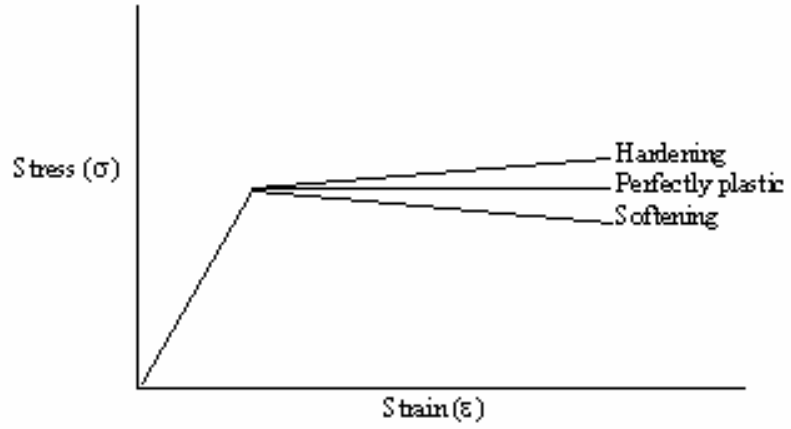

Figure 2.1 Stress strain behavior of material

2.1.1 YIELD FUNCTION

Response of materials, when subjected to a generalized state of stress, depends on the interaction of individual stress components. In plasticity theory this interaction of stress components are defined in terms of a yield function. The yield function is a function of the stress components such that:

$$f = f\left(\sigma_{ij}\right) \tag{2.1}$$

The material is in elastic state if

$$f = f\left(\sigma_{ij}\right) < 0 \tag{2.2}$$

The material is in plastic state if

$$f = f\left(\sigma_{ij}\right) = 0 \tag{2.3}$$

Many such yield functions are available to describe the behavior of materials. For cohesive materials subjected to undrained loading, the Tresca and the von Mises yield function are often used (Murff, 2002). Details of material behavior and yield function are presented in Chapter IV. Plasticity theory is valid for only well behaved stable materials. Drucker's Stability Postulates define a "stable" material as follows:

a) During the application of incremental forces, the work done by these forces on the displacements they produce is positive.

b) Over the cycle of application and removal of the forces, the new work produced by these is non-negative.

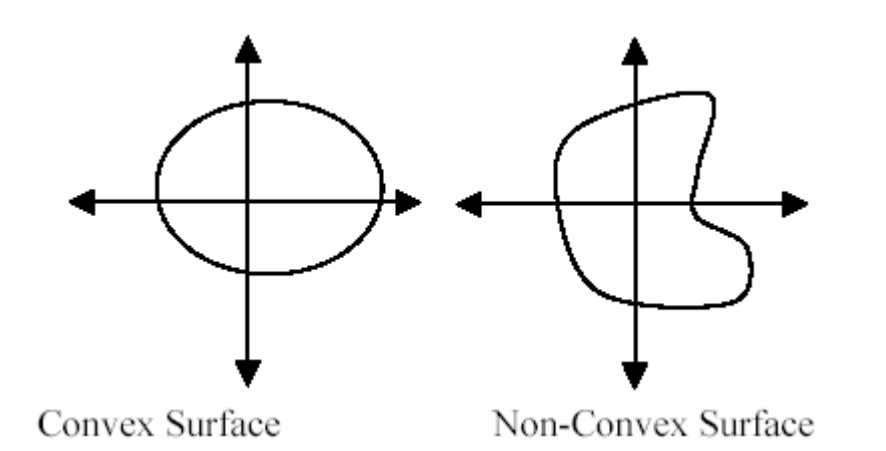

Figure 2.2 Convexity of yield surface

A stable material has a convex yield surface (Figure 2.2) and a unique stress-strain relationship exists for that material (Chen and Han,1988).

2.1.2 FLOW RULE

The post yield behavior of the material is defined in terms of the flow rule, which associates the plastic strain increment to the yield surface. For associated flow, the "direction" of the plastic strain increment is normal to the yield surface. Associated flow means that at point on the yield surface, the natural tendency of the material is to deform in the direction given by the gradient to the yield surface at that point.

$$\dot{\varepsilon}_{ij}^{\,p} = \lambda \frac{\partial f(\sigma_{ij})}{\partial \sigma_{ij}} \tag{2.4}$$

where,

$\lambda = a$ *positive scalar multiplier*

$f =$ *the plastic potential which is the same as the yield function for associated flow*

$\sigma_{ij} =$ *the stress state corresponding to* $\dot{\varepsilon}_{ij}^{p}$

2.1.3 HARDENING RULE

The hardening rule mathematically describes the increase in strength of a material when it is loaded beyond the elastic range. For elastic perfectly plastic material, there is no hardening.

2.1.4 LOWER AND UPPER BOUND THEOREMS

The upper bound and the lower bound methods are two approaches for estimating collapse load of a system. In the lower bound method, equilibrium and the yield condition are satisfied without considering the deformation mechanism. The lower bound theorem states that “if any stress distribution throughout the structure can be found which is everywhere in equilibrium internally and balances certain external loads and at the same time does not violate the yield condition, those loads will be carried safely by the structure” (Drucker and Prager, 1952).

In the upper bound method, the strain compatibility and the yield condition are satisfied and the collapse load is estimated without considering equilibrium. The upper bound theorem states that “if an estimate of the plastic collapse load of a body is made by equating internal rate of dissipation of energy to the rate at which external forces do

work in any postulated (kinematically admissible) mechanism of deformation of the body, the estimate will be either high or correct" (Drucker and Prager,1952).

2.1.5 UPPER BOUND ANALYSIS PROCEDURE

In the upper bound method, a kinematically admissible mechanism is postulated in terms of a prescribed velocity field. The postulated velocity field satisfies strain compatibility requirements and the velocity boundary conditions. The external work is then equated to the rate of internal energy dissipation to solve for the unknown collapse load. In order to find the best upper bound, the unknown collapse load is then minimized with respect to optimization parameters, which describes the mechanism.

The upper bound plastic limit analysis procedure is as follows (Murff, 2002)

- Define a failure mechanism for the unknown collapse load F by prescribing a kinematically admissible velocity field v_i.
- For the given velocity field, compute the strain rate field $\dot{\varepsilon}_{ij} = \frac{\partial v_i}{\partial x_j}$
- Compute the external rate of work , $\dot{W} = Fv_i$
- Compute the external rate of work done by the soil unit weight in gravitational field , $\dot{W}_g = \int_V v_z \gamma' dV$

- Compute total internal rate of energy dissipation by adding the total rate of energy dissipation for all regions, $\dot{D}_T = \sum_{k=1}^{n} \int_V \dot{D}_k \, dV$

- Equate the rate of external work to rate of internal energy dissipation $Fv_i = \dot{D}_T - W_g$

- Minimize the value of F by varying the optimization parameters.

In the upper bound method, the prescribed mechanism can be made of two types of velocity fields: continuously deforming region and slip surfaces. For each of these two types of velocity field the rate of unit internal dissipation for undrained cohesive material is calculated as below (Murff, 2002).

For continuously deforming region:

Von Mises yield scriterion: $\dot{D} = S_u (2\dot{\varepsilon}_{ij}\dot{\varepsilon}_{ij})^{1/2}$ (2.5)

Tresca yield criterion: $\dot{D} = 2S_u \left|\dot{\varepsilon}_{sm}\right| = S_u \left|\dot{\gamma}\right|_{\max}$ (2.6)

For slip surface:

$\dot{D} = S_u \left|v_r\right|$, where v_r is the slip velocity. (2.7)

2.2 PULLOUT CAPACITY OF AXIALLY LOADED PILES

The pullout capacity of axially loaded piles depends on two components: reverse end bearing and shaft resistance. In case of piles, about 90 to 95% of the total soil resistance is due to the shaft resistance (Clukey and Phillips, 2002).However; in case of suction caissons, the shaft resistance accounts for a much lower percentage of the total resistance. The shaft resistance is around 40 to 60% of total resistance, for typical suction anchors presently being used in the Gulf of Mexico (Clukey and Phillips, 2002). Thus, reverse end bearing is significant for suction caissons especially for shorter caissons. For reverse end bearing to develop, a perfect seal is required at the caisson bottom and the soil. This seal may not be present if drainage occurs inside the caisson. If the skin friction resistance inside the caisson is more than the end bearing resistance, a soil plug failure will occur. Thus depending on the occurrence of soil plugging, two failure modes are possible. These are as follows (Han, 2002):

- If soil plugging occurs, the total resistance comprises of the side resistance developed inside and outside of the caisson wall and the end bearing of the annular caisson tip.
- If soil plugging does not occur, the total resistance comprises of the side resistance developed on the outside of the caisson and the end bearing of the full caisson bottom.

2.2.1 REVERSE END BEARING

When the caisson is loaded vertically and a perfect seal occurs between the caisson bottom and the soil, a soil failure mechanism is developed, as shown in Figure 2.3. The resistance developed due to this failure mode is called the reverse end bearing.

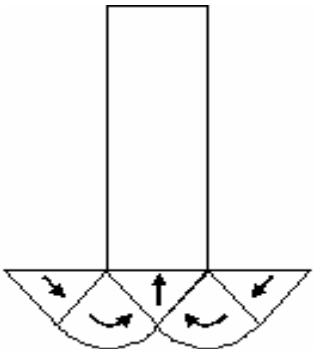

Figure 2.3 Reverse end bearing failure

The maximum vertical resistance at the bottom of the suction caisson for purely vertical loading is $V_{b0} = \pi R^2 S_{uavg} N_{ab}$, where R is the caisson radius, S_{uavg} is the average shear strength between the caisson tip and one diameter below the caisson tip and N_{ab} is the tip bearing resistance factor (Aubeny et al., 2003a).The value of N_{ab} is between 10.5 and 12 (Aubeny et al., 2003a).

2.2.2 SHAFT RESISTANCE

The unit shaft resistance for undrained loading condition is $P_a = N_{as}(\psi) S_u$,where N_{as} is the axial resistance factor, S_u is the undrained shear strength at a depth and ψ is

the angle of inclination of the load (Aubeny et al., 2003a).The N_{as} value depends on the inclination of the load. For purely vertical load, $N_{as} = \pi$ .For horizontal loading $N_{as} = 0$.

2.3 RESISTANCE OF LATERALLY LOADED PILE

Early investigation of laterally loaded piles was carried out by Broms (1964).He expressed the ultimate lateral resistance *P*, which is the net horizontal force per unit projected area of the pile. Thus the horizontal resisting force *ΔH* acting along a vertical length *Δz* for a pile with diameter *D*, is given by:

$$\Delta H = PD\Delta z$$

For cohesive soils, $P = N_{ps}S_u$ where N_{ps} is a dimensionless unit resistance factor and S_u is the undrained strength. Matlock (1970) and Reese (1975) have proposed empirical estimates of N_{ps}. Later Hamilton et al. (1991) and Murff and Hamilton (1993) developed quasi-upper bound methods for estimating the value of N_{ps}. Aubeny et al. (2001b) developed simplified methods for estimating lateral resistance.

2.3.1 ANALYSIS OF FLOW AROUND ZONE

Randolph and Houlsby (1984) developed a solution for lateral pressure acting on an infinitely long translating cylinder by using classical plasticity methods. They found that if the failure load is divided by the product of the soil strength times the caisson diameter times the unit length, they could express the failure load in terms of a non-dimensional number N_p. The N_p value, which they computed, varied between 9.14 for a

perfectly smooth caisson to 11.94 for a perfectly rough cylinder. These flow-around solutions assume that full suction will be developed and no gap shall form at the back of the caisson.

2.3.2 EFFECT OF FREE SURFACE

Murff and Hamilton (1993) presented a three dimensional quasi upper bound formulation for predicting the ultimate capacity of laterally loaded piles. Their proposed method accounted for effects of reduced resistance at free surface and the tip resistance at the bottom. In this formulation, they assumed that yielding could occur in soil as well as in the pile. Based on this they could compute the total ultimate resistance for the laterally loaded pile. They could also predict the variation of lateral resistance (P-ultimate) along the length of the pile. Their method could handle a variety of conditions such as linearly varying soil profile, gap formation behind the caisson, full or reduced adhesion, soil weight and depth of load application. The three dimensional mechanism (Figure 2.3 to Figure 2.6) which they proposed comprised of a conical wedge near the free surface and a flow around zone below the wedge (Randolph and Houlsby, 1984).If full suction is mobilized then on the “windward” side of the caisson an active wedge is formed. If full suction is not mobilized then a gap is formed on the “windward” side, which extends down to the flow around zone. Thus in the case of the gap formation, no resistance is developed in the back of the caisson.

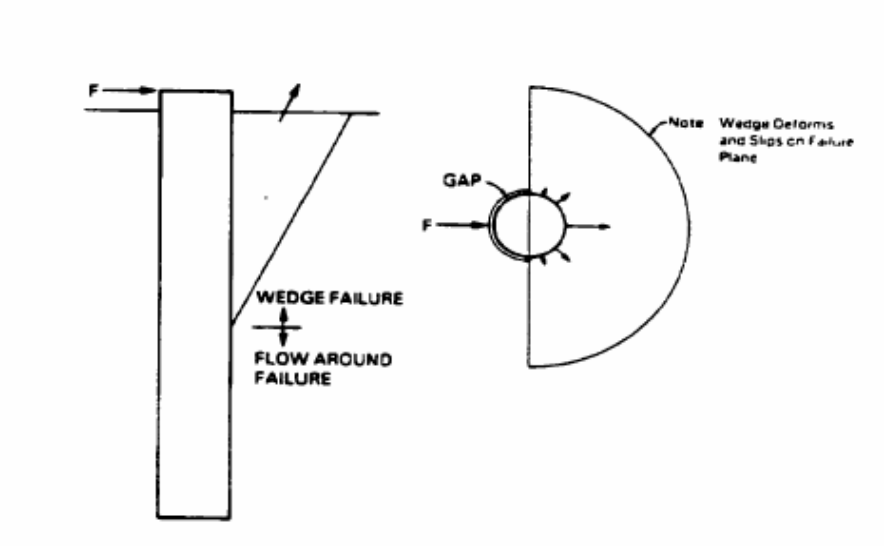

Figure 2.4 Soil deformation mechanism (Murff and Hamilton ,1993)

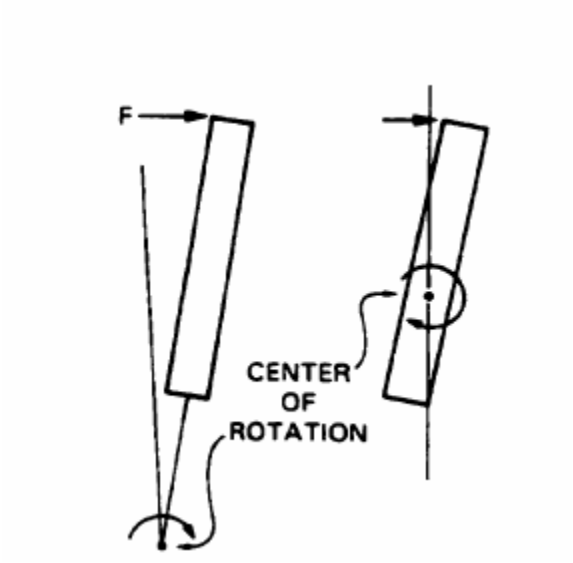

Figure 2.5 Caisson deformation mechanism (Murff and Hamilton ,1993)

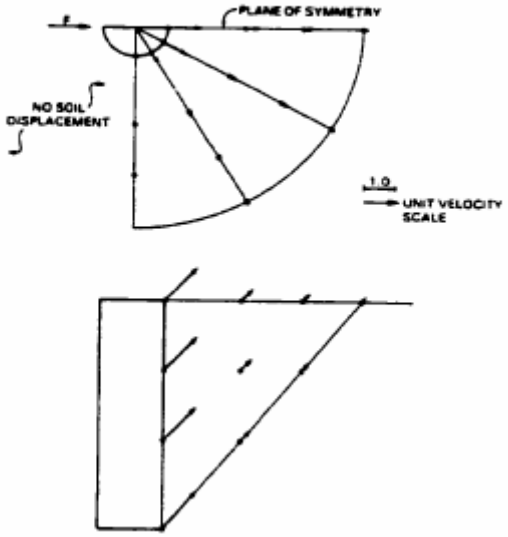

Figure 2.6 Translation mechanism: plan and cross section (Murff and Hamilton ,1993)

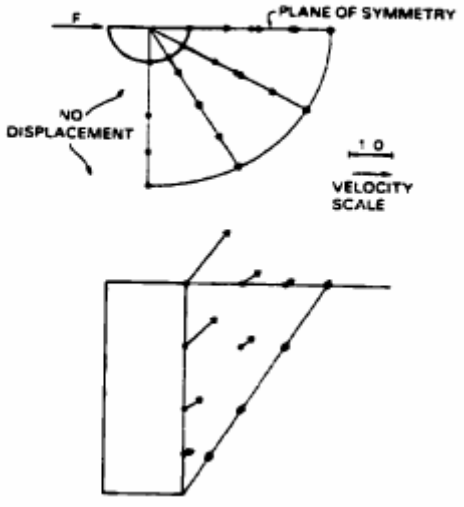

Figure 2.7 Rotation mechanism: plan and cross section (Murff and Hamilton ,1993)

The geometry of the failure mechanism (Figure 2.7) was described in terms of four optimization variables, c, r_o, z_o and α. The optimization parameter c is used to represent the distance of the rotation point from the caisson top given by z_o /c. The radial extent of the wedge was described by the parameter r_o .The depth of the wedge was given by z_o .The radial variation of the velocity of the wedge is described in terms of an exponent α .

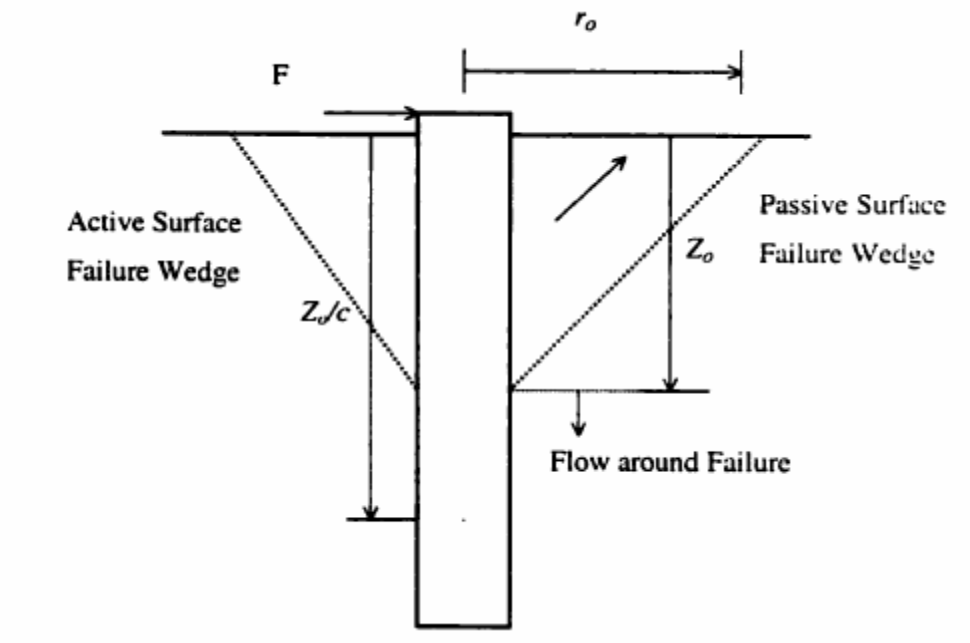

Figure 2.8 Failure mechanism and optimization variable (Han, 2002)

Using their upper bound method, Murff and Hamilton derived relationships for a non-dimensional lateral bearing capacity factor N_p, which related the lateral unit resistance on the side of a caisson P to soil strength S_u given by the $P = N_p S_u$. N_p is a

function of depth and the type of soil profile. Murff and Hamilton proposed relationships for N_p varying with depth for uniform and linearly varying soil profiles.

2.3.3 SIMPLIFIED UPPER BOUND FOR LATERAL LOADING

Based on the original upper bound solution developed by Murff and Hamilton (1993), Aubeny et al. (2001b) proposed a simplified procedure for predicting the lateral capacity, which was later extended to account for general loading condition by Aubeny et al. (2003a). The theoretical foundation of simplification is the concept of generalized stress and strains where the resistances are generalized stresses and displacements and rotations are generalized strains Aubeny et al. (2003a). The simplified method proposed by Aubeny et al. (2001b) reduced the number of optimization variables from 4 (original method Murff and Hamilton, 1993) to 1 (the depth of the center of rotation L_0).

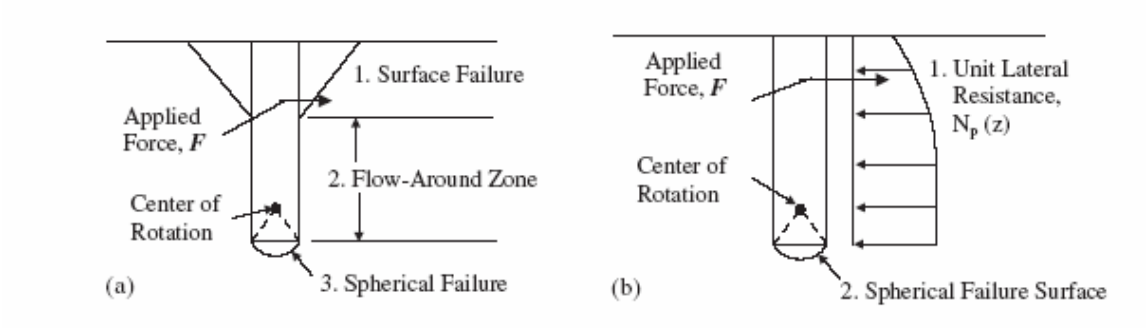

Figure 2.9 (a) failure mechanism assumed by Murff and Hamilton (1993); and (b) simplified analysis by Aubeny et al. (2001b)

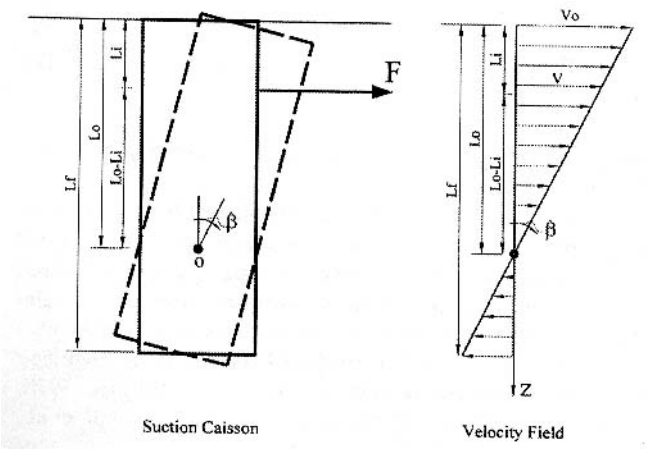

Figure 2.10 Failure mechanism: simplified method (Aubeny et al., 2001b)

The energy dissipation in the simplified method (Aubeny et al., 2001b) is computed by integrating the product of unit resistance P_l times the local displacement over the projected side area of the caisson.

2.4 SIMPLIFIED UPPER BOUND FOR INCLINED LOADING

The simplified method discussed above was modified to account for inclined loading condition Aubeny et al. (2003a). The external load *F* this case is inclined at an angle ψ, which is measured from horizontal. Li is the location at which the line of action of the load *F* intersects the caisson centerline. Knowing the value of Li, the load attachment point can be obtained by projecting the line of action of the load *F* to the caisson boundary.

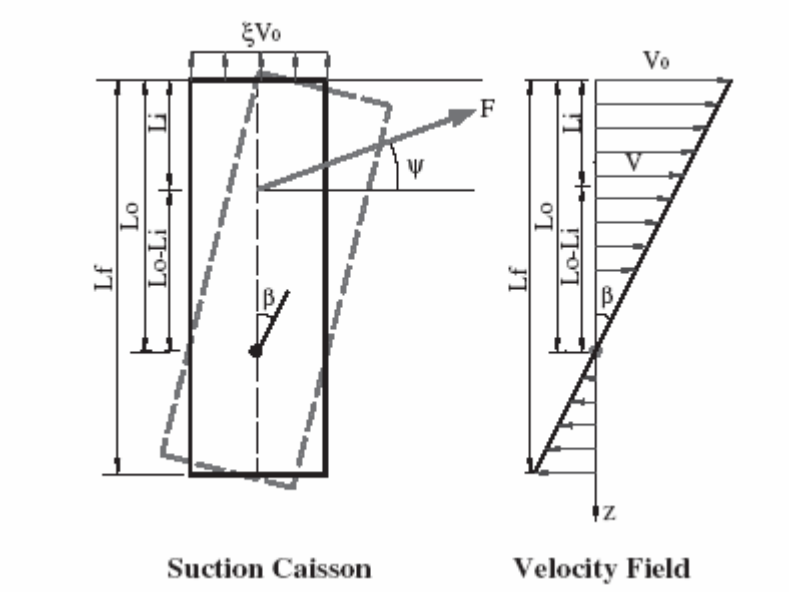

Figure 2.11 Failure mechanism: simplified method (Aubeny et al., 2003a)

The capacity (minimum value of *F*) is obtained by optimizing the failure mechanism (Figure 2.10) with respect to two parameters: the center of rotation of the rotating caisson, Lo; and a parameter ξ, which related the magnitude of vertical to horizontal motion.

2.4.1 SIDE RESISTANCE

The ultimate unit axial and lateral resistance per unit-projected area along the side of the caisson was expressed by P_a and P_l (Aubeny et al., 2003a).

$$P_a = N_{as}(\psi) S_u \tag{2.8}$$

$$P_l = N_{ps}(\psi, z) S_u \tag{2.9}$$

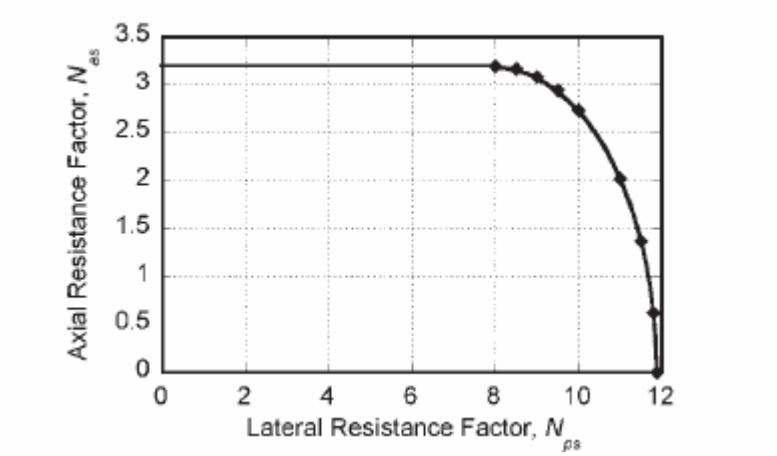

Figure 2.12 Axial and lateral resistance factors on side of caisson

Interaction diagrams of N_{as} and N_{ps} (Figure 2.12) were developed by finite element method for uniform and linearly varying soil profiles. For purely vertical loading, $N_{as}=\pi$ for a circular caisson and $N_{ps} = 0$ for all values of z (Aubeny et al., 2003a).

For purely horizontal loading, $N_{as}=0$ while N_{ps} becomes the lateral resistance factor associated with a P-ultimate analysis of laterally loaded piles (Aubeny et al., 2003a).

2.4.2 TIP RESISTANCE

The tip resistance also affects the moment resistance and the vertical resistance. For short stubby caissons, this effect is more significant. In case of longer caissons, the tip resistance becomes relatively less compared to the total resistance. Aubeny et al. (2003a) has proposed a simplified formula for the interaction of moment resistance and the vertical resistance.

$$f = \left(\frac{V_b}{V_{b0}}\right)^2 + \left(\frac{M_b}{M_{b0}}\right)^2 - 1 = 0 \tag{2.10}$$

V_b is the vertical resistance of the base M_b is the moment resistance. The subscript "0" indicates the maximum capacity when no other component is present.

CHAPTER III

SITE CHARACTERISTICS OF GULF OF MEXICO AND THE NORTH SEA

This chapter presents a discussion of site characteristics and undrained strength profiles in the Gulf of Mexico (GOM) and the North Sea, two of the most active deepwater exploration zones today. The undrained shear strength is one of the most important parameters, affecting the ultimate capacity of suction caissons in clays. Therefore, in order to carry out any meaningful ultimate strength assessment with finite elements, careful attention must be paid to the undrained strength parameter. In this chapter, typical undrained strength profiles from the Gulf of Mexico and the North Sea are described and based on these profiles, representative profiles for the finite element study are selected.

3.1 SITE CHARACTERISTICS OF THE GULF OF MEXICO (GOM)

The predominant soil condition in deepwater Gulf of Mexico is normally consolidated clay with relatively small undrained strengths at the mudline. The typical undrained strength at the mudline is around 2-5 kPa and increases linearly at a rate of 1.0-2.0 kPa/m(Aubeny et al., 2001b). These soils are highly plastic in nature with LL in the range of 65 to 100 and, the PI's around 25-40.The water content is often more than 100% at mudline, and around 35% at depths greater than 150ft. Figure 3.1 shows a typical range of undrained strengths vs depth for the Gulf of Mexico.

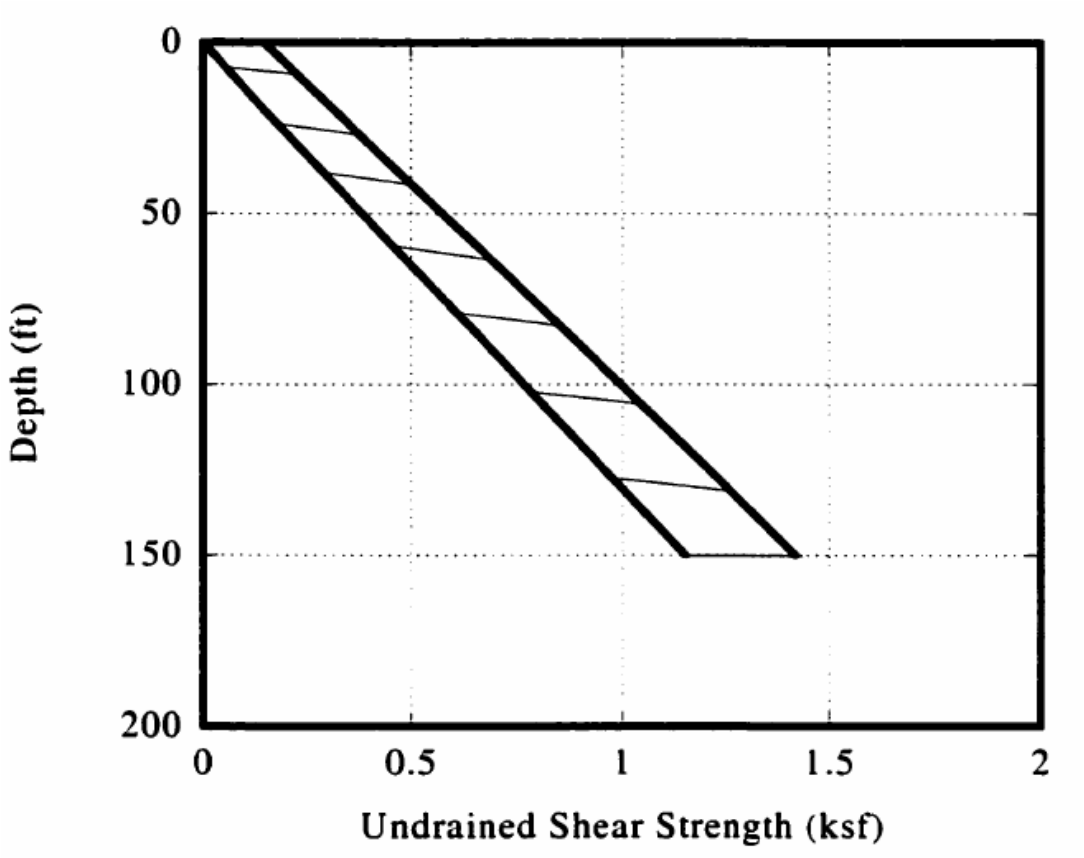

Figure 3.1 Undrained shear strength profile in GOM (Aubeny et al., 2001b)

Bradshaw et al. (2000) in a recent study conducted in plateau areas of the Texas-Louisiana continental slope of the Gulf of Mexico (Figure 3.2) reported that the plateau sites are normally consolidated at depths over 4 meters with a zone of apparent overconsolidation in the upper few meters (Figure 3.3). It was also reported that the sediments from the apparently overconsolidated zone showed greater normalized strength and less contractive behavior than the deeper normally consolidated clay. Figure 3.3 shows a typical undrained strength profile.

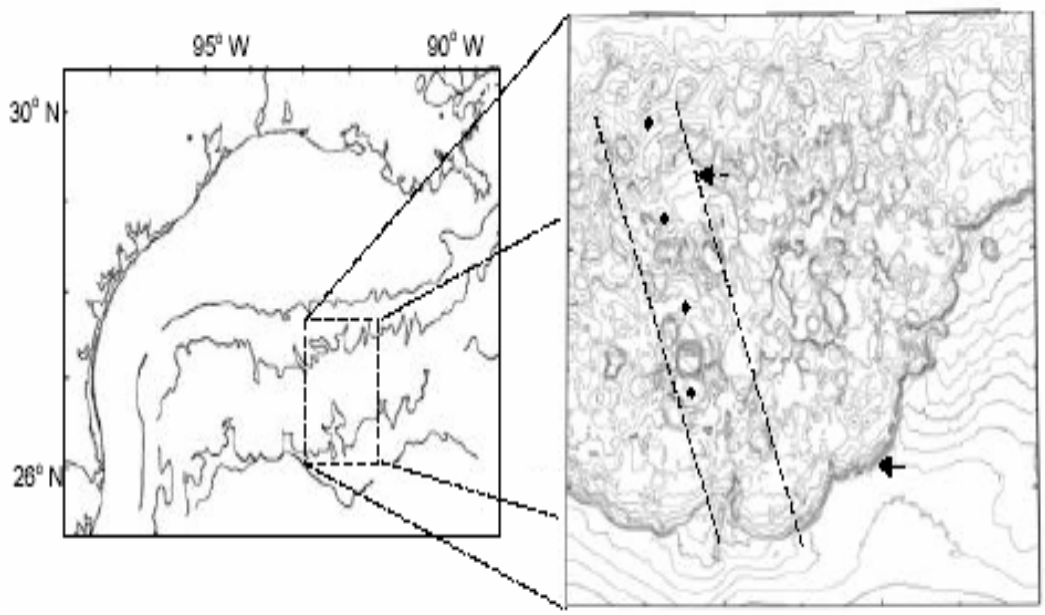

Figure 3.2 Location of selected study cores (Bradshaw et al., 2000)

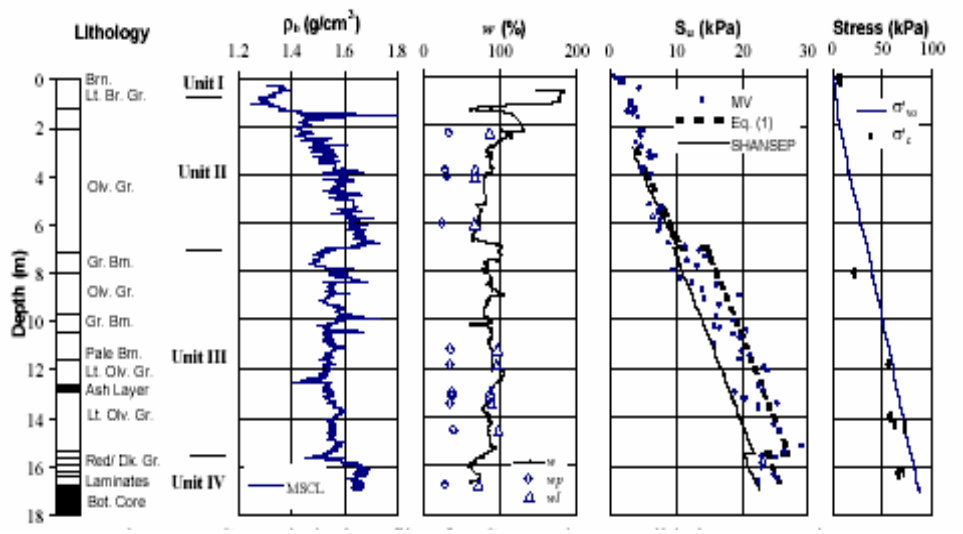

Figure 3.3 Soil profile (Bradshaw et al., 2000)

3.2 SITE CHARACTERISTICS OF THE NORTH SEA

Soils are mainly stiff overconsolidated clays and sands in many south and central North Sea areas (Aubeny et al., 2001b) due to glaciation. Normally consolidated clays also occur in deeper waters. Figure 3.4 shows typical North Sea soil profiles.

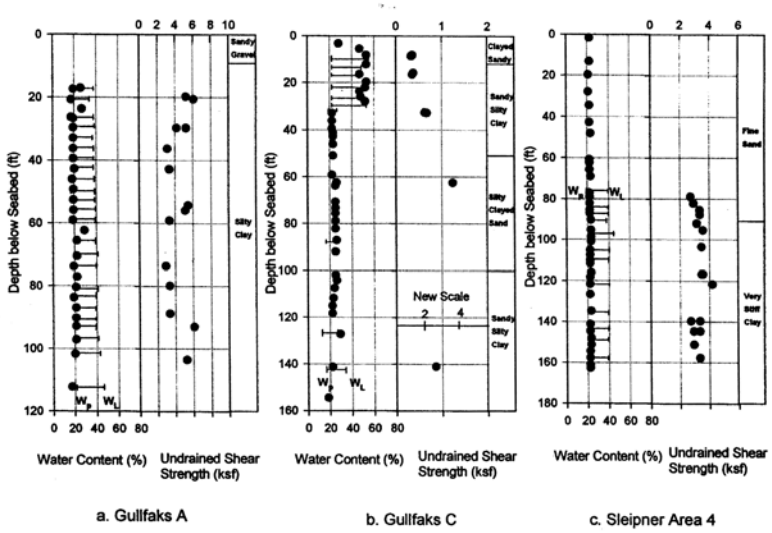

Figure 3.4 Typical North Sea profile (Lunne et al., 1985)

As an example, the Gullfaks “A” site consist of moderately to highly overconsolidated glaciomarine clays with LL=41-50 and water content around the plastic limit. The overconsolidation ratio typically ranges from 3-5 .The undrained shear strength ranges from 3000 psf to around 6000 psf. The water depth at the Gullfaks “A” site is around 440 ft (Aubeny et al., 2001b). The Gullfaks “C” site comprises normally consolidated to lightly over clays with OCR’s around 1-2. The undrained shear strength at the mudline ranges from around 400 psf to 600 psf depending on depth. The water depth at Gullfaks “C” site is around 720 ft (Aubeny et al., 2001b). The top 70 ft in the

Sleipner area comprises dense fine sand underlain by moderately overconsolidated glaciomarine clay with OCR ranging from 1-3. The undrained strength of clays at this site ranges from 2000-4000 psf.

Lacasse et al. (1979) conducted a series of pressuremeter tests to evaluate the stress-strain and the strength characteristics of two Norwegian clays of marine origin, the Onsoy and the Drammen clays.

The marine deposits at the Onsoy site consists of a weathered desiccated crust of less than one meter thick, which is underlain by 8 m of soft clay and 12 m of medium plastic clay with natural water contents of the clay is between 60 to 65% (Lacasse et al., 1979).

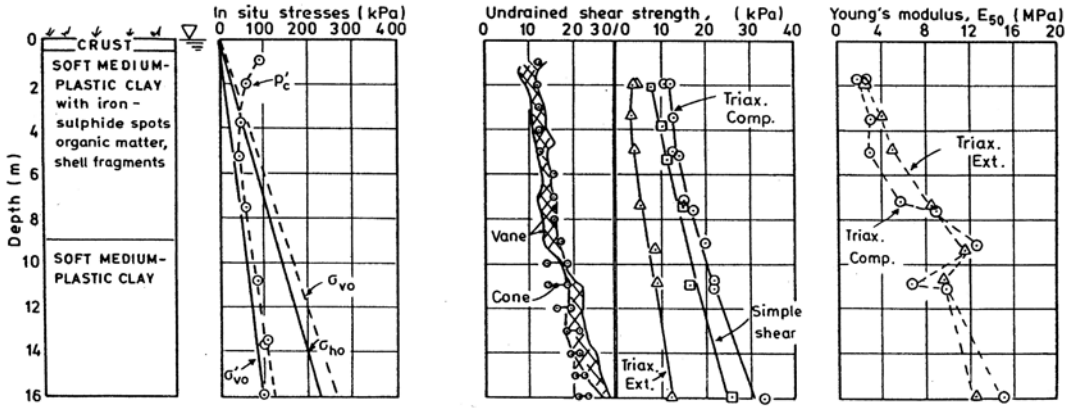

Figure 3.5 Site characteristics at Onsoy site (NGI)

As can be seen from Figure 3.5, the undrained strength measured from the triaxial compression test at this site is nearly uniform at about 10-kPa up to a depth of 5 m and

then increasing linearly at a rate of about 2 kPa/m. The Drammen site (Figure 3.6) comprises marine deposits consisting of about 10 m of thick plastic clay with PI around 30% and water content of around 55 – 60 % . This clay is underlain by a 30 m layer of lean clay with water content around 30 – 35 % and PI of 10%. The OCR in the lean clay and the plastic clay ranges from 1.15 to 1.5.

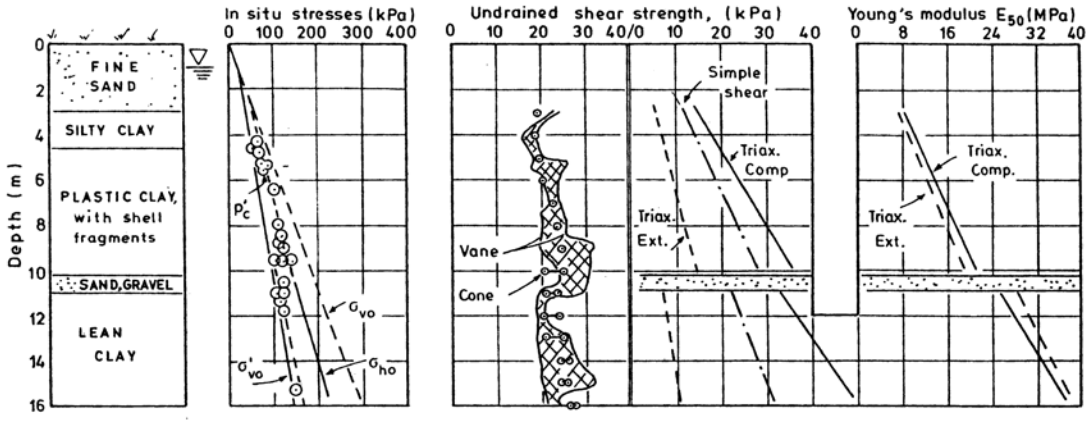

Figure 3.6 Site characteristics at Drammen test site (NGI)

3.3 UNCERTAINITY IN UNDRAINED STRENGTH

A fair amount of uncertainty is associated with the undrained strength in each of the test sites as seen from the soil profiles in the earlier section. Therefore, the foundation design needs account for these uncertainties (Gilbert and Murff, 2001b) in the selection of design criteria and in selection of the design strength profile. On the other hand, using an overly conservative profile may result in an uneconomic foundation

design; therefore, engineering judgment needs to be applied when selecting a suitable design profile.

3.4 REPRESENTATIVE SOIL PROFILE FOR FE ANALYSES

Based on the study of typical profiles in the Gulf of Mexico and the North Sea, the design soil profiles for this study were selected. Soil profile (P1) is a uniform profile, which was selected as a benchmark profile since a closed form solution for lateral load capacity for infinitely long caisson is available (Randolph and Houlsby, 1984). Profile P2 is representative of the typical soil profile in the Gulf of Mexico. Profile P3 is a profile of a lightly overconsolidated soil, which is also typical of sites in the GOM and the North Sea. Profile P4 is a profile, which is typical of stronger soils in the North Sea but which are still relatively soft. The specific undrained strengths of the four profiles are as listed in table 3.1.Undrained strength profile is shown in Figure 3.7.

Table 3.1 Representative strength profiles

PROFILE	CHARECTERISTIC REGION	STRENGTH EQUATION
P1	BENCHMARK PROFILE	S_U =1 (kPa)
P2	GULF OF MEXICO	S_U =1.25 z (kPa)
P3	GULF OF MEXICO AND NORTH SEA	S_U =5 + 1.25 z (kPa)
P4	NORTH SEA	S_U =10(kPa) for z <= 5m , S_U =2 z(kPa) for z > 5m ,

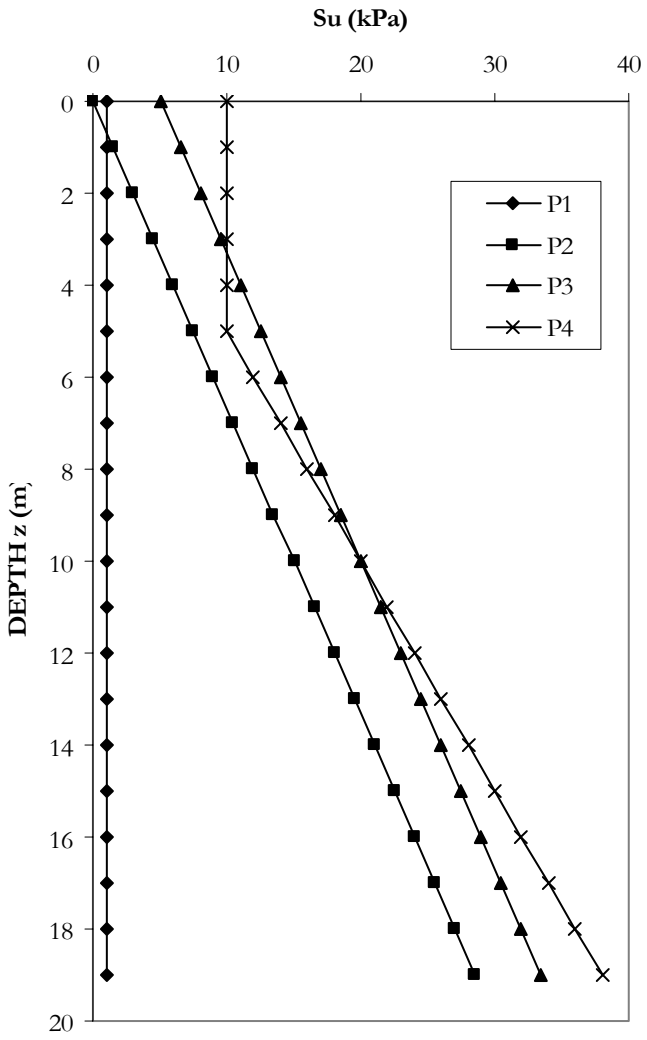

Figure 3.7 Strength profiles for FE analyses

CHAPTER IV

FINITE ELEMENT MODELING OF UNDRAINED BEHAVIOR

Finite element analysis is a numerical technique, which is being used to solve a wide range of real world problem. Versatility is the forte of this technique. Application of the method ranges from modeling prosthetic heart valve components to simulations of space structures like solar sails, space radars, and reflector antennas (ABAQUS website). Of more relevance here, the finite element method has been used to simulate various kinds of geotechnical problems such as dynamic soil-structure interaction of nuclear structures, modeling of ground water flow, estimation of collapse loads of foundations, simulating large water retaining structures such as earth dams, modeling of tunnels, estimating the ultimate capacity of piles and pile groups etc. Each of these different classes of problems has a unique physical behavior (Desai and Siriwarddane, 1984) which is represented by a set of governing partial differential equation. In order to model a problem accurately using the finite element method, it is essential to understand the physical nature of the problem, boundary conditions, and theoretical limitations (Cook, 1995). Some of these modeling issues are addressed in this chapter.

4.1 PHYSICAL NATURE OF THE CURRENT PROBLEM

The suction caisson is embedded in the seafloor by drawdown or negative pressure, which is applied to the inside of the caisson. During installation, the soil surrounding the caisson wall is disturbed or remolded. As time progresses the surrounding soil reconsolidates and regains a percentage of its original strength. The

time required for soil to reconsolidate depends on the soil permeability, stiffness and the problem geometry.

The caisson is installed in the desired location, connected to the anchor line, which is later connected to the floating structure. Depending on the type of floating structure, the type of mooring system and the anchor line attachment point, the loading angle may vary from zero to ninety degrees. Once the caisson is loaded, the caisson transmits the load to the surrounding soil. The pore pressure in the soil increases which is then gradually dissipated during loading, resulting in increase of the effective stress. As time progresses, the effective stress increases and as a result the factor of safety also increases. Thus, the most critical case in this problem is right after the installation. There may also be occasions during the service life of the floating system where it is subjected to severe environmental loads due to wave and wind action. These loads will be transmitted very rapidly to the foundation. Suction caissons in such situations may also be subjected to storm induced cyclic loading.

Furthermore, to add to the complexity of the problem, the shear strength of soil is dependent on the direction of shearing, in other words, soils exhibit marked anisotropy. The stress strain response also depends on the rate of loading. These two issues are not addressed in this study.

Theoretically it is possible to model most of these aspects, however to simplify the analysis and at the same time model the problem in a reasonably representative manner, some assumptions are made which are discussed in the next section.

4.2 BASIC ASSUMPTIONS

The following are the basic assumptions of the current problem.

- The soil is a single-phase material, i.e. the response of the soil is completely characterized by the total stress or the undrained strength parameter Su.
- The soil is isotropic, i.e. the shear strength of the material is independent of the mode of shearing.
- The response of the soil is independent of the rate of loading, i.e. the material is rate independent.
- The soil is elastic, perfectly plastic material i.e. the material does not harden or soften after first yield has occurred.
- The material follows the normality rule, i.e. the plastic strain increment is normal to the yield surface.
- The caisson is perfectly rigid, i.e. there is no relative deformation within the caisson.
- No gap is formed on the back of the caisson (active soil wedge).
- There is no slip between the caisson and the soil but there is a zone of reduced strength also known as the smear zone, which is less than or equal to the thickness of the skirt wall.

- The attachment point of the anchor line is a perfect hinge and no moment is developed at the attachment point.

4.3 MATERIAL BEHAVIOR UNDER UNDRAINED CONDITION

Normally consolidated soils under undrained loading conditions exhibit linear behavior at very low strain levels with very little post yield gradient. The response of the material is very strongly dependent on the sensitivity. For very sensitive clays, a post yield reduction in strength is observed (Figure 4.1).

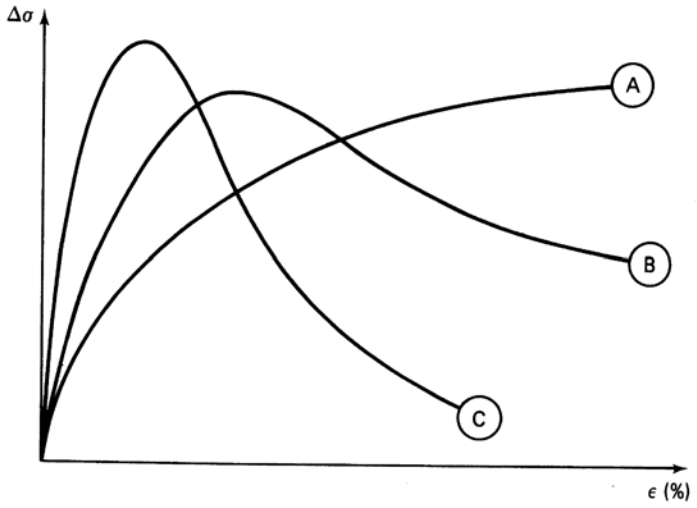

Figure 4.1 Typical stress strain curve for (A) remolded clays (B) medium sensitive clays (C)highly sensitive clays (Holtz and Kovacs, 1981)

Figure 4.2 shows the stress strain response of marine clays in the Gulf of Mexico (Bradshaw et al., 2000). It can be seen that, even at very large strains there is no strain softening.

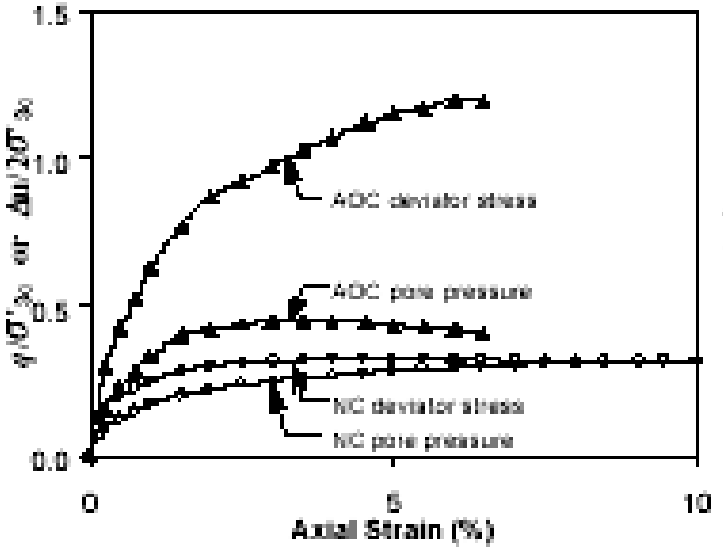

Figure 4.2 Stress strain behavior of NC clay in GOM (Bradshaw et al., 2000)

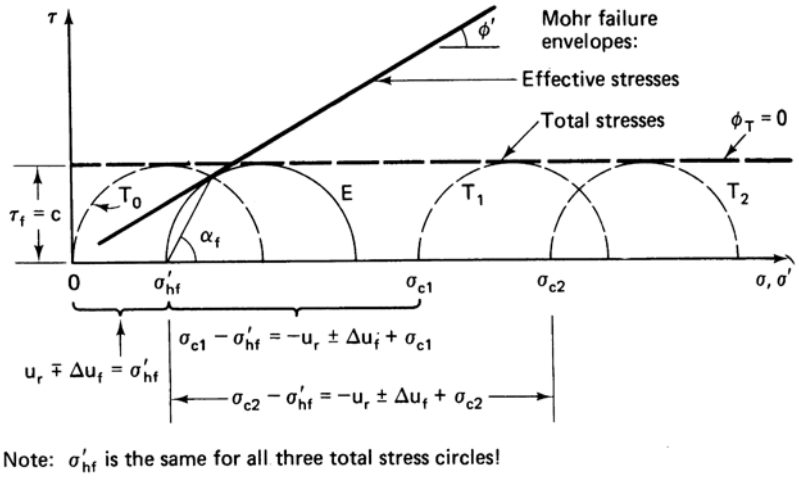

Figure 4.3 Failure envelopes under biaxial undrained loading (Holtz and Kovacs, 1981)

4.4 MATERIAL MODEL

A classical Prandtl-Reuss model was adopted to simulate the soil constitutive behavior. This model features linearly elastic behavior beneath the yield surface, a von Mises yield criterion with perfectly plastic behavior at yield (Figure 4.4), and an associated flow rule (Figure 4.5).

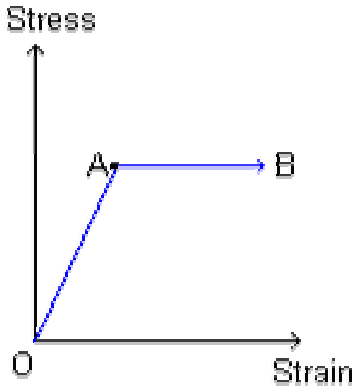

Figure 4.4 Idealized elastic-perfectly plastic response

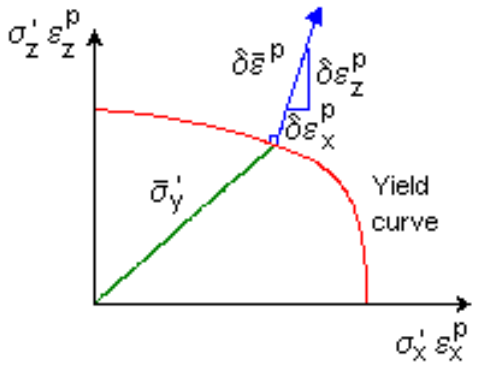

Figure 4.5 Associated flow; plastic strain increments are normal to yield surface

This constitutive model is isotropic in the sense that the stress-strain behavior is independent of the coordinate frame. However, shear strength will depend on shearing mode.

ABAQUS characterizes the von Mises yield surface in terms of the yield strength Y (Figure 4.6). This is related to the direct simple shear strength (Chapter III) used in this study to characterize soil-shearing resistance by the following relationship.

$$Y = \sqrt{3} S_U^{DSS} \tag{4.1}$$

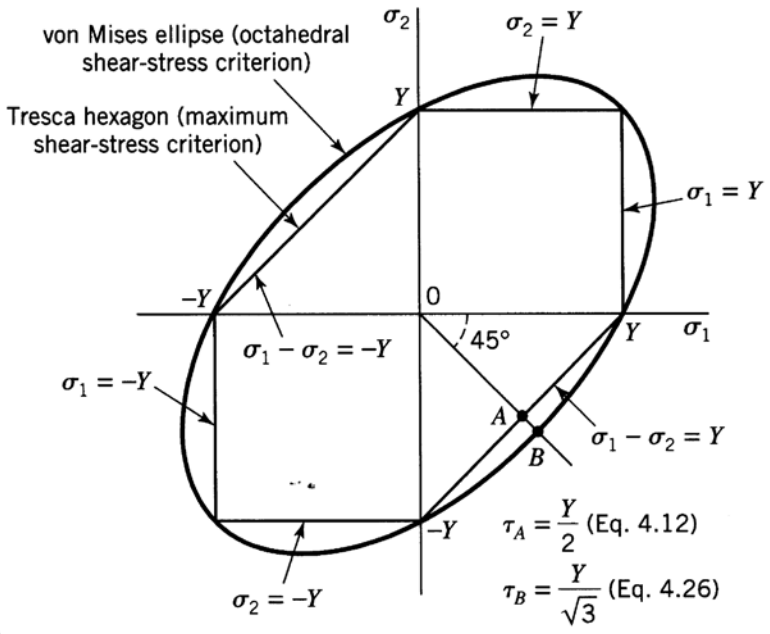

Figure 4.6 von Mises and Tresca yield surface under biaxial loading. Point A and B the location of pure shear on the yield surface (Boresi and Schmidt, 2002)

The von Mises yield function implies that the shear strength is independent of the hydrostatic stress ((Figure 4.7). This condition is true in case of the undrained condition as seen from Figure 4.3 where it is seen that the Mohr circle simply translates without growing in size.

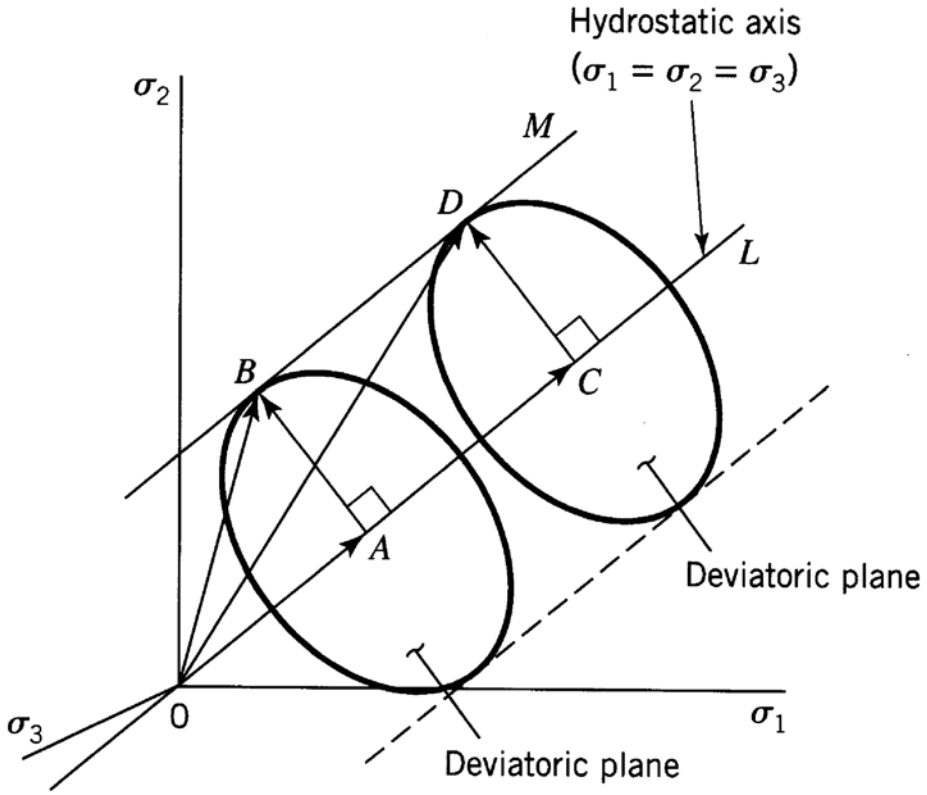

Figure 4.7 Effect of hydrostatic stress on von Mises criterion (Boresi and Schmidt, 2002)

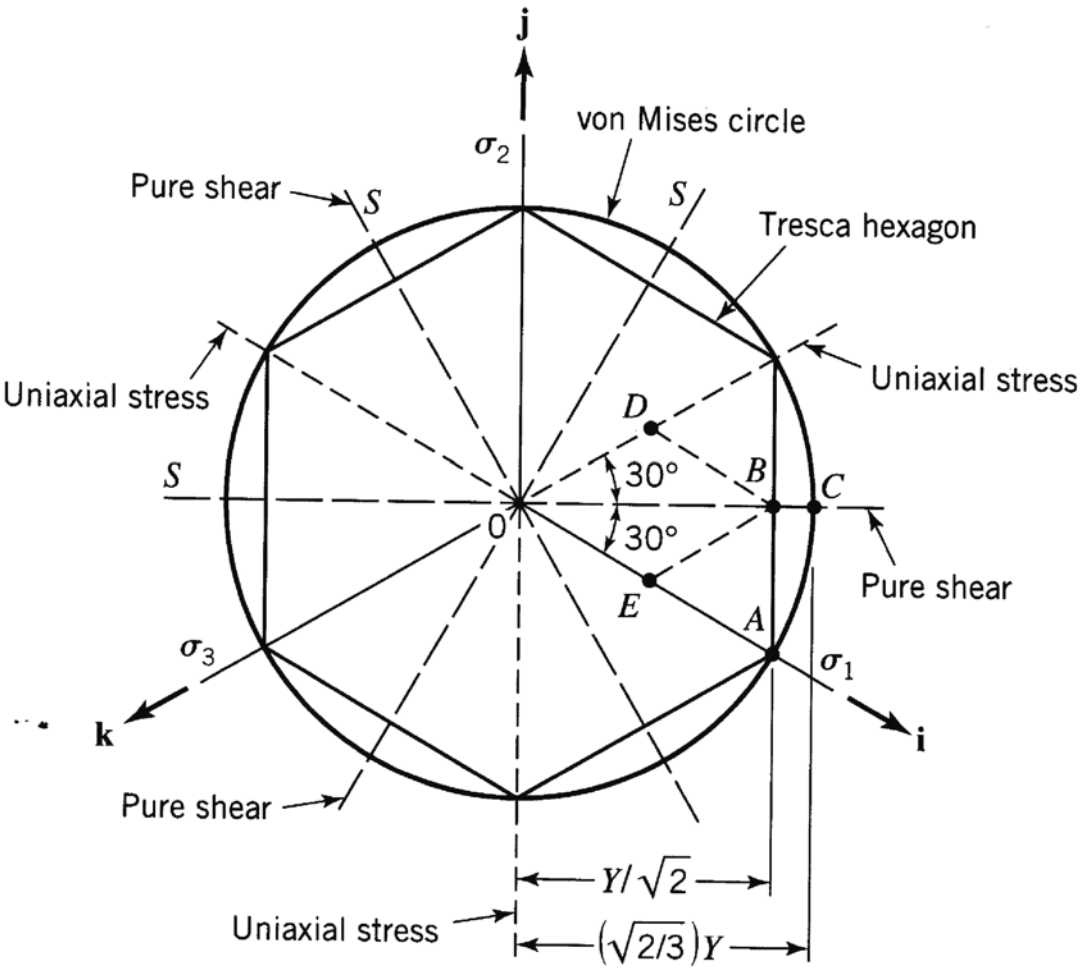

Figure 4.8 von Mises and Tresca yield criteria on π plane (Boresi and Schmidt, 2002)

The initial elastic modulus of the soil is assumed to be small, i.e. E/s_u^{DSS} = 500. This is done in order to increase the computational speed and avoid numerical problems. Even though the elastic stiffness of the system is underestimated, this however does not

affect the ultimate capacities (Moon, 2000) and only the elastic displacements are overestimated.

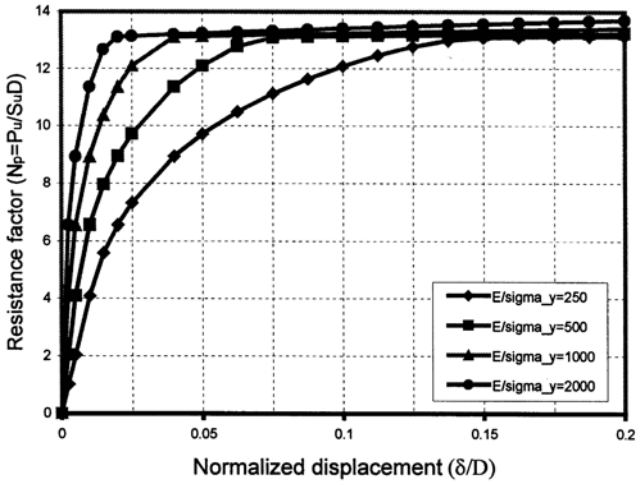

Figure 4.9 Effect of initial elastic stiffness on ultimate capacity (Moon, 2000)

4.5 FINITE ELEMENT MODEL

Finite element analyses were carried out using the ABAQUS 6.3 (HKS, 2000) computer program. Undrained conditions imply an incompressible material for which mean stress cannot be determined from displacements. Hybrid displacement-pressure (mean stress) elements provide an effective means for numerical modeling of this condition. The ABAQUS element library offers a number of hybrid elements. A 3D 8-node hybrid brick element (C3D8H) was selected for the FEM simulations.

The suction caisson was modeled using the RIGID BODY option. A RIGID BODY is a group of nodes or elements whose motion is governed by the motion of a

single node also called the rigid body reference node. The applied load for load-controlled analyses was enforced on the rigid body reference node.

Taking advantage of symmetry about the plane in which the load is applied, only one-half (180 degrees) of the problem had to be modeled. Different mesh discretization was used for each aspect ratio (L/D ratio) of caisson geometry. The details of individual mesh are discussed in the next chapter.

The displacements at the outer boundary and at the base of the mesh were assumed to be zero. All the nodes at these boundaries were constrained by imposing zero displacements. The nodes at the plane of symmetry were constrained in the normal direction of the plane.

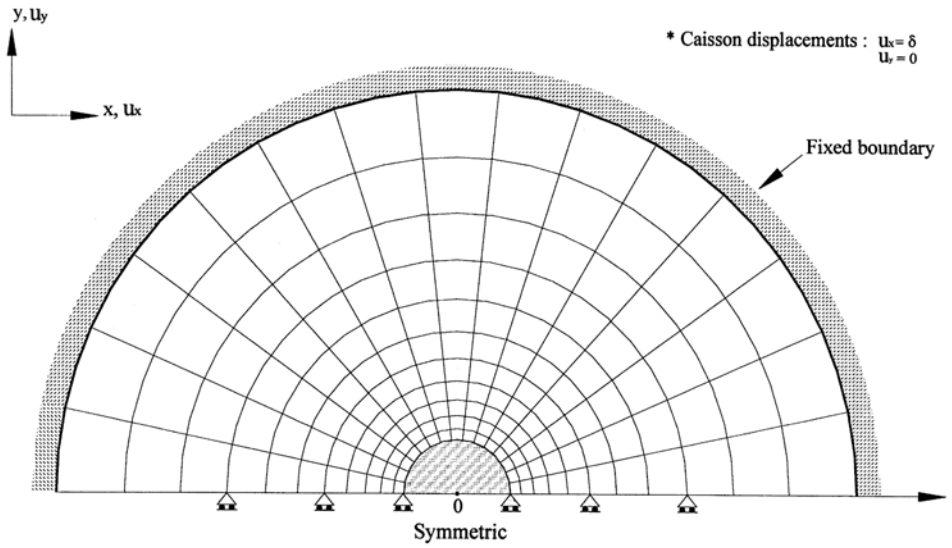

Figure 4.10 Boundary condition (Moon, 2000)

4.6 TYPES OF FINITE ELEMENT ANALYSES PERFORMED

Both load controlled and displacement controlled analyses (Sukumaran et al., 1999) were performed. For the pure horizontal and the vertical loading cases, displacements were applied to obtain ultimate capacity. For inclined loading conditions, a load controlled procedure was followed.

In the displacement-controlled analyses, the horizontal and the vertical displacement were prescribed at the rigid body reference node located at the top of the vertical centerline. The prescribed displacement at the rigid body node was increased progressively to a sufficiently large value, where there was essentially no increase in reaction forces in the rigid body node.

In the load-controlled analyses, the load applied to the rigid body reference node located at the top of the vertical centerline was increased in steps. The step sizes were automatically computed by ABAQUS automatic incrementation scheme. The load was increased to a magnitude where the slope of the load-displacement curve was nearly zero. In some of the analyses, the load-displacement curve was extrapolated to approximate a tangential stiffness of zero.

4.7 KINEMATIC CONSTRAINTS

Kinematic constraints were applied to the rigid body in order to obtain the maximum capacity of the caisson at a particular load angle. From previous studies (Moon, 2000 and Han, 2002) it was shown that maximum capacity is obtained in a pure translational mechanism. Details of kinematics constrains are discussed below.

4.7.1 OPTIMAL LOADING, NO ROTATION

If the load is attached at its optimal location, the caisson will experience pure translation with no rotation. This corresponds to a condition in which the maximum pullout resistance of the caisson is mobilized. This case was simulated in ABAQUS by applying the load to the caisson (modeled as a rigid body) at an arbitrary reference point while specifying a condition of no rotation. Through this procedure, the FEM analyses calculate an ultimate load as well as the magnitude of the moment required to restrain the caisson against rotation. With the ultimate force and restraining moment known, the distance of the optimal load application point from the reference point is computed simply by dividing the restraining moment by the ultimate load. The reference point

used in these simulations was on the centerline at the top of the caisson. Ultimate load capacity for conditions of optimal loading was evaluated for load inclinations of 0, 15, 30, 45, 60, and 90 degrees.

4.7.2 LOAD ATTACHMENT ABOVE AND BELOW OPTIMUM

If the load attachment point is above or below its optimal depth, the caisson will rotate with a corresponding reduction in pullout capacity. A few FEM simulations for this type of condition were performed for a load inclination of 30 degrees.

For the short caisson (L/D=1.5), attachment depths of 2.5m and 6m were considered. For the slender caisson (L/D=5), attachment depths of 12.5m and 20m were considered. The upper and lower attachment depths in both cases correspond to attachment depths that are respectively above and below the optimum depth.

CHAPTER V

RESULTS OF FINITE ELEMENT STUDY

This chapter documents the 3D Finite Element study carried out for estimation of ultimate load capacity of suction caisson anchors. These FEM studies were performed to provide a basis for evaluating the simplified plasticity models for estimating the load capacity of suction caissons for general conditions of inclined loading, ranging from purely horizontal to purely vertical loading. Two sets of studies were performed; the first set was performed in conjunction with University Western Australia (UWA) and Norwegian Geotechnical Institute (NGI). Finite element analyses were carried out for two test cases: one short (C2 caisson with L/D=1.5) and one slender (C3 caisson with L/D=5) caisson. The short caisson was analyzed for a strength profile typical of normally consolidated conditions. The slender caisson was analyzed for a lightly overconsolidated strength profile. The particular areas of focus these studies were to compare the various FEM simulations carried out at UWA, NGI and TAMU. The FEM simulations were also compared to the predictions made by the various simplified methods which included the magnitude of the ultimate load capacity, vertical-horizontal load interaction effects, the location of the optimal load attachment point, and the effects of anchor rotation. Details of this study were reported in the technical report titled "Deepwater Anchor Design Practice Phase II Report to American Petroleum Institute" (NGI 2003).

The second study developed a family of load interaction curves for various caisson aspect ratios in typical soil profiles of the Gulf of Mexico and the North Sea. This study

mainly focused on the optimum capacity estimation and the location of the load attachment point. The study also explored the effect of reduction in soil strength due to disturbance created by the caisson penetration process. This effect was simulated by assigning a reduced strength to the disturbed zone (Table 5.3). Finite element analyses were carried out for four different caisson aspect ratios (L/D=2, 4, 6, 8). All caissons were analyzed for four different strength profiles P1, P2, P3 and P4 (Table 3.1). All analyses assumed fully undrained conditions, and no separation was assumed to occur between the soil-caisson interface on the active side of the caisson.

5.1 DESCRIPTION OF STUDY-I

Finite element analyses were carried out for two test cases: one short (L/D=1.5) and one slender (L/D=5) caisson. All analyses assumed fully undrained conditions, and no separation was assumed to occur between the soil-caisson interface on the active side of the caisson. For these set of analyses, the weight of the caisson was also included. FEM analyses were performed for the following conditions:

Optimal loading, no rotation. If the load is attached at its optimal location, the caisson will experience pure translation with no rotation. This corresponds to a condition in which the maximum pullout resistance of the caisson is mobilized. This case was simulated in ABAQUS by applying the load to the caisson (modeled as a rigid body) at an arbitrary reference point while specifying a condition of no rotation. Through this procedure, the FEM analyses calculated an ultimate load as well as the magnitude of the moment required to restrain the caisson against rotation. With the ultimate horizontal

force (H) and restraining moment (RM) known, the distance of the optimal load application point from the reference point (Li) is computed simply by dividing the restraining moment by the ultimate load. The reference point (attachment point) used in these simulations was on the centerline at the top of the caisson. Ultimate load capacity for conditions of optimal loading was evaluated for load inclinations of 0, 15, 30, 45, 60, 75, and 90 degrees.

Load attachment above and below optimum. If the load attachment point is above or below its optimal depth, the caisson will rotate with a corresponding reduction in pullout capacity. FEM simulations for this type of condition were performed for a load inclination of 30 degrees. For the short caisson, attachment depths of 2.5m and 6m were considered. For the slender caisson, attachment depths of 12.5m and 20m were considered. The upper and lower attachment depths in both cases correspond to attachment depths that are respectively above and below the optimum depth.

Details of soil data, anchor geometry data and mesh discretization are presented in following sections

5.2 SOIL DATA

The soil was modeled as a weightless material with undrained strength in direct simple shear (S_u) as summarized in Table 5.1. Shear strength at the soil-caisson interface was taken as 0.65 times S_u.

Table 5.1 Soil strength data

CAISSON TYPE	C2	C3
UNDRAINED STRENGTH	Su=1.25.z (kPa)	Su=10 (kPa) (z<5m) Su=2.z (kPa) (z>5m)

5.3 ANCHOR DETAILS

The following anchor geometries were used for the analyses (Table 5.2).

Table 5.2 Anchor geometry details

CAISSON TYPE	C2	C3
LENGTH (L)	7.5 m	25 m
DIAMETER (D)	5 m	5 m
L/D RATIO	1.5	5
SUBMERGED WEIGHT	330 kN	1100 kN
STRUCTURAL MODEL	RIGID CYLINDER	RIGID CYLINDER

5.4 MESH DISCRETIZATION

The details of the meshes used for the analyses are as follows:

Table 5.3 Mesh discretization details

CAISSON TYPE	TYPE C2 (Figure 5.1)	TYPE C3 (Figure 5.2)
DIVISION OF LENGTH	20	50
DIVISION OF RADIUS	10	3
SECTORS IN PLAN	18	18
DISTANCE FROM THE CAISSON BASE TO BOTTOM BOUNDARY	7.5 m	25 m
DISTANCE FROM RADIUS TO OUTER BOUNDARY	47.5 m	47.5 m
DIVISION FROM BASE TO BOTTOM BOUNDARY	20	10
DIVISION FROM RADIUS TO OUTER BOUNDARY	24	24
REFINEMENT FACTOR FROM BASE TO BOTTOM BOUNDARY	1	0.9
REFINEMENT FACTOR FROM RADIUS TO OUTER BOUNDARY	0.85	0.85
BOTTOM BOUNDARY CONDITION	FIXED	FIXED
RADIAL BOUNDARY CONDITION	FIXED	FIXED
PLANE OF SYMMETRY BOUNDARY CONDITION	RESTRAINED NORMAL TO PLANE	RESTRAINED NORMAL TO PLANE
TOTAL NUMBER OF ELEMENTS	24480	36720
SMAER ZONE	0.17 m	0.20m

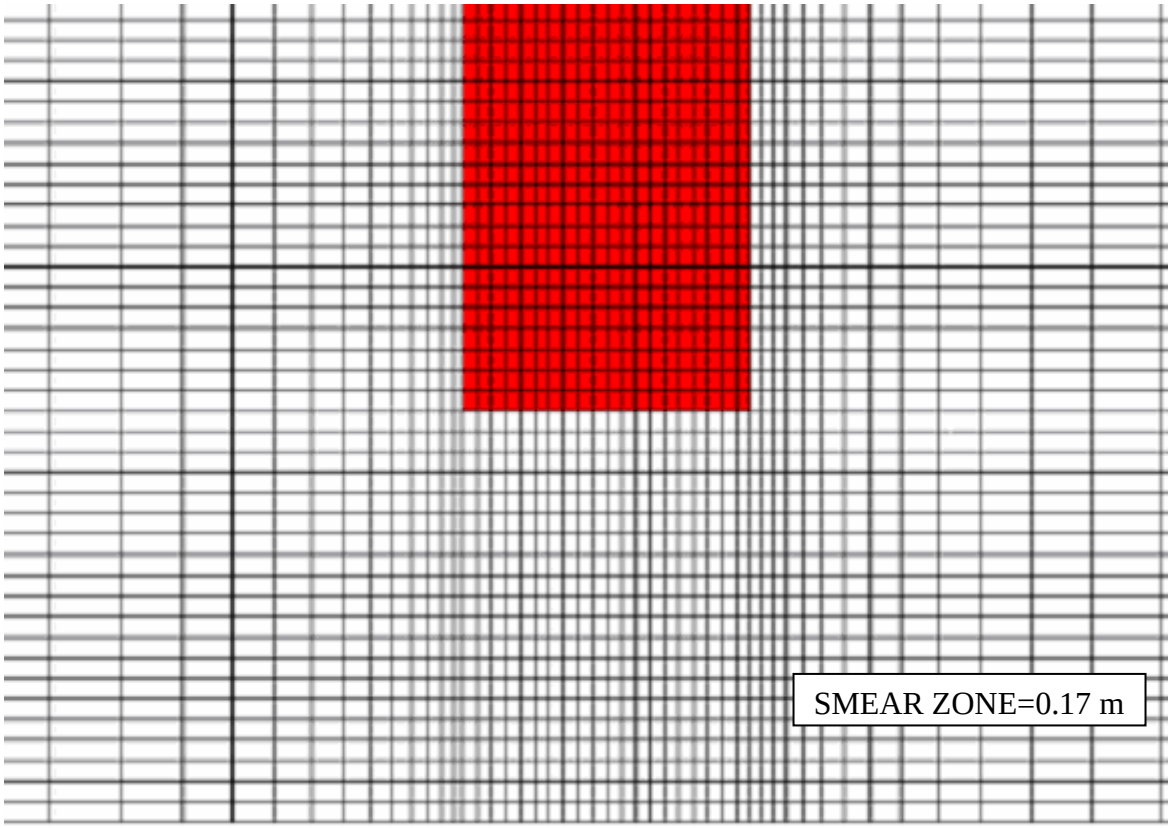

Figure 5.1 Magnified view of mesh for C2 type caisson

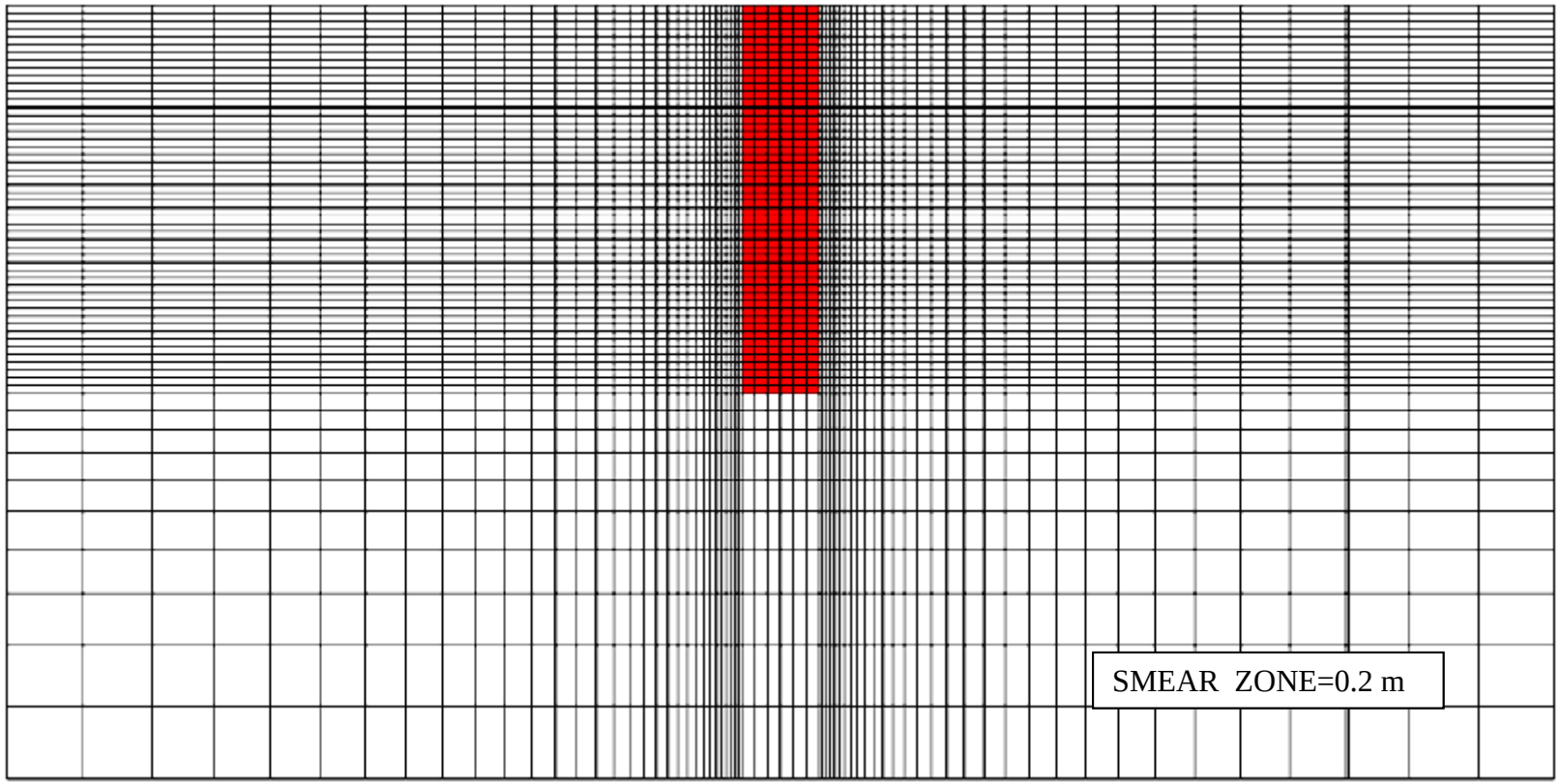

Figure 5.2 Mesh for C3 type caisson

5.5 ANALYSES RESULTS FOR THE SHORT CAISSON (C2)

No rotation. The horizontal-vertical load interaction diagram for the no-rotation condition is shown in Figure 5.3. Figure 5.4 shows the same predictions in terms of the total resultant load versus inclination angle. Distance of the optimal load application point from the rigid body reference point (Li) is normalized by the length of the caisson (L). These predictions are tabulated in Table 5.4.

Table 5.4 Ultimate capacity of C2 caisson

L (m)	D (m)	α	δ (deg)	H (kN)	V (kN)	RM (kN-m)	Li/L
7.5	5	0.65	0.0	1729.00	0.00	9248.00	0.713
7.5	5	0.65	15.0	1729.00	463.20	9370.00	0.723
7.5	5	0.65	30.0	1727.60	997.40	9068.00	0.700
7.5	5	0.65	45.0	1622.00	1622.00	8540.00	0.702
7.5	5	0.65	60.0	1257.80	2178.00	6538.00	0.693
7.5	5	0.65	75.0	667.80	2492.00	3232.00	0.645
7.5	5	0.65	90.0	0.00	2560.00	0.00	-NA-

The predictions indicate that the load capacity interaction effects occur primarily between inclination angles of 15 and 75 degrees. That is, for load inclination angles less than 30 degrees the horizontal capacity is essentially unaffected by the vertical load components, and for inclination angles greater than 75 degrees the vertical load capacity is unaffected by the horizontal load capacity.

The optimal load attachment depth (Table 5.4) is such that the resultant load intersects the centerline at very close to 0.7 times the caisson length for load inclination

angles up to 60 degrees. The computations show that the optimal depth decreases somewhat at a load inclination angle of 75 degrees. However, at angles 75 degrees or greater, the caisson load capacity is dominated by the vertical capacity and the optimal attachment depth begins to lose its relevance.

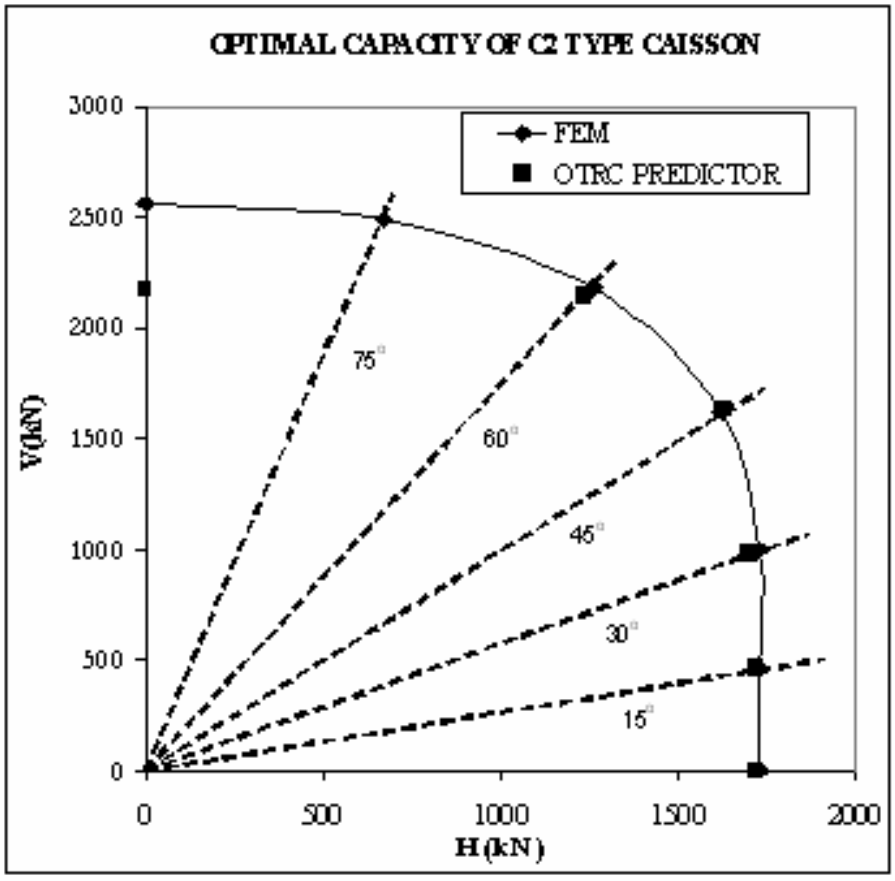

Figure 5.3 Optimal capacity of C2 type caisson

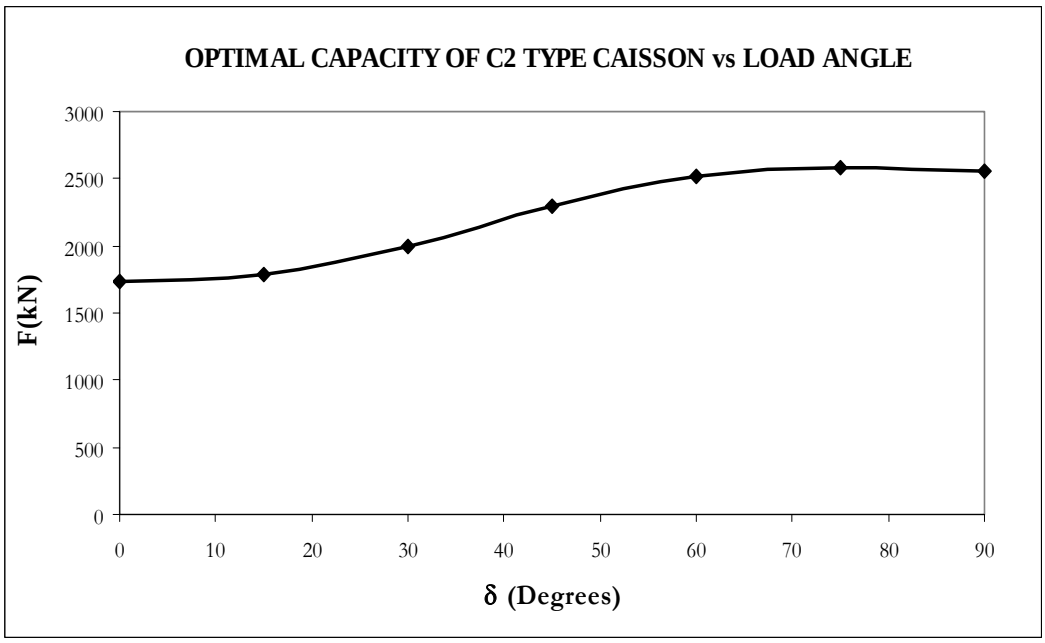

Figure 5.4 Variation of optimal capacity of C2 type caisson with load inclination

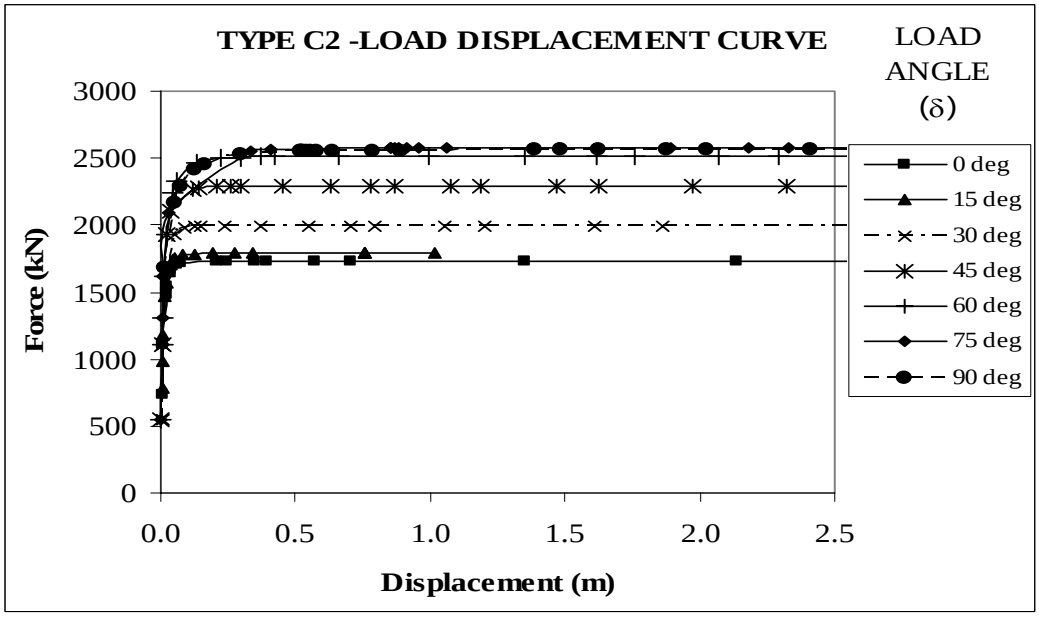

Figure 5.5 Load displacement curve for C2 caisson

Load-displacement curves for various load inclinations for the case of no rotation are shown in Figure 5.1. For horizontal loading, the ultimate load capacity is mobilized at a relatively small displacement, less than 0.1m or 0.02 caisson diameters. As the load inclination angle is increased, the displacement required for mobilization of ultimate load capacity progressively increases. For purely vertical loading, the displacement at which the ultimate load is mobilized is about 0.4m or 0.08 diameters.

Rotation. Three analyses were performed for the case in which rotation of the caisson is permitted to occur, all for the case of a 30-degree load inclination angle. In the first case the load was attached at a depth of 2.5m below the mudline; i.e., above the optimum load attachment depth. The results of these analyses are presented in Table 5.5.

Table 5.5 Variation of ultimate capacity of C2 type caisson with attachment point

H	V	F	δ (deg)	Z
1311.00	756.80	1513.76	30.0	-2.500
1727.60	997.40	1994.85	30.0	-3.806
1139.00	657.60	1315.20	30.0	-6.000

The rotation of the caisson in this case resulted in about a 25 percent reduction in the ultimate total load capacity. Similarly, when the load was applied below the optimum attachment depth, 6m below the mudline, the ultimate total load capacity was reduced by about 35 percent.

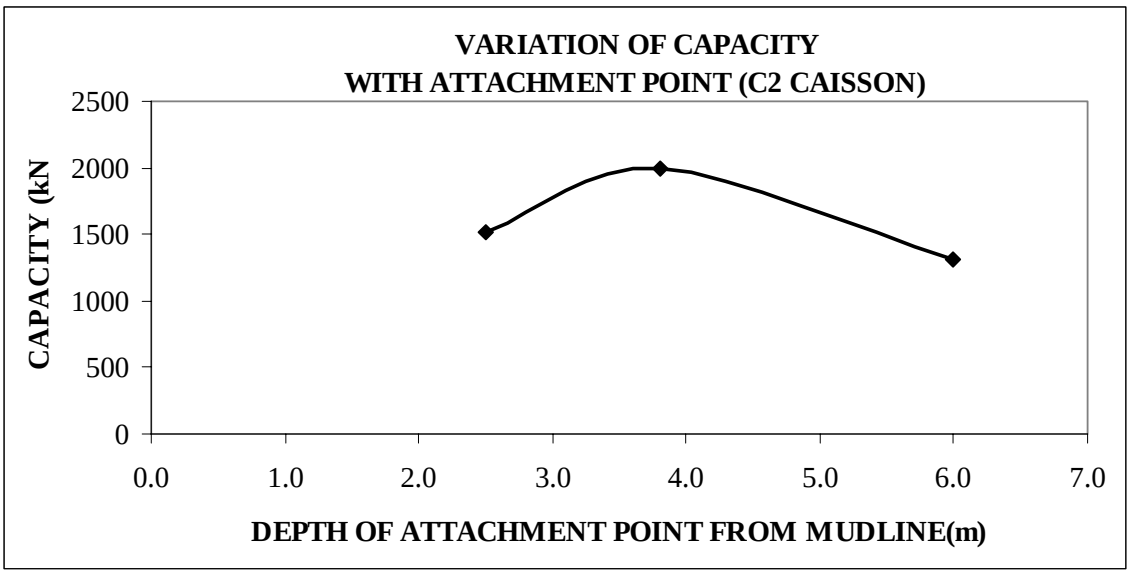

Figure 5.6 Variation of optimal capacity with attachment point

The variation of optimum capacity with attachment point is shown in Figure 5.6. When the load was attached at the optimal load attachment depth indicated in Table 5.4, the ultimate total load capacity was identical to that computed for the case in which the caisson was restrained against rotation.

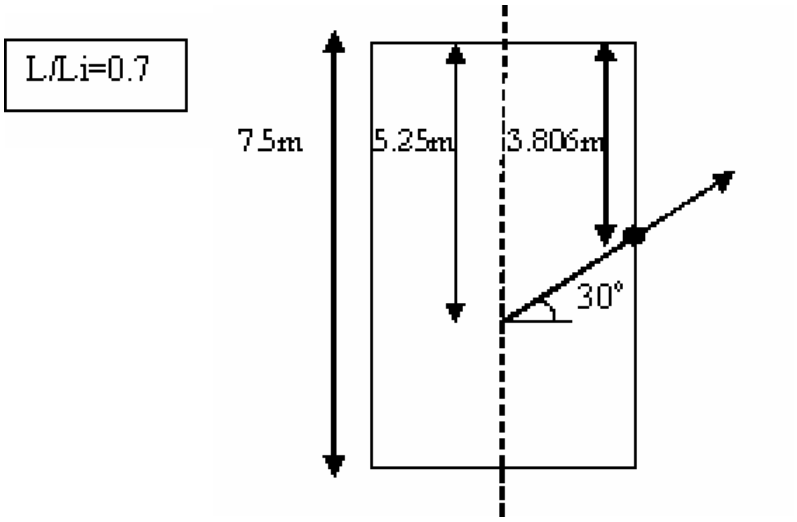

Figure 5.7 Load attachment point for maximum capacity when rotation is allowed

The load attachment point for the optimum capacity in this case was obtained by projecting the line of action of the external force on the caisson periphery (Figure 5.7). This essentially confirms the validity of the results presented in Table 5.4; i.e., when the load is attached at its optimal location, the caisson will not rotate even if it is unconstrained against rotation.

Figure 5.8, Figure 5.9 and Figure 5.10 shows the failure mechanism of the C2 caisson for different attachment point. When the load is attached at the optimum attachment point (Figure 5.10), the failure mechanism is purely translational. When the load attachment point is above or below the optimum, a rotational mode of failure is seen.

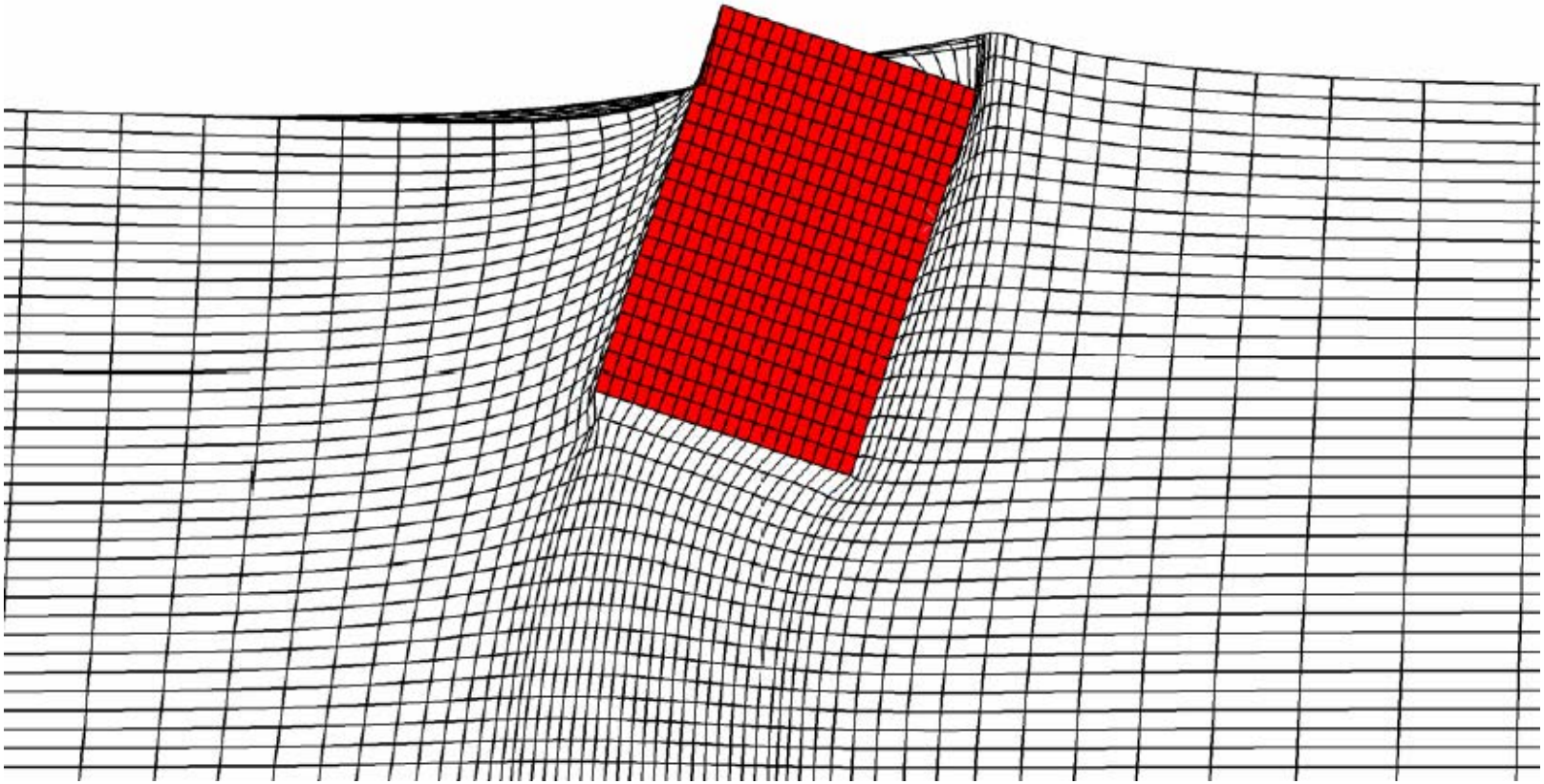

Figure 5.8 Failure mechanism when attachment point is above the optimum attachment point

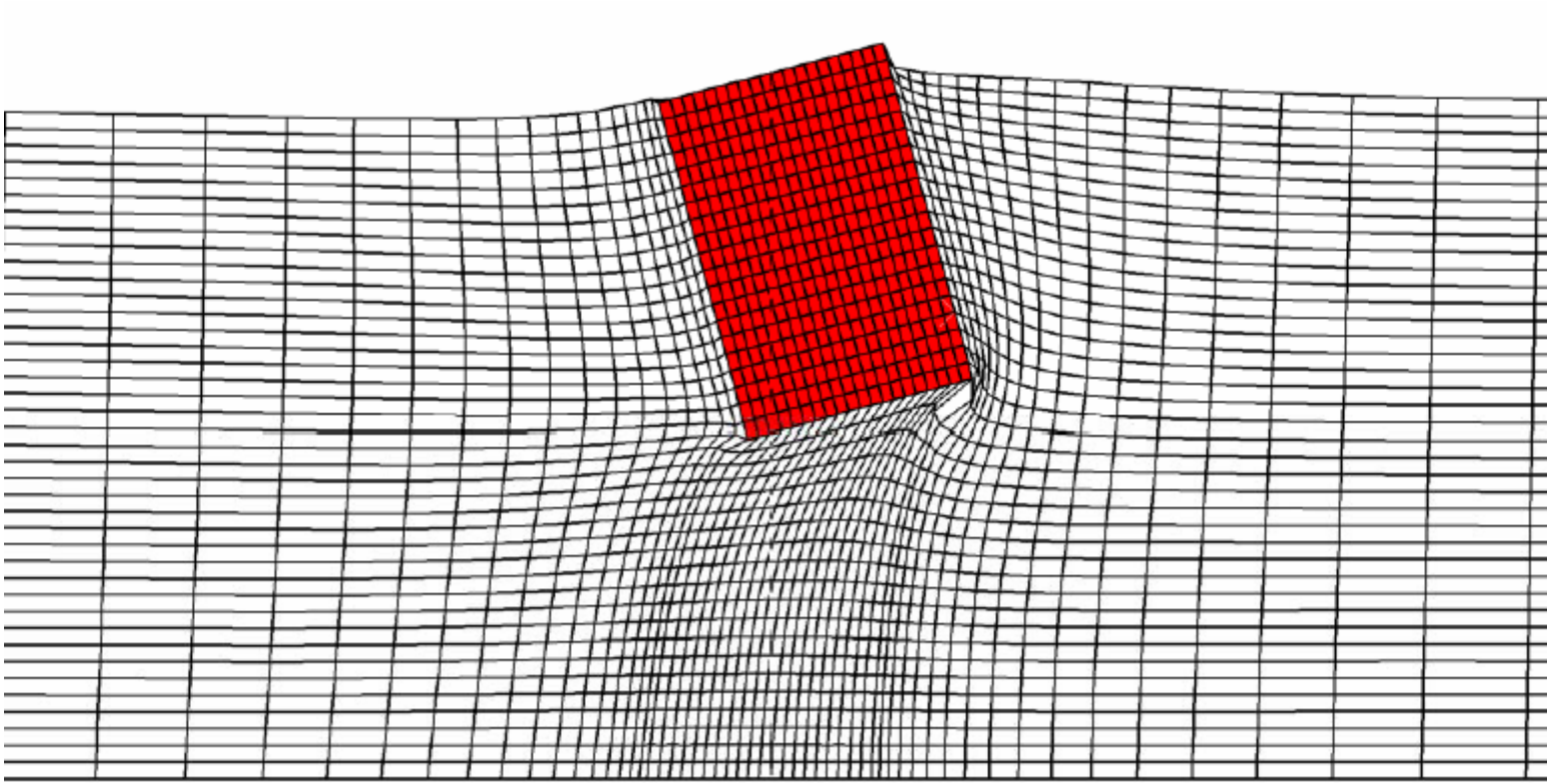

Figure 5.9 Failure mechanism when attachment point is below the optimum attachment point

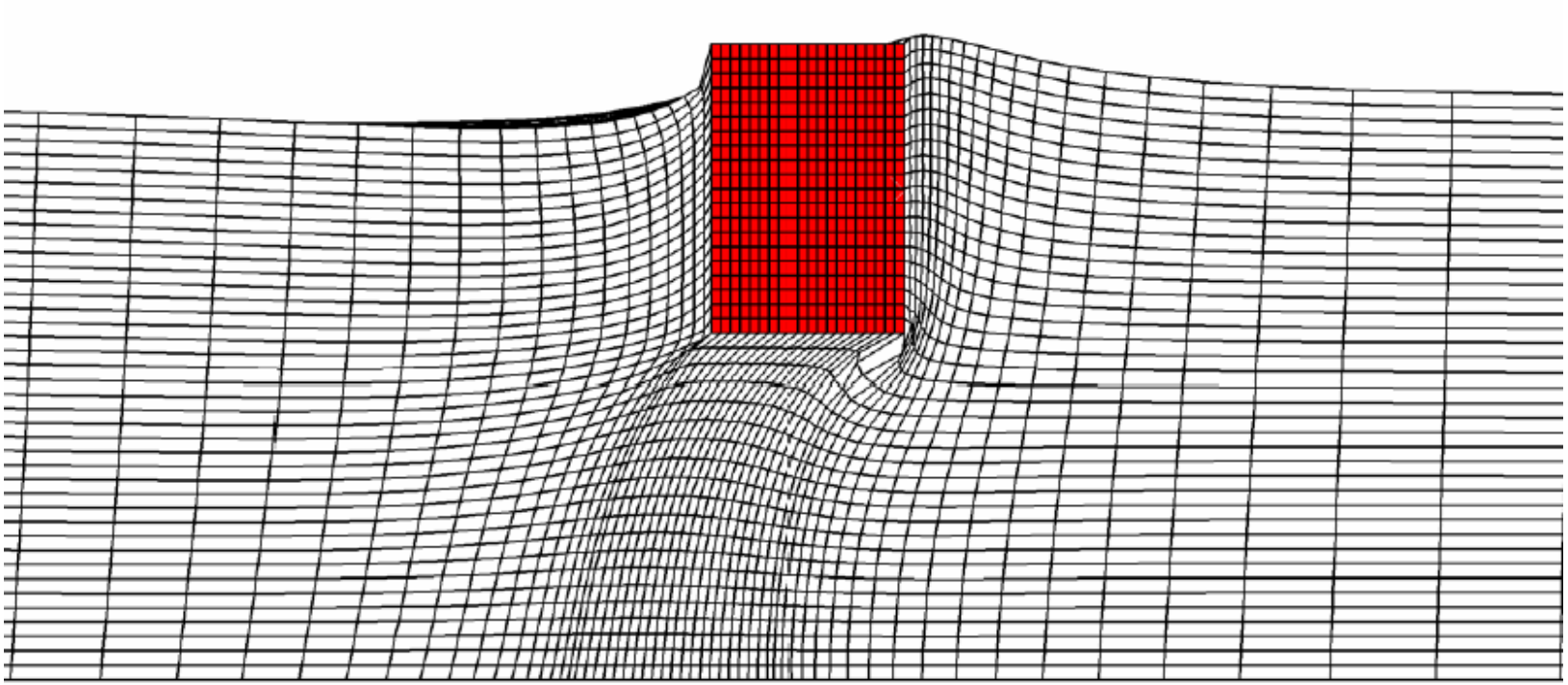

Figure 5.10 Failure mechanism when attachment point is the optimum attachment point

5.6 ANALYSES RESULTS FOR THE SLENDER CAISSON (C3)

No rotation. The horizontal-vertical load interaction diagram for the no-rotation condition is shown in Figure 5.11.Figure 5.12 shows the same predictions in terms of the total resultant load versus inclination angle. These predictions are also tabulated in Table 5.6.

Table 5.6 Ultimate capacity of C3 caisson

L (m)	D (m)	α	δ (deg)	H (kN)	V (kN)	RM (kN-m)	Li/L
25	5	0.65	0.0	3.903E+04	0.000E+00	6.7962E+05	0.696
25	5	0.65	15.0	3.738E+04	1.002E+04	6.4530E+05	0.691
25	5	0.65	30.0	2.991E+04	1.727E+04	5.0596E+05	0.677
25	5	0.65	45.0	1.952E+04	1.952E+04	2.9818E+05	0.611
25	5	0.65	60.0	1.162E+04	2.013E+04	1.6168E+05	0.556
25	5	0.65	90.0	0.000E+00	1.968E+04	-	

The predictions indicate that the load capacity interaction effect for the slender caisson (C3) occur at lower load inclination angles than for the case of the short caisson (C2). That is, the interaction effects occur primarily at load inclination angles between 15 and 45 degrees. The optimal depth (Table 5.6) at which the resultant load intersects the centerline is approximately 0.7 times the caisson length for horizontal loads and decreases somewhat with increasing load attachment angle.

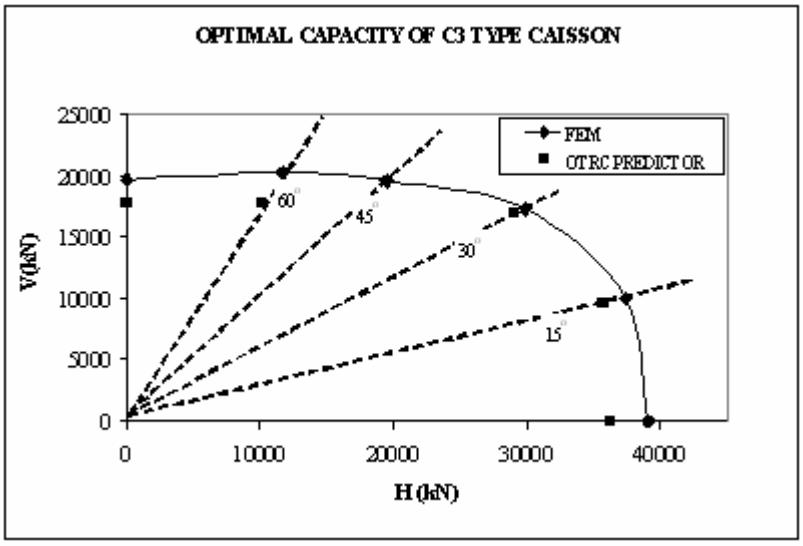

Figure 5.11 Optimal capacity of C3 type caisson

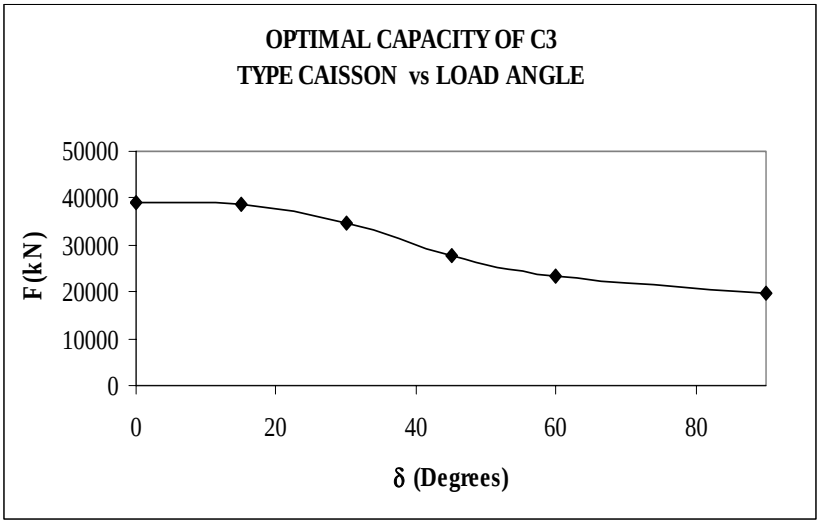

Figure 5.12 Variation of optimal capacity of C3 type caisson with load inclination

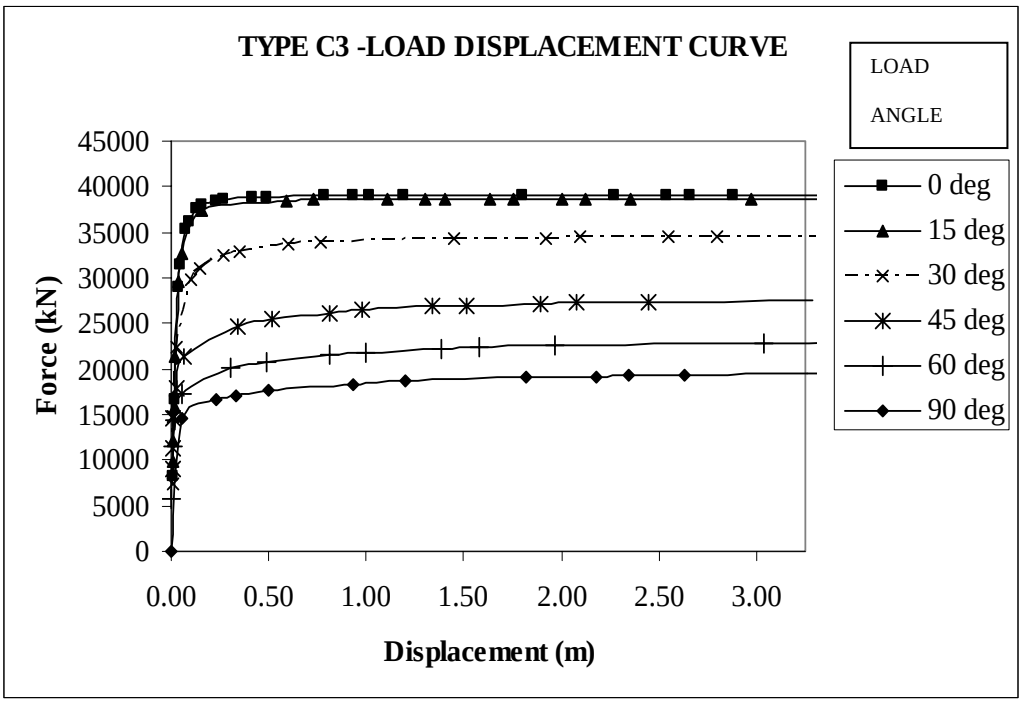

Figure 5.13 Load displacement curve for C3 caisson

Load-displacement curves for various load inclinations for the case of no rotation are shown in Figure 5.11. Regarding the displacement levels at which full resistance is mobilized, similar trends occur here as for the C2 case; that is, the displacement required to mobilize the ultimate capacity increases with increasing load inclination angle. However, the overall magnitudes of these displacements are substantially higher than for the C2 case. For example, for horizontal loading the ultimate capacity is mobilized at 0.4m displacement for the slender (C3) case versus about 0.1m for the short case. At a load attachment angle of 60 degrees about 2m of displacement was required to mobilize the ultimate resistance.

Rotation. Two analyses were performed (Table 5.7) for the case in which rotation of the caisson is permitted to occur, all for the case of a 30-degree load inclination angle. In the first case the load was attached at a depth of 12.5m below the mudline; i.e., above the optimum load attachment depth. The rotation of the caisson in this case resulted in about a 15 percent reduction in the ultimate total load capacity. A similar reduction occurred when the load was applied below the optimum attachment depth, 20m below the mudline.

Table 5.7 Variation of ultimate capacity of C3 type caisson with attachment point

H	V	F	δ (deg)	Z
14574.00	29147.21	30.0	-12.500	14574.00
14578.00	29156.14	30.0	-20.000	14578.00

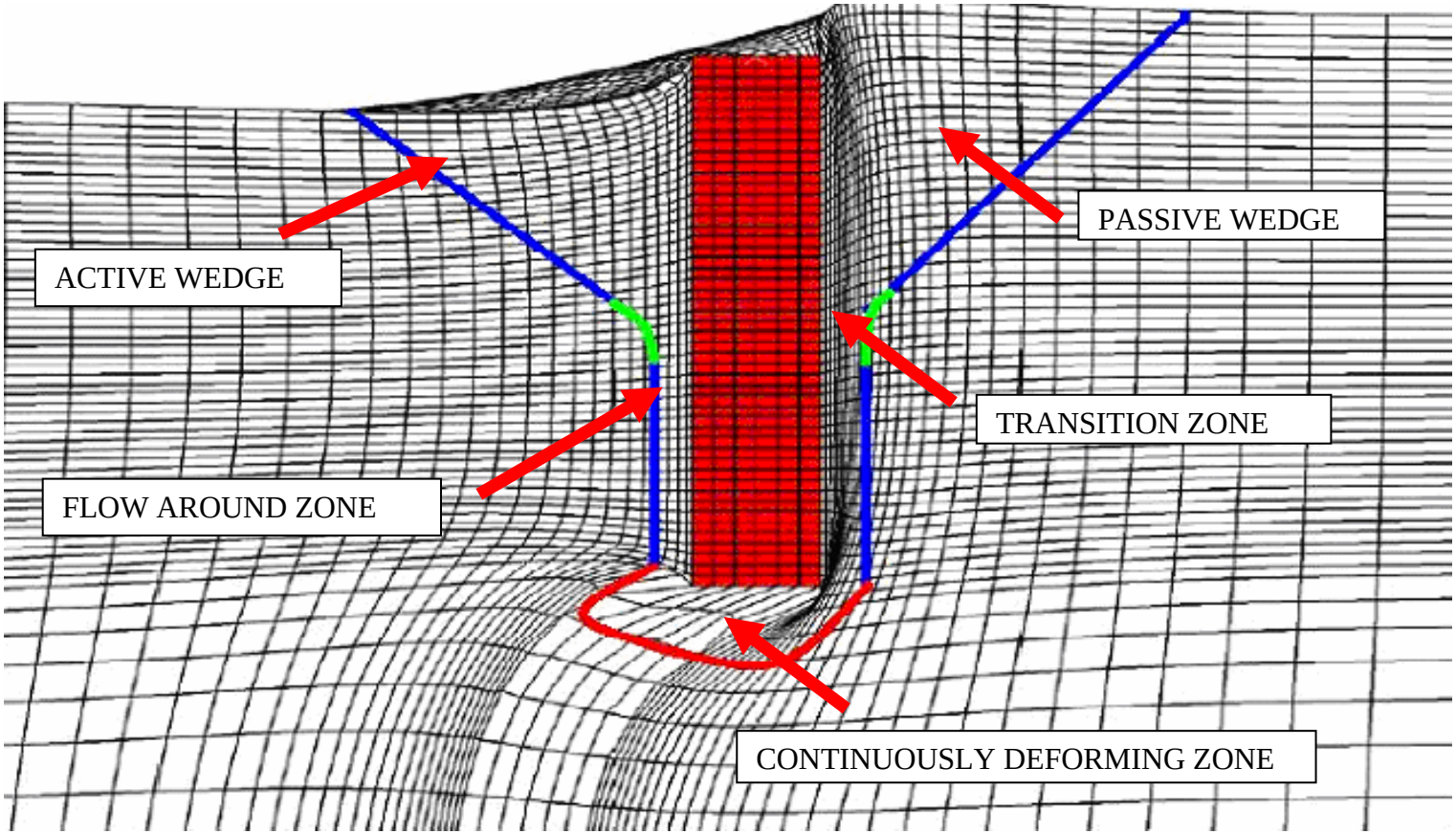

Figure 5.14 Various energy dissipation zones

5.7 ENERGY DISSPATION ZONES IN SOIL

Figure 5.14 shows the zones of energy dissipation in soil surrounding the caisson. Near the surface, active and passive wedges are formed. Below the wedge a flow around zone exist. It is interesting to note that at the bottom; a continuously deforming zone is seen instead of a rigid sphere. This is because; it is much easier for the soil to flow under the caisson near the bottom than to flow around it.

5.8 COMPARISION OF FEM AND OTRC PREDICTOR RESULTS

For the C2 type caisson, excellent agreement is seen between FEM solution and predictor method for load angles 0 to 60 degrees.The predictor method underestimated vertical capacity by about 15 % (Figure 5.3)

For the C3 type caisson, in general good agreement is seen between FEM solution and predictor method .Predictor method underestimated vertical capacity by about 10 % and horizontal capacity by 7% (Figure 5.11)

5.9 DESCRIPTION OF STUDY-II

The objective of the second study was to develop load interaction curves for various caisson aspect ratios in typical soil profiles of the Gulf of Mexico and the North Sea. Based on the experience gained from the first study, the meshes were optimized. The lateral extent of the mesh was reduced. More number of elements was used below the caisson as in it was seen in the previous study that the vertical capacity was over predicted for the C3 type caisson. The family of load interaction curves developed form this study is presented in APPENDIX -B.

5.10 ANCHOR DETAILS

The following anchor geometries were used for the various analyses carried out for determination of ultimate capacity (Table 5.8).

Table 5.8 Anchor geometry details

CAISSON TYPE	TYPE 1	TYPE 2	TYPE 3	TYPE 4
LENGTH (L)	10 m	20 m	30 m	40 m
DIAMETER (D)	5 m	5 m	5 m	5 m
L/D RATIO	2	4	6	8
STRUCTURAL MODEL	RIGID CYLINDER	RIGID CYLINDER	RIGID CYLINDER	RIGID CYLINDER

Note: - The anchors were considered weightless in each of this case.

5.11 MESH DISCRETIZATION

The details of the meshes (Table 5.9) used for the analyses are as follows:

Table 5.9 Mesh discretization details

CAISSON TYPE	TYPE 1 (Figure 5.15)	TYPE 2 (Figure 5.16)	TYPE 3 (Figure 5.17)	TYPE 4 (Figure 5.18)
DIVISION OF LENGTH	15	30	45	60
DIVISION OF RADIUS	5	5	5	5
SECTORS IN PLAN	18	18	18	18
DISTANCE FROM THE CAISSON BASE TO BOTTOM BOUNDARY	15m	15m	15m	15m
DISTANCE FROM RADIUS TO OUTER BOUNDARY	30m	30m	30m	30m
DIVISION FROM BASE TO BOTTOM BOUNDARY	15	15	15	15
DIVISION FROM RADIUS TO OUTER BOUNDARY	20	20	20	20
REFINEMENT FACTOR FROM BASE TO BOTTOM BOUNDARY	0.8	0.8	0.8	0.8
REFINEMENT FACTOR FROM RADIUS TO OUTER BOUNDARY	0.8	0.8	0.8	0.8
BOTTOM BOUNDARY CONDITION	FIXED	FIXED	FIXED	FIXED
RADIAL BOUNDARY CONDITION	FIXED	FIXED	FIXED	FIXED
PLANE OF SYMMETRY BOUNDARY CONDITION	RESTRAINED NORMAL TO PLANE	RESTRAINED NORMAL TO PLANE	RESTRAINED NORMAL TO PLANE	RESTRAINED NORMAL TO PLANE
TOTAL NUMBER OF ELEMENTS	13500	20250	27000	33750
SMEAR ZONE	0.0875m	0.0875m	0.0875m	0.0875m

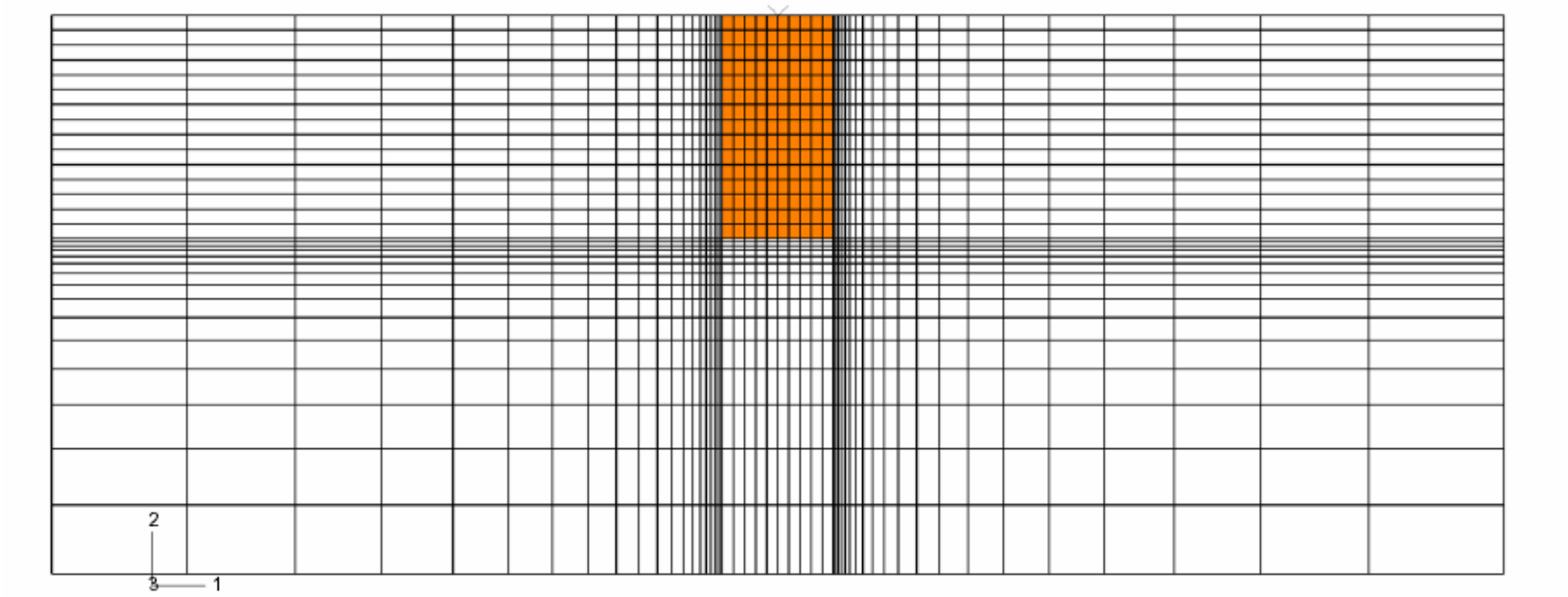

Figure 5.15 Mesh for caisson with L/D=2

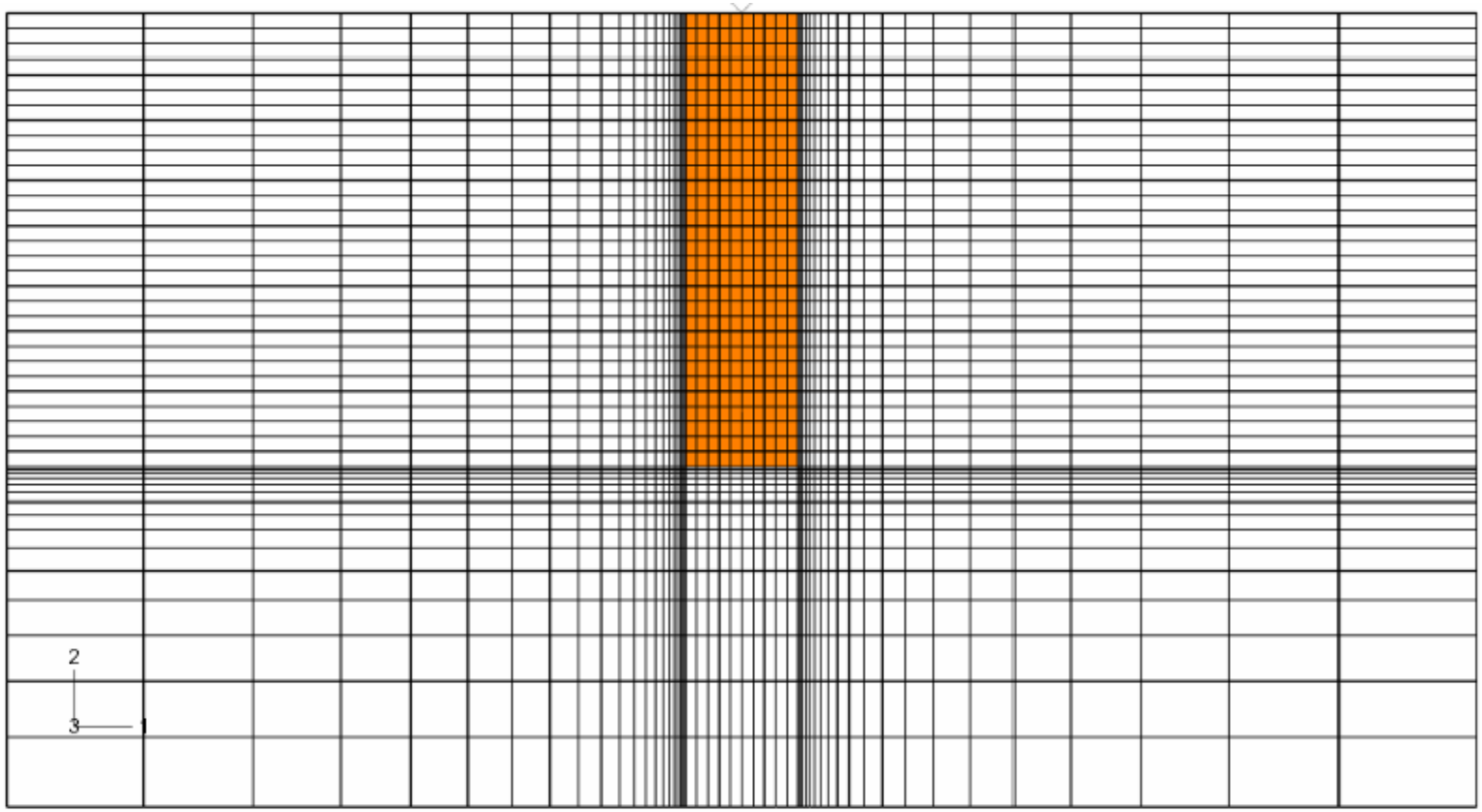

Figure 5.16 Mesh for caisson with L/D=4

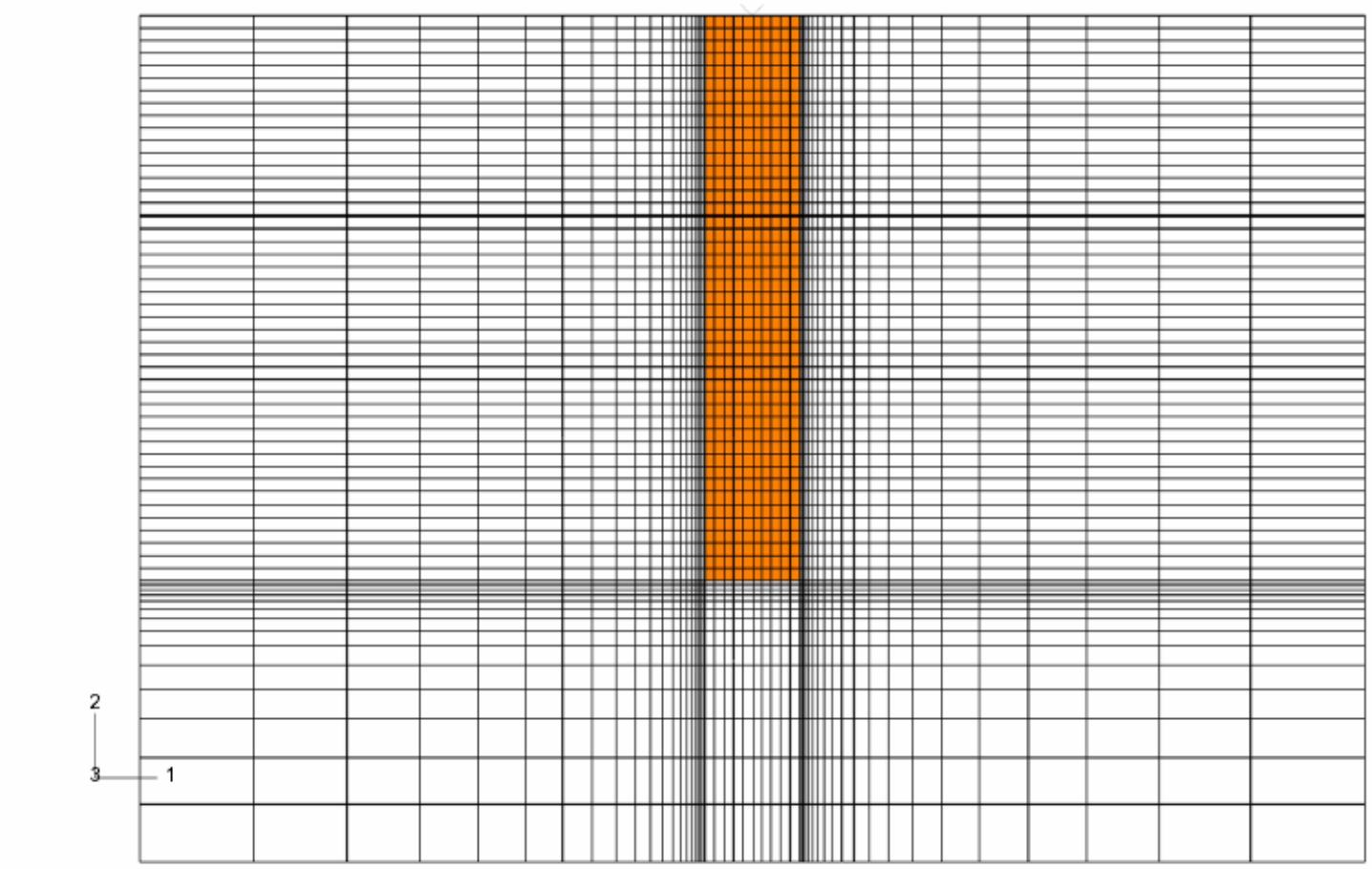

Figure 5.17 Mesh for caisson with L/D=6

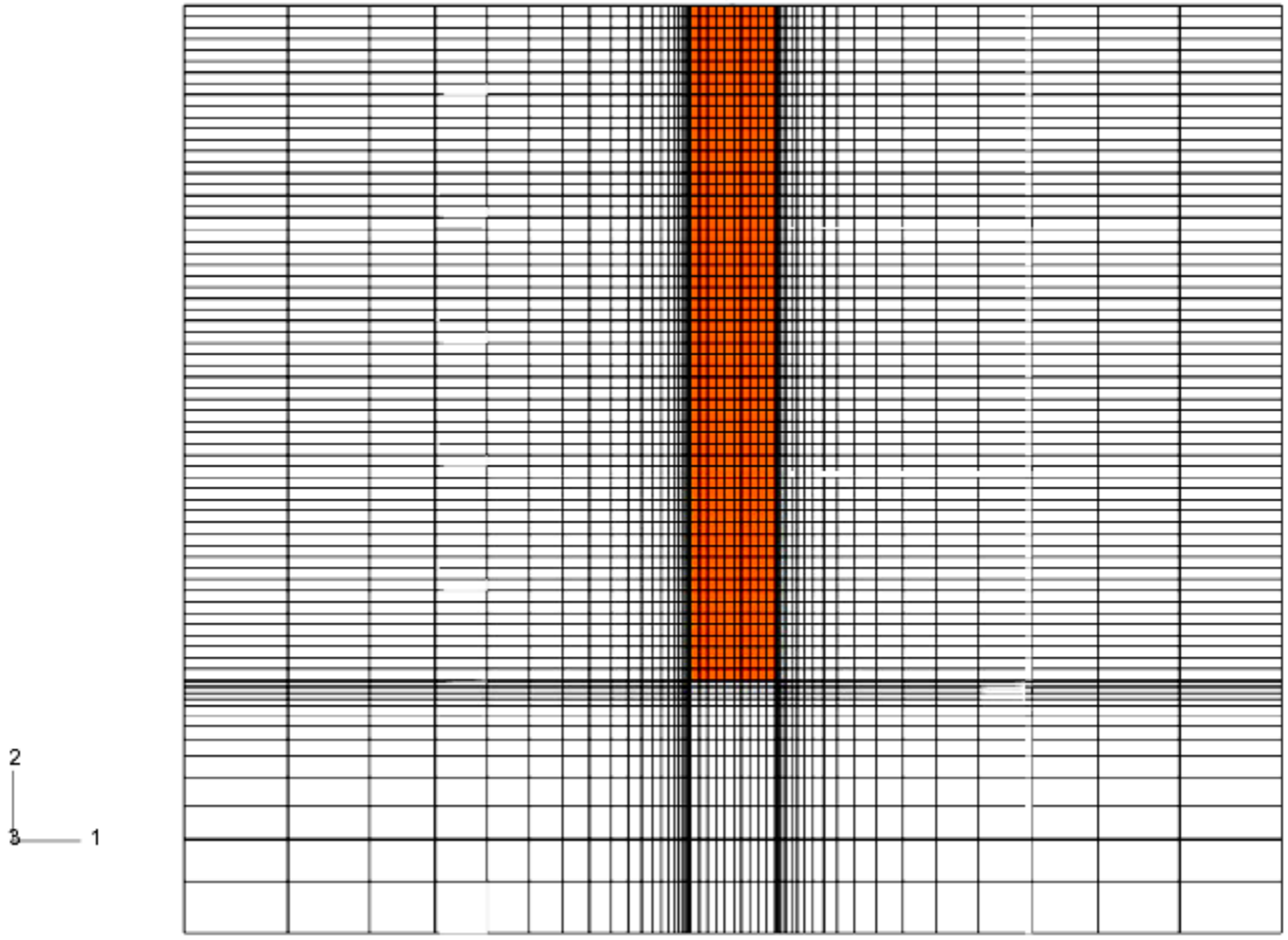

Figure 5.18 Mesh for caisson with L/D=8

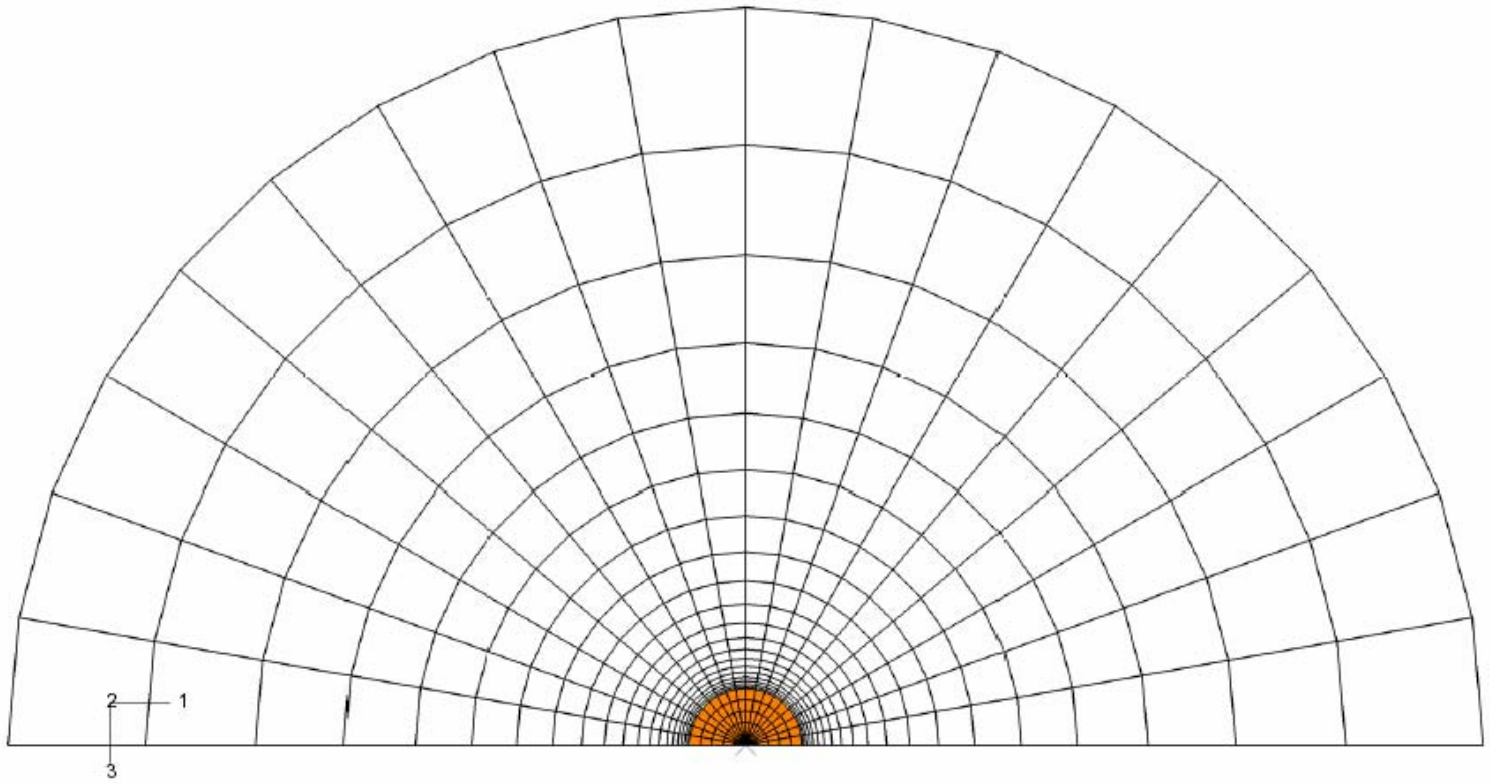

Figure 5.19 Top view of mesh

5.12 ANALYSES RESULTS

The ultimate capacity calculate from the finite element study is presented in form of a normalized load interaction diagram. The normalized plots are presented in term of two parameters N_H and the N_V. These two parameters are defined as follows.

$$N_H = \frac{H}{LDS_{u\_AVG}}$$

$$N_V = \frac{V}{LDS_{u\_AVG}}$$

Where,

H = Horizontal component of ultimate load

V = Vertical component of ultimate load

L = Length of caisson

D = Diameter of caisson

S_{u_AVG} = Shear strength, computed at L/2 For the soil profile P4, the value S_{u_AVG} values for each aspect ratio of the caisson was computed by fitting a curve (Figure 5.20 to Figure 5.23) using least square method and computing the shear strength value of the best-fit curve at L/2.The best-fit strength values are shown in Table 5.10 to Table 5.13.

Table 5.10 Best fit soil strength for caisson with L/D=2 ; soil profile P4

Z(m)	Su (kPa)	$SU_{1\ BEST\ FIT}$	$SU_{0\ BEST\ FIT}$	$Su_{AVG\ BEST\ FIT}$
0.00	5.00	1.5000	2.5000	10.0000
5.00	5.00			
10.00	20.00			

Table 5.11 Best fit soil strength for caisson with L/D=4; soil profile P4

Z(m)	Su (kPa)	$SU_{1\ BEST\ FIT}$	$SU_{0\ BEST\ FIT}$	$Su_{AVG\ BEST\ FIT}$
0.00	5.00	1.8846	0.9615	19.8077
5.00	5.00			
20.00	40.00			

Table 5.12 Best fit soil strength for caisson with L/D=6; soil profile P4

Z(m)	Su (kPa)	$SU_{1\ BEST\ FIT}$	$SU_{0\ BEST\ FIT}$	$Su_{AVG\ BEST\ FIT}$
0.00	5.00	1.9516	0.5645	29.8387
5.00	5.00			
30.00	60.00			

Table 5.13 Best fit soil strength for caisson with L/D=8; soil profile P4

Z(m)	Su (kPa)	$SU_{1\ BEST\ FIT}$	$SU_{0\ BEST\ FIT}$	$Su_{AVG\ BEST\ FIT}$
0.00	5.00	1.9737	0.3947	39.8684
5.00	5.00			
40.00	80.00			

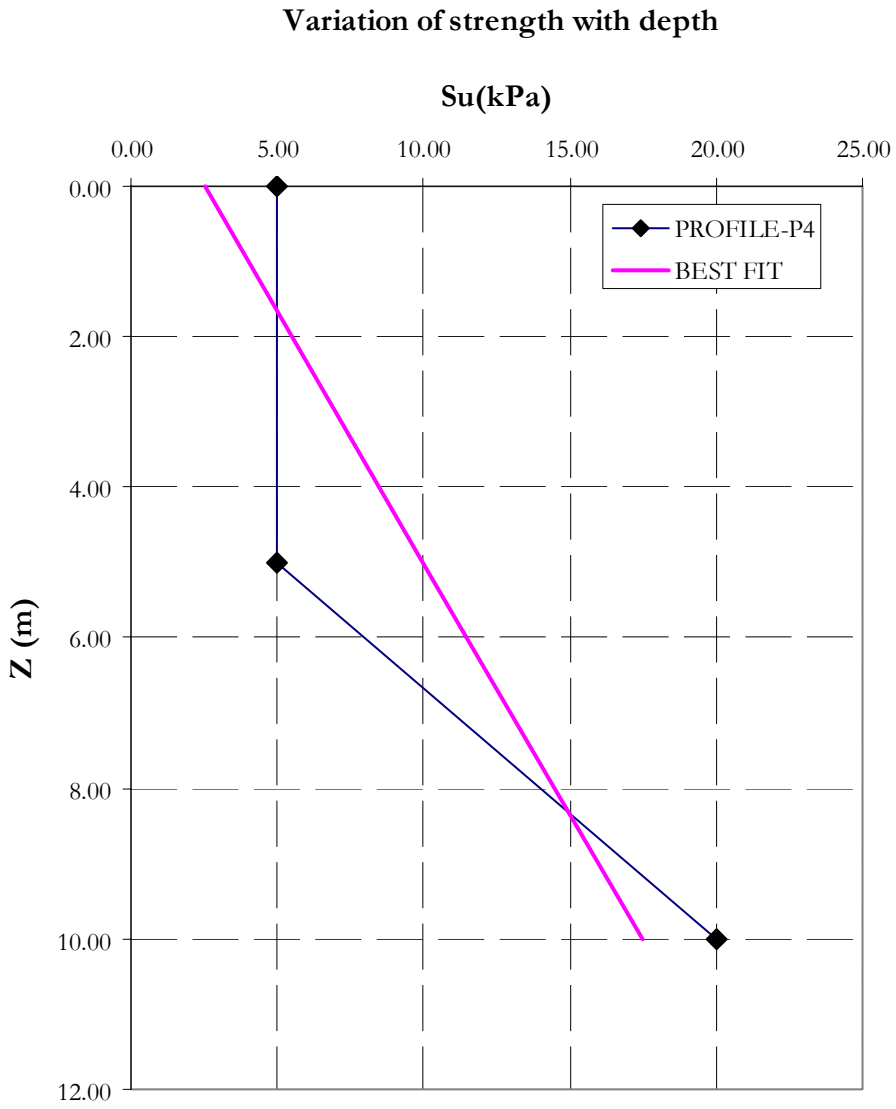

Figure 5.20 Best fit strength profile for caisson with L/D=2

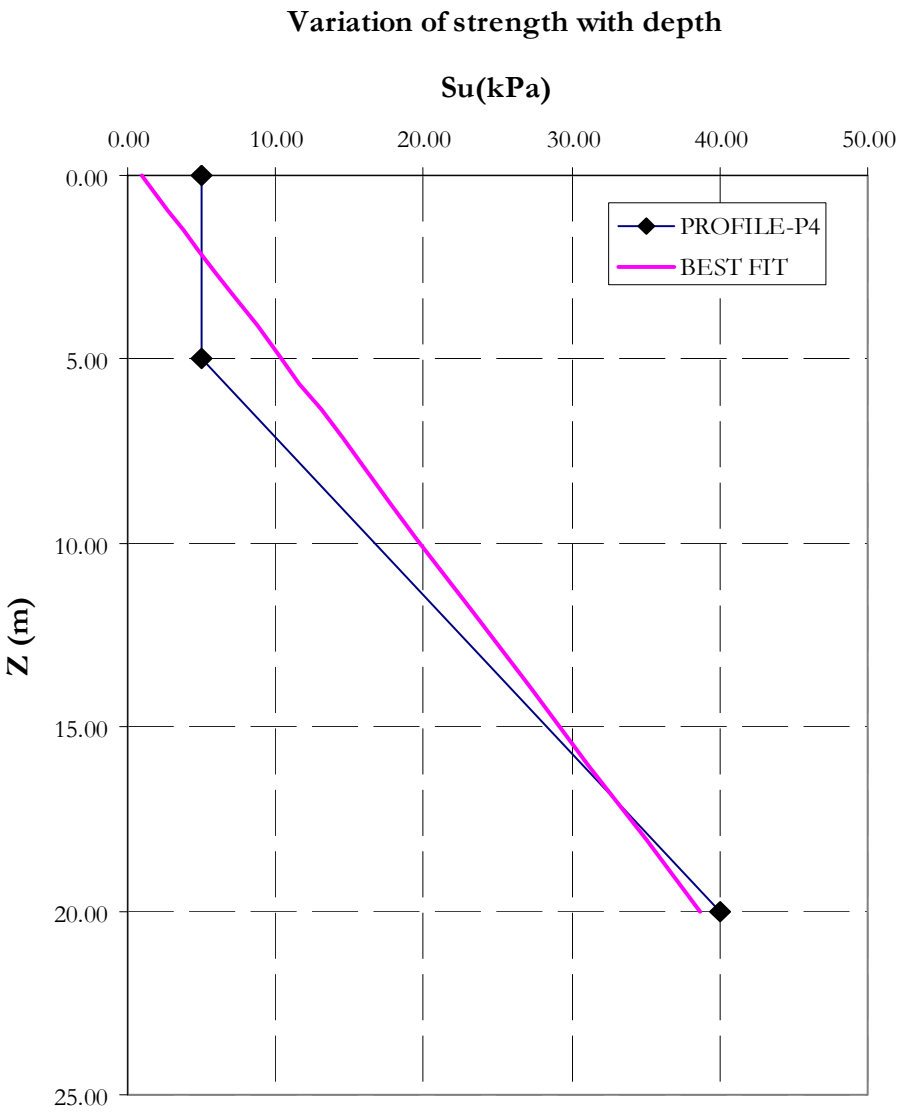

Figure 5.21 Best fit strength profile for caisson with L/D=4

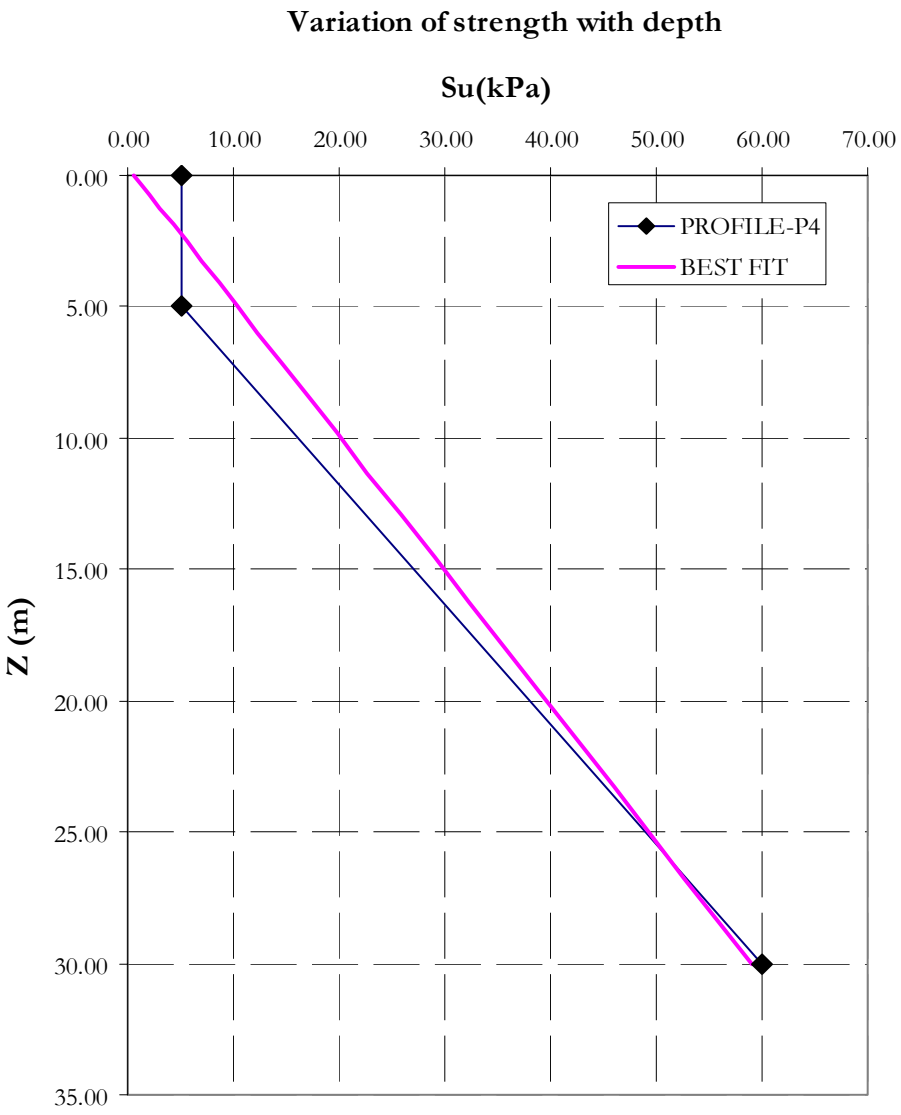

Figure 5.22 Best fit strength profile for caisson with L/D=6

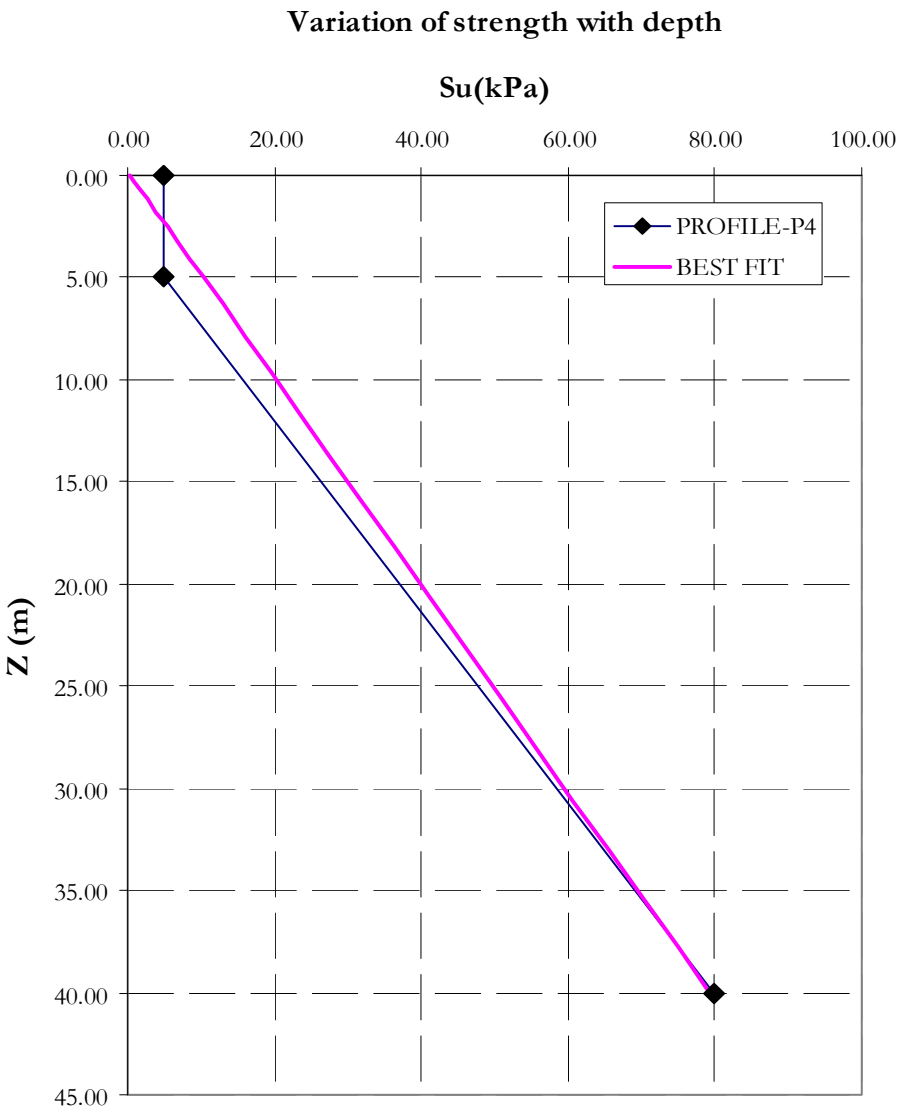

Figure 5.23 Best fit strength profile for caisson with L/D=8

5.13 ACCURACY OF FINITE ELEMENT SOLUTION

In order to determine the accuracy of the accuracy of the finite element solutions, the ultimate lateral load computed by the finite element method for the uniform soil profile P1 (Table 3.1) was compared with the exact solution published by Randolph and Houlsby (1984). The exact solution for the infinitely long caisson is N_H =11.94. Compared to the value of N_H =11.94 for the infinitely long caisson, the ultimate normalized lateral resistance for a caisson with aspect ratio of L/D=8 for the uniform soil profile P1 was found to be N_H =11.58. This value also compares favorably with limiting value of N_p=12 (Murff and Hamilton, 1993).

5.14 NORMALIZED LOAD INTERACTION CURVES

The optimum load interaction curves (APPENDIX B) for the no rotation case are plotted for caisson aspect ratios of 2, 4, 6 and 8. The curves are plotted for the load angles 0, 15, 30, 45, 60 and 90 degrees. Normalized plots were generated for the full adhesion case (α=1) and the reduced adhesion case (α=0.65). These normalized plots present a convenient way of estimating the capacity of the suction caissons. Appropriate N_H and N_V for a particular load angle can be obtained from the curve and these values can then be multiplied with the actual caisson dimensions (length and diameter) and an average shear strength value to obtain the ultimate capacity. Normalized load interaction curves are presented at the end of this chapter.

5.15 EFFECT OF LOAD INCLINATION

The predictions indicate that the load capacity interaction effects occur primarily between inclination angles of 15 and 60 degrees for the shorter caisson (L/D=2) where as for the intermediate and the longer caissons (L/D=4, 6 and 8) the interaction effect is observed between inclination angles of 15 and 30.Figure 5.24 shows a typical interaction curve for the shorter caisson.

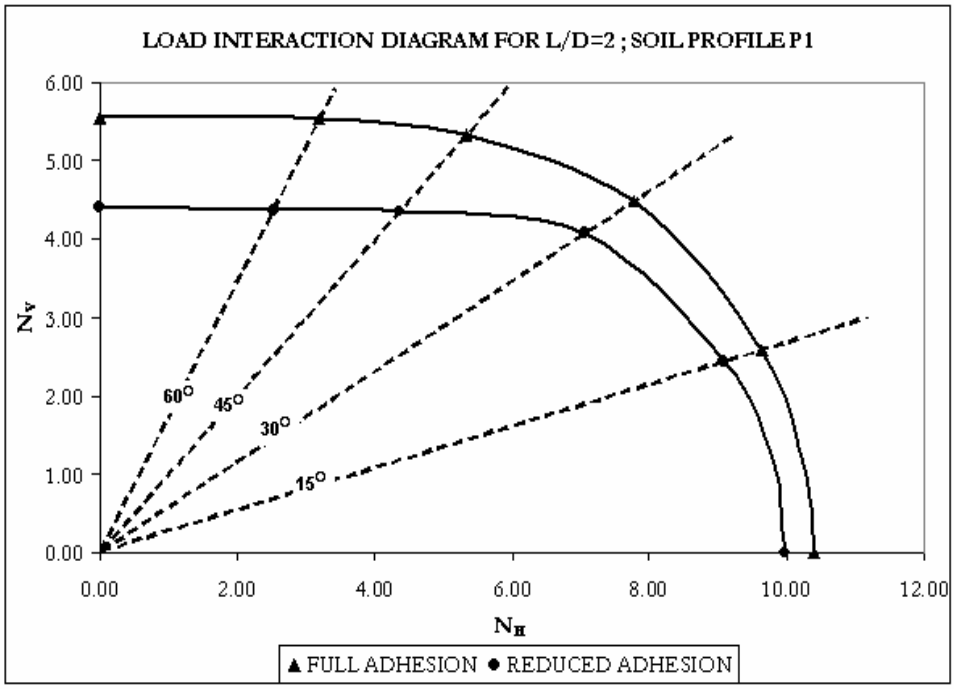

Figure 5.24 Load interaction diagram for L/D=2; soil profile P1

Thus for the shorter caisson (L/D=2), for load inclination angles less than 15 degrees, the horizontal capacity is essentially unaffected by the vertical load components, and for inclination angles greater than 60 degrees the vertical load capacity is unaffected by the horizontal load capacity. For the intermediate and the longer

caissons (L/D=4, 6 and 8), the horizontal capacity is unaffected by the vertical load component for load inclinations upto 15 degrees and the vertical capacity is unaffected by the vertical load component for load inclinations for inclination angles greater than 30 degrees. Figure 5.25 shows a typical interaction curve for the longer caisson.

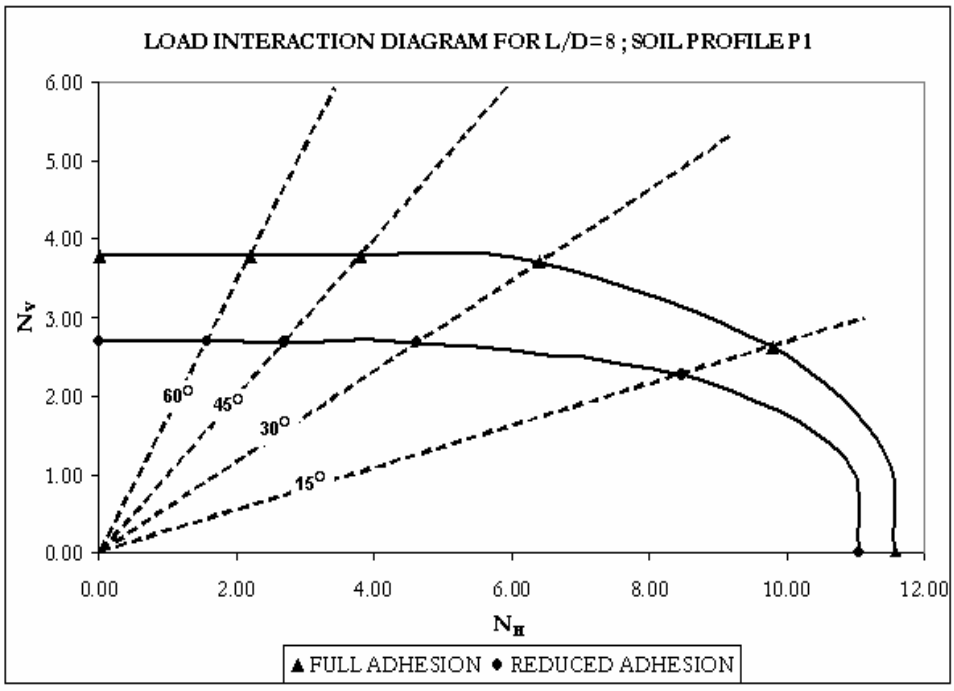

Figure 5.25 Load interaction diagram for L/D=8; soil profile P1

5.16 EFFECT OF LOAD ATTACHMENT POINT

It is observed that for soil profiles P2, P3 and P4 (Table 3.1),the optimal load attachment depth is such that the resultant load intersects the centerline (Li/L) at very close to 0.7 times the caisson length for load inclination angles up to 60 degrees (Appendix C, table C.9 to table C.32). For the uniform soil profiles P1, (Appendix C, Table C.1 to Table C.8) the optimal load attachment depth intersects the centerline at 0.55 times the caisson length. This indicates the point of intersection of the centerline and the resultant load (Li/L) is strongly influenced by the soil profile. This also indicate that the limiting values of (Li/L) for an infinitely long caisson in uniform profile P1 would be 0.5 , and for the normally consolidated profile (P2) the limiting value of (Li/L) would be 0.66. This is because, for the infinitely long caisson, the capacity would be governed by the flow around mechanism. This would give a rectangular distribution of the resisting force on the caisson for P1 profile and a triangular distribution for P2. In order to maintain the no rotation condition for optimum capacity, the load attachment in such a case must be located at the same depth as the centroid of the resisting force.

5.17 EFFECT OF REDUCED ADHESION

The effect of reduced adhesion is computed in term of a non-dimensional number Rf, which is calculated by dividing of ultimate capacity with reduced adhesion case (α=0.65) by the ultimate capacity with full adhesion case (α=1).The effect of reduced adhesion is plotted in Figure 5.26 to Figure 5.29. For all the cases analyzed, it is observed that reduced adhesion effect the vertical capacity more then the horizontal

capacity. It is also observed that in case of the vertical capacity, the reduced adhesion affects the longer caisson more the shorter caisson. For the horizontal capacity, the Rf is around 0.95 for all profile (Table 5.14 to Table 5.17), that is the maximum mobilized horizontal capacity for the reduced adhesion case is 0.95 times the maximum mobilized capacity for full adhesion. For the vertical capacity however, the Rf is depended on the type of profile. For profile P1 (Table 5.14), the Rf value for the vertical capacity varied from 0.8 for the short caisson to 0.71 for the long caisson. For the other three profiles (P2, P3, P4) (Table 5.15 to Table 5.17), the Rf value for the vertical capacity varied between 0.84 for the short caisson to 0.74 for the long caisson.

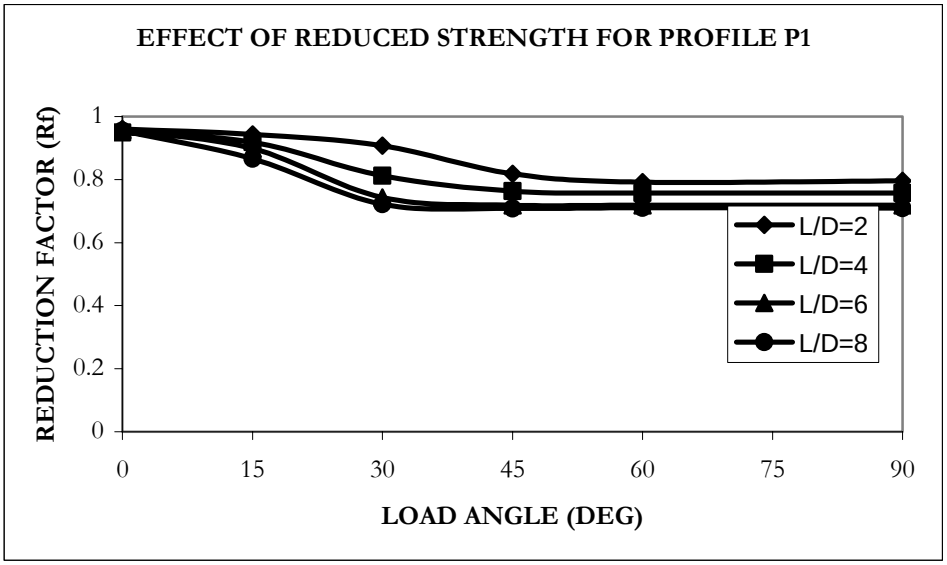

Figure 5.26 Effect of reduced adhesion for profile P1

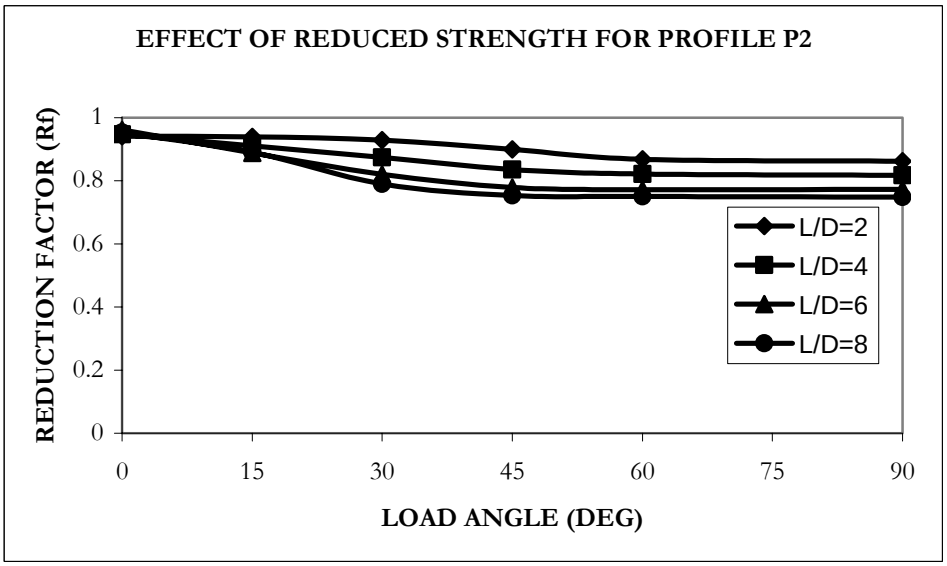

Figure 5.27 Effect of reduced adhesion for profile P2

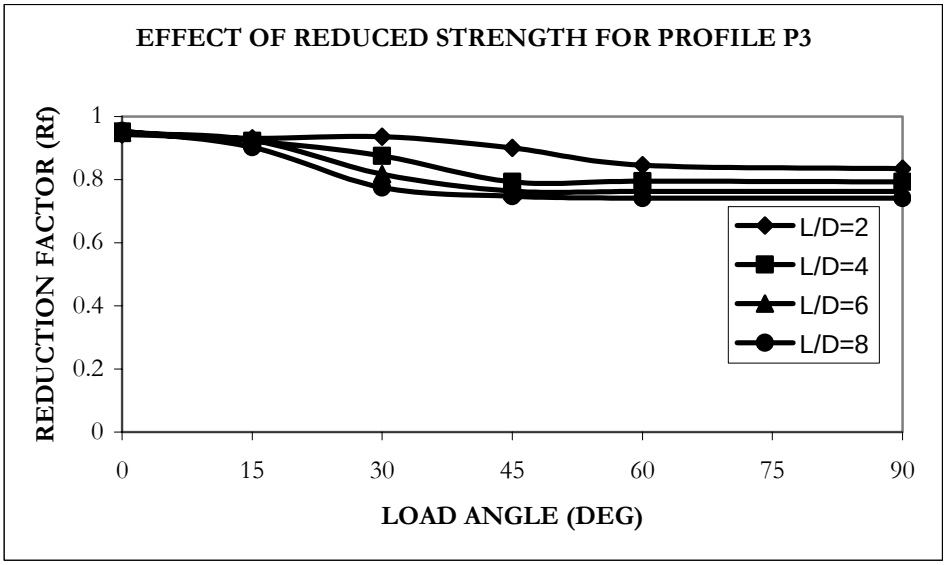

Figure 5.28 Effect of reduced adhesion for profile P3

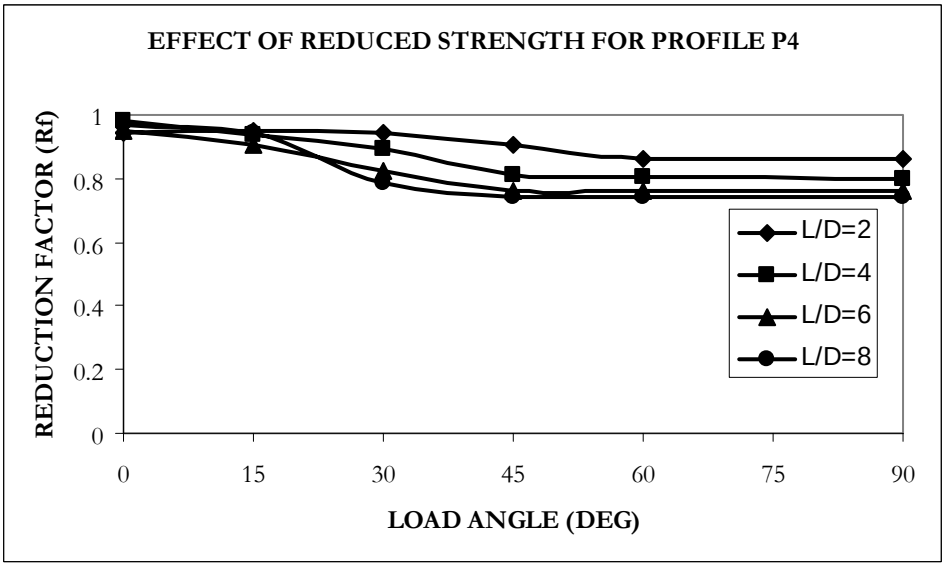

Figure 5.29 Effect of reduced adhesion for profile P1

Table 5.14 Effect of reduced adhesion for profile P1

δ (deg)	L/D=2			L/D=4			L/D=6			L/D=8		
	α=1	α=0.65	Rf	α=1	α=0.65	Rf	α=1	α=0.65	Rf	α=1	α=0.65	Rf
0	5.194E+02	4.988E+02	0.96	1.112E+03	1.055E+03	0.95	1.706E+03	1.634E+03	0.96	2.316E+03	2.212E+03	0.96
15	4.989E+02	4.706E+02	0.94	9.978E+02	9.164E+02	0.92	1.497E+03	1.346E+03	0.90	2.028E+03	1.756E+03	0.87
30	4.489E+02	4.076E+02	0.91	7.963E+02	6.464E+02	0.81	1.151E+03	8.550E+02	0.74	1.481E+03	1.069E+03	0.72
45	3.770E+02	3.086E+02	0.82	6.126E+02	4.674E+02	0.76	8.443E+02	6.063E+02	0.72	1.071E+03	7.585E+02	0.71
60	3.196E+02	2.529E+02	0.79	5.035E+02	3.813E+02	0.76	6.910E+02	4.966E+02	0.72	8.743E+02	6.208E+02	0.71
90	2.775E+02	2.210E+02	0.80	4.372E+02	3.309E+02	0.76	5.984E+02	4.298E+02	0.72	7.578E+02	5.377E+02	0.71

Table 5.15 Effect of reduced adhesion for profile P2

δ (deg)	L/D=2			L/D=4			L/D=6			L/D=8		
	α=1	α=0.65	Rf	α=1	α=0.65	Rf	α=1	α=0.65	Rf	α=1	α=0.65	Rf
0	3.256E+03	3.064E+03	0.94	1.459E+04	1.382E+04	0.95	3.343E+04	3.214E+04	0.96	6.027E+04	5.745E+04	0.95
15	3.323E+03	3.120E+03	0.94	1.380E+04	1.257E+04	0.91	3.013E+04	2.677E+04	0.89	5.263E+04	4.683E+04	0.89
30	3.368E+03	3.129E+03	0.93	1.200E+04	1.049E+04	0.87	2.468E+04	2.024E+04	0.82	4.157E+04	3.285E+04	0.79
45	3.388E+03	3.046E+03	0.90	9.871E+03	8.248E+03	0.84	1.917E+04	1.492E+04	0.78	3.112E+04	2.345E+04	0.75
60	3.105E+03	2.695E+03	0.87	8.277E+03	6.794E+03	0.82	1.579E+04	1.217E+04	0.77	2.553E+04	1.915E+04	0.75
90	2.740E+03	2.362E+03	0.86	7.238E+03	5.916E+03	0.82	1.367E+04	1.056E+04	0.77	2.218E+04	1.659E+04	0.75

Table 5.16 Effect of reduced adhesion for profile P3

δ (deg)	L/D=2			L/D=4			L/D=6			L/D=8		
	α=1	α=0.65	Rf	α=1	α=0.65	Rf	α=1	α=0.65	Rf	α=1	α=0.65	Rf
0	5.984E+03	5.644E+03	0.94	2.058E+04	1.960E+04	0.95	4.288E+04	4.067E+04	0.95	7.229E+04	6.896E+04	0.95
15	6.028E+03	5.613E+03	0.93	1.889E+04	1.742E+04	0.92	3.781E+04	3.496E+04	0.92	6.236E+04	5.629E+04	0.90
30	5.755E+03	5.390E+03	0.94	1.609E+04	1.408E+04	0.88	3.046E+04	2.490E+04	0.82	4.899E+04	3.795E+04	0.77
45	5.221E+03	4.704E+03	0.90	1.317E+04	1.044E+04	0.79	2.351E+04	1.795E+04	0.76	3.642E+04	2.723E+04	0.75
60	4.713E+03	3.986E+03	0.85	1.079E+04	8.579E+03	0.79	1.922E+04	1.465E+04	0.76	2.995E+04	2.221E+04	0.74
90	4.158E+03	3.472E+03	0.84	9.384E+03	7.442E+03	0.79	1.664E+04	1.268E+04	0.76	2.596E+04	1.924E+04	0.74

Table 5.17 Effect of reduced adhesion for profile P4

δ (deg)	L/D=2			L/D=4			L/D=6			L/D=8		
	α=1	α=0.65	Rf	α=1	α=0.65	Rf	α=1	α=0.65	Rf	α=1	α=0.65	Rf
0	6.720E+03	6.338E+03	0.94	2.409E+04	2.356E+04	0.98	5.309E+04	5.047E+04	0.95	9.186E+04	8.916E+04	0.97
15	6.653E+03	6.313E+03	0.95	2.296E+04	2.153E+04	0.94	4.869E+04	4.420E+04	0.91	8.383E+04	7.920E+04	0.94
30	6.413E+03	6.053E+03	0.94	2.002E+04	1.789E+04	0.89	4.041E+04	3.323E+04	0.82	6.729E+04	5.296E+04	0.79
45	6.005E+03	5.448E+03	0.91	1.650E+04	1.341E+04	0.81	3.168E+04	2.405E+04	0.76	5.059E+04	3.751E+04	0.74
60	5.408E+03	4.646E+03	0.86	1.372E+04	1.103E+04	0.80	2.589E+04	1.969E+04	0.76	4.136E+04	3.068E+04	0.74
90	4.690E+03	4.044E+03	0.86	1.192E+04	9.549E+03	0.80	2.241E+04	1.706E+04	0.76	3.583E+04	2.654E+04	0.74

CHAPTER VI

CONCLUSIONS AND RECOMMENDATIONS

The 3D finite element analyses provided valuable results for estimating the undrained capacity of suction caissons in typical normally and lightly overconsolidated soil profiles seen in the Gulf of Mexico and the North Sea. The study also provided an excellent check of independent finite element studies conducted by three different groups. The finite element studies provided a means for checking the results of simplified capacity prediction methods. Based on the study, several important conclusions were reached which are outlined in this chapter. The finite element study did not account for all the factors, which may affect the capacity of suction anchors. Several of these factors needs to be investigated in future studies, details of which are presented at the final section of this chapter.

6.1 CONCLUSIONS

Study of actual soil profiles (Chapter III) has shown that a great deal of scatter is associated with the measured shear strength values. In order to establish the design strength profile, the undrained shear strength need to be correctly estimated by proper interpretation of in situ and laboratory test data. The actual undrained strength then needs to be adjusted by assessing the uncertainties and risks the associated with the project in order to establish the design strength profile. Establishing the design soil profile is the key to designing reliable suction anchors.

The load attachment point strongly determines the failure mechanism (rotation or translation mode) of the caisson. The ultimate capacity that is mobilized depends very strongly on the mode of failure. The study has shown that the point of intersection of the centerline and the resultant load (Li/L) is strongly influenced by the soil profile. Theoretically, it is possible to compute the exact location of the optimal attachment point. However, it must be realized that the actual soil profile will always be different from the design soil profile, which in turn shall affect the location of the optimum attachment point. Therefore, the design capacity of the caisson needs to be suitably adjusted to account for possible reduction in capacity due to the rotational failure mode.

The finite element predictions have shown that the load interaction effect is maximum for load angles between 15 and 60 degrees for the shorter caisson (L/D=2) where as for the intermediate and the longer caissons (L/D=4, 6 and 8) the interaction effect is observed between inclination angles of 15 and 30 degrees. This load interaction effect may strongly affect the factor of safety, which is shown graphically by the double-headed arrow in figure 6.1. For point “B”, the factor of safety is much lower in the vertical direction even though the resultant magnitudes of the loads are the same for both points “A” and “B”. The angle of loading is dependent on the mooring system as explained in Chapter I. Design should take into account the uncertainty in the angle and its effects.

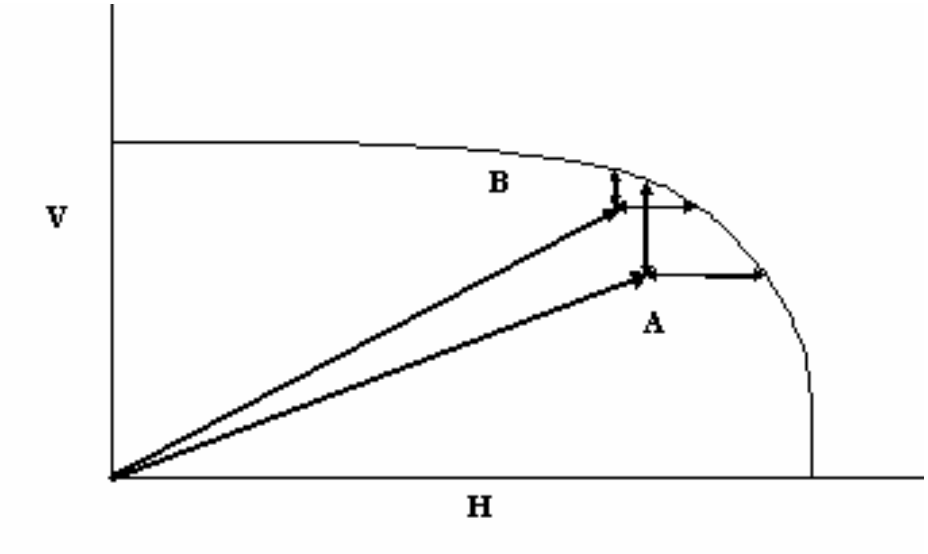

Figure 6.1 Variation of factor of safety with angle of loading

The remolding and reconsolidation of the soil during the caisson installation also affects the capacity of the caisson. This effect is more predominant on the vertical capacity than the horizontal capacity. The effect of reduced adhesion would be most crucial when the mooring line capacity is dominated by vertical capacity as maximum reduction occurs at this point. The post set-up strength on the outside skirt wall was specified as 0.65 times the shear strength in this study. This value need to be estimated as accurately as possible when designing anchors for vertically moored structures such as TLPs.

6.2 RECOMMENDATIONS

Potential for crack at the active side. In this study, the primary assumption was undrained loading condition with no gap forming on the active side of the caisson.

However, in shallow water depths, and for overconsolidated clays the formation of a gap on the active side is a very real possibility when the anchor is subjected to a long duration monotonic loading. Studies need to be conducted to prediction of formation of gap on the active side in order to better understand the problem

Effect of cyclic loading. Moored structures are subjected to severe environmental cyclic loading which in turn is transmitted to the anchors. The effect of cyclic loading needs to be investigated.

Set-up. The effect of installation and setup should be investigated. It may be necessary to model the entire installation process. This will be computationally very intensive as adaptive refining of the mesh will be required because of the penetration process is a large strain, large displacement process. Limited studies in this area were performed by Maniar and Tassoulas (2003).

REFERENCES

Aubeny, C.P., Murff, J.D., and Roesset, J.M. (2001a). "Geotechnical issues in deep and ultra deep waters." *International Journal of Geomechanics.*, 1(2), 225-247.

Aubeny, C.P., Moon, S.K., and Murff, J.D. (2001b). "Lateral undrained resistance of suction caisson anchors." *International Journal of Offshore and Polar Engineering.*, 11(2), 95-103.

Aubeny, C.P., Han, S.W., and Murff, J.D. (2003a). "Inclined load capacity of suction caissons." *International Journal for Numerical and Analytical Methods in Geomechanics.*, 27(14), 1235-1254.

Aubeny, C.P., Han, S.W., and Murff, J.D. (2003b). "Refined model for inclined load capacity of suction caissons." *22nd International Conference on Offshore Mechanics and Arctic Engineering*, Cancun.

Boresi, A.P., and Schmidt, R.J. (2002). *Advanced Mechanics of Material*, John Wiley & Sons, Inc., New York.

Bradshaw, A. S., Silva, A. J., and Bryant, W. R. (2000). "Stress-strain and strength behavior of marine clays from continental slope, Gulf of Mexico." *Engineering Mechanics Divisions, American Society of Civil Engineering (EMD 2000) Conference*, Austin, TX.

Bransby, M.F., and Randolph, M.F. (1998). "Combined loading of skirted foundations." *Geotechnique.*, 48(5), 637-655.

Broms, B.B. (1964). "Lateral resistance of piles in cohesive soil." *J.Soil Mech. and Found.Div., ASCE*, 90(2), 27-63.

Chen, W.F. (1975). *Limit Analysis and Soil Plasticity*, Elsevier Scientific Publishing Co., New York.

Chen, W.F., and Han, D.J. (1988). *Plasticity for Structural Engineers,* Springer Verlag, New York.

Clukey, E.C., and Phillips, R. (2002). "Centrifuge model tests to verify suction caisson capacities for taut and semi-taut legged mooring systems." *Deep Offshore Technology Conference for Deep Water Oil Exploration and Drilling,* New Orleans, Louisiana.

COFS (2001). "Installation and pull-out capacity of stiffened suction caissons in cohesive sediments." *COFS Internal Research Report*, Centre for Offshore Foundation Systems, Crawly, Western Australia.

Colliat, J.L., Boisard, P., Anderson, K., and Schroeder, K. (1995). "Caisson foundations as alternative anchors for permanent mooring of a process barge offshore Congo." *Offshore Tech., Conf., OTC* 7797, Houston, TX.

Cook, R. D. (1995). *Finite Element Modeling for Stress - Solutions Manual for the Analytical Problems*, John Wiley and Sons, New York.

Desai, C.S., and Siriwarddane, H.J. (1984). *Constitutive Laws for Engineering Materials with Emphasis on Geologic Materials,* Prentice- Hall, New Jersey.

Drucker, D.C., and Prager, W. (1952). "Soil mechanics and plastic analysis or limit design." *Quarterly of Appl. Math.*, 10(2), 157-165.

Gilbert, R.B., and Murff, J.D. (2001a). "Design Methodologies and Criteria for Suction Caissons for Deepwater Mooring Applications." *Workshop Report,* Offshore Technology Research Center, College Station,Texas.

Gilbert, R.B., and Murff, J.D. (2001b). "Identifying uncertainties in the design of suction caisson foundations." *Proc. OTRC 2001 International Conference Honoring Professor Wayne.A.Dunlap,* Houston, 231-242.

Hamilton, J. M., Phillips, R., Dunnavant, T.W., and Murff, J.D. (1991). "Centrifuge study of laterally loaded pile behavior in clay." *Proc., Int. Conf. Centrifuge 1991, ISSMFE,* Boulder, Colorado, 285-292.

Han, S.W. (2002). *The Capacity of Suction Caisson in Isotropic and Anisotropic Cohesive Soils under General Loading Conditions*, Dissertation, Dept. of Civil Eng., Texas A&M University, College Station, Texas.

Holtz, R.D., and Kovacs, W.D. (1981). *An Introduction to Geotechnical Engineering*, Prentice-Hall, Inc., Englewood Cliffs, New Jersey.

HKS. (2000). *ABAQUS Version 6.3 User's Manuals,* Hibbitt, Karlson and Sorensen Inc., Providence, Rhode Island.

Lacasse, S., and Lunne, T. (1979). "In situ testing program in Norwegian clays-Description of proposed test sites." *NGI, Internal Report* 52155-9, Oslo, Norway.

Lunne, T., Christoffersen, H. P., and Tjelta, T. I. (1985). "Engineering use of piezocone data in North Sea clays." *11th International Conference of Soil Mechanics and Foundation Engineering*, 2, 907-912.

Maniar, D.R., and Tassoulas, J.R. (2003). "Simulation of suction caisson behavior during and after installation in normally consolidated soil." *16th ASCE Engineering Mechanics Conference*, University of Washington, Seattle.

Matlock, H. (1970). "Correlations for design of laterally loaded piles in soft clay." *Proc. 2nd Offshore Tech.Conf.*, Houston, TX, 1,577-594.

MMS. (2000). *Deepwater Gulf of Mexico: America's Emerging Frontier,* Minerals Management Service, New Orleans, Louisiana.

Moon, S.K. (2000). *Lateral Resistance of Suction Caisson Anchors*, M. Eng. Report, Dept. of Civil Eng., Texas A&M University, College Station, Texas.

Murff, J.D. (1980). "Vane shear testing of anisotropic, cohesive soils." *International Journal for Numerical and Analytical Methods in Geomechanics.*, 4, 285-289.

Murff, J.D. (2002). *Theoretical Soil Mechanics Class Notes*, Department of Civil Engineering, Texas A&M University, College Station, Texas.

Murff, J.D., and Hamilton, J.M. (1993). "P-Ultimate for undrained analysis of laterally loaded piles." *ASCE Journal of Geotechnical Engineering*., 119(1), 91-107.

NGI (2003). "Deepwater anchor design practice phase II report to American Petroleum Institute." *Norwegian Geotechnical Institute*, Oslo, Norway.

Pavlicek, R.W. (1992). "Axial tensile load capacity of suction piles." Report 1/93-B40100, *Offshore Technology Research Center*, Austin,TX.

Prager, W. (1959). *An Introduction to Theory of Plasticity*, Addison Wesley, Reading, Massachusetts.

Randolph, M.F., and Houlsby, G.T. (1984). "The limiting pressure on a circular pile loaded laterally in cohesive soil." *Geotechnique.*, 34(4) 613-623.

Randolph, M.F., O'Neill, M.P., Stewart, D.P., and Erbrich, E. (1998). "Performance of suction anchors in fine-grained calcareous soils." *Proc. Offshore Tech. Conf., Paper No*.8831, 521-529.

Reese, L.C., Cox, W.R., and Koop, R.D. (1975). "Field testing and analysis of laterally loaded piles in stiff clay." *Proc., 7th Offshore Tech. Conf.*, Houston, TX, 2, 473-483.

Sukumaran, B., and McCarron, W.O. (1999). "Total and effective stress analysis of suction caisson for Gulf of Mexico conditions." *OTRC 99 International Conference on Analysis, Design, Construction, and Testing of Deep Foundations*, Austin, TX, 247-260.

Sukumaran, B., and McCarron, W.O., Jeanjean, P., and Abouseeda, H. (1999). “Efficient finite element techniques for limit analysis of suction caissons under lateral loads.” *Computers and Geotechnics.*, 24(2), 89-108.

Vryhof Anchors. (2000). *Vryhof Anchor Manual,* Vryhof Anchors bv, The Netherlands.

APPENDIX A

LIST OF SYMBOLS

α = Reduction factor in strength due to remolding

δ = Inclination of anchor load with respect to horizontal

D= Diameter of caisson

H= Horizontal component of optimum capacity

L= Length of caisson

Li= Distance of the load application point from the rigid body reference point.

N_H= Normalized horizontal capacity

N_V= Normalized vertical capacity.

RM= Reaction moment at rigid body node

S_u = Undrained shear strength of soil.

S_U^{DSS} = Undrained shear strength of soil in direct simple

S_{U_AVG} = Undrained shear strength of soil Shear strength, computed at L/2

V= Vertical component of optimum capacity

z=Distance of the load application point from midline

Z= Distance from midline

APPENDIX B

LOAD INTERACTION CURVES

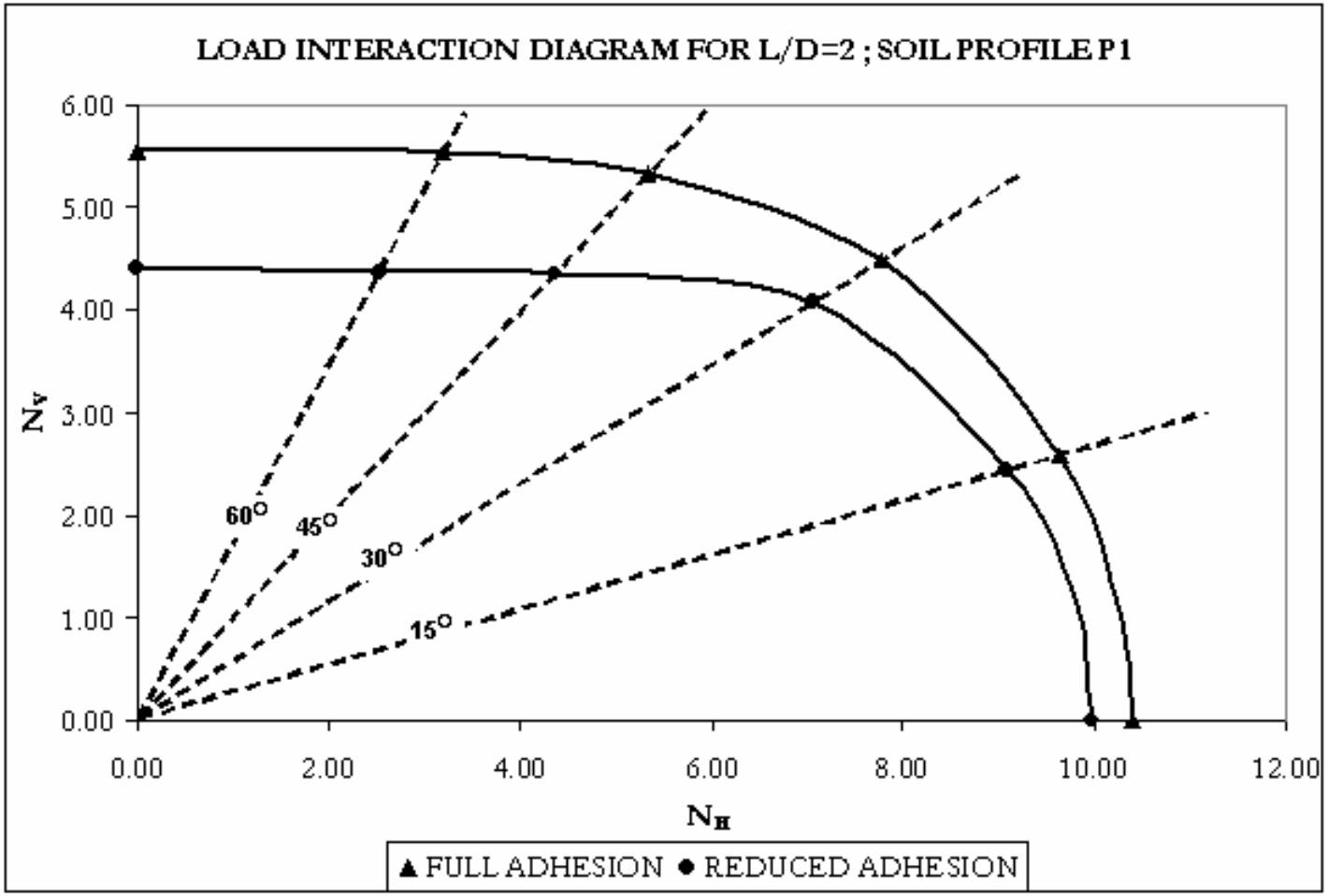

Figure B.1 Load interaction diagram for L/D=2; soil profile P1

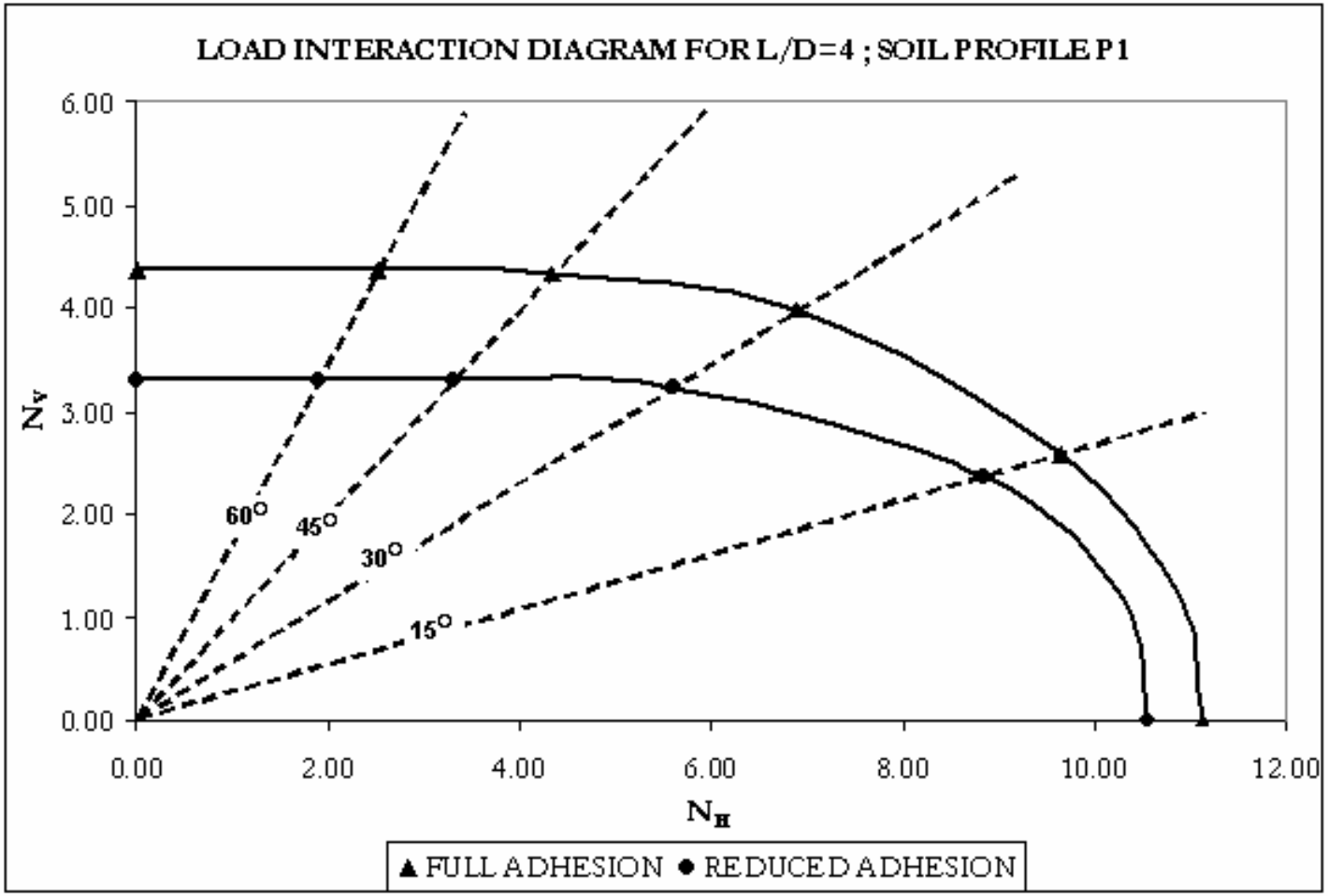

Figure B.2 Load interaction diagram for L/D=4; soil profile P1

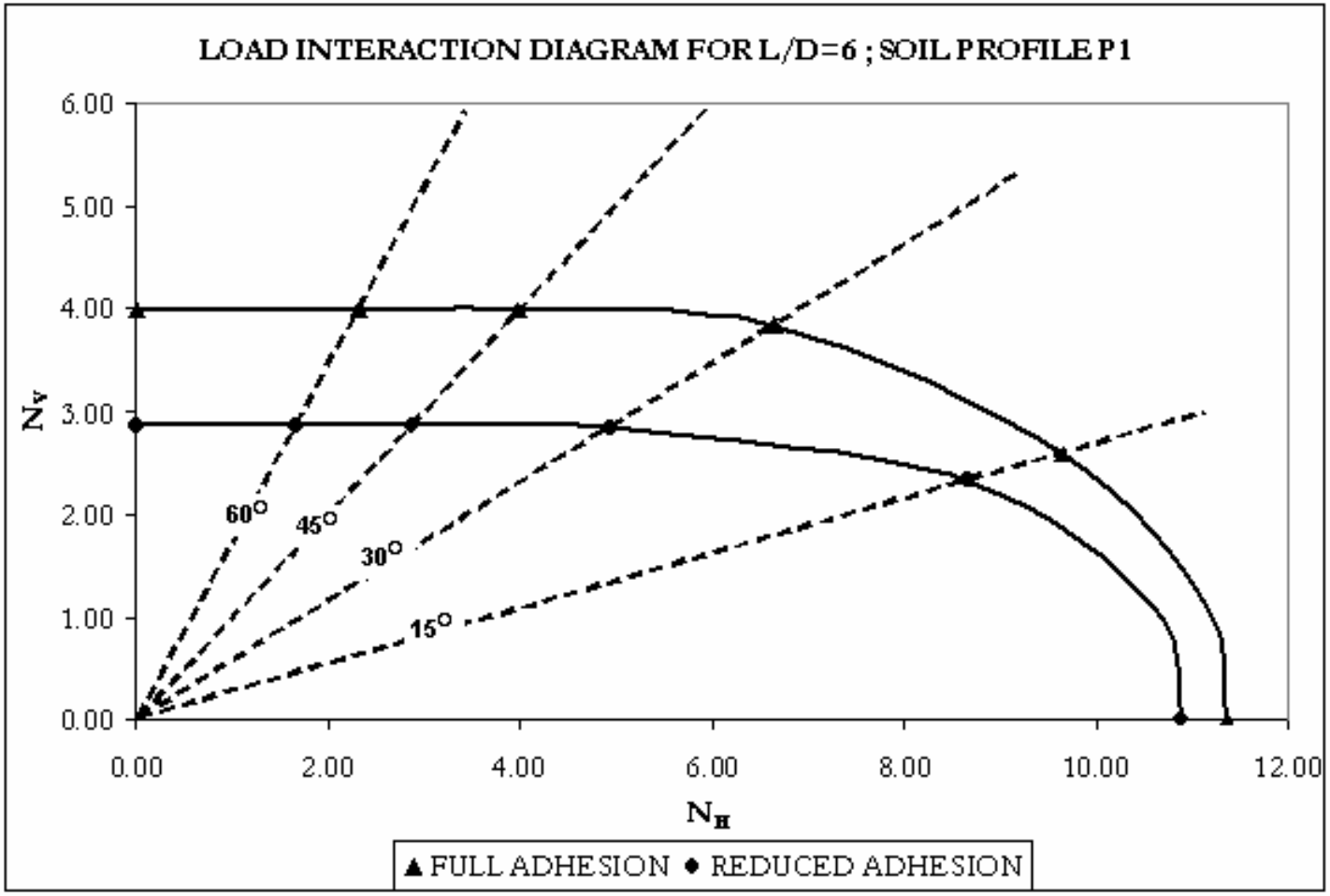

Figure B.3 Load interaction diagram for L/D=6; soil profile P1

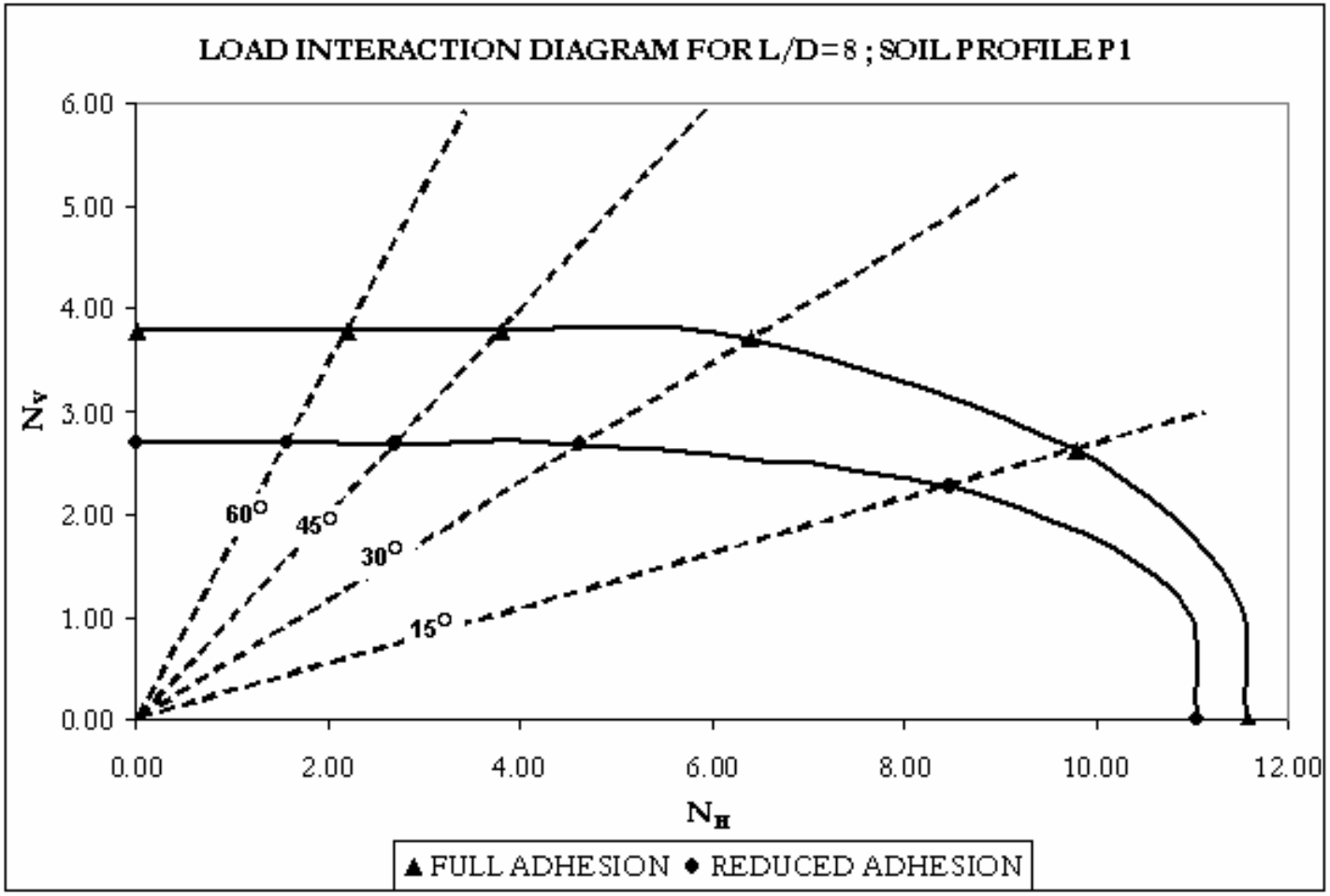

Figure B.4 Load interaction diagram for L/D=8; soil profile P1

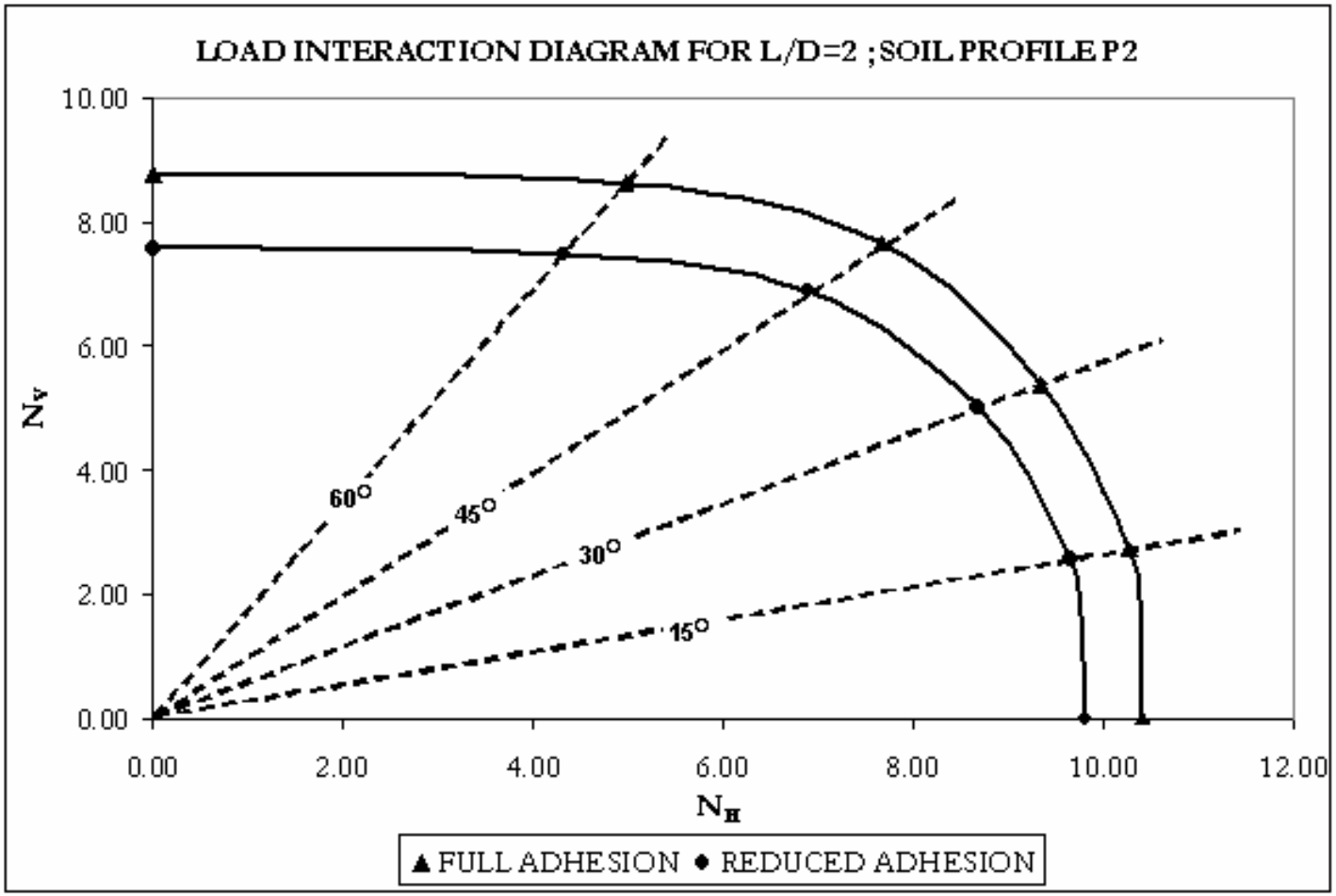

Figure B.5 Load interaction diagram for L/D=2; soil profile P2

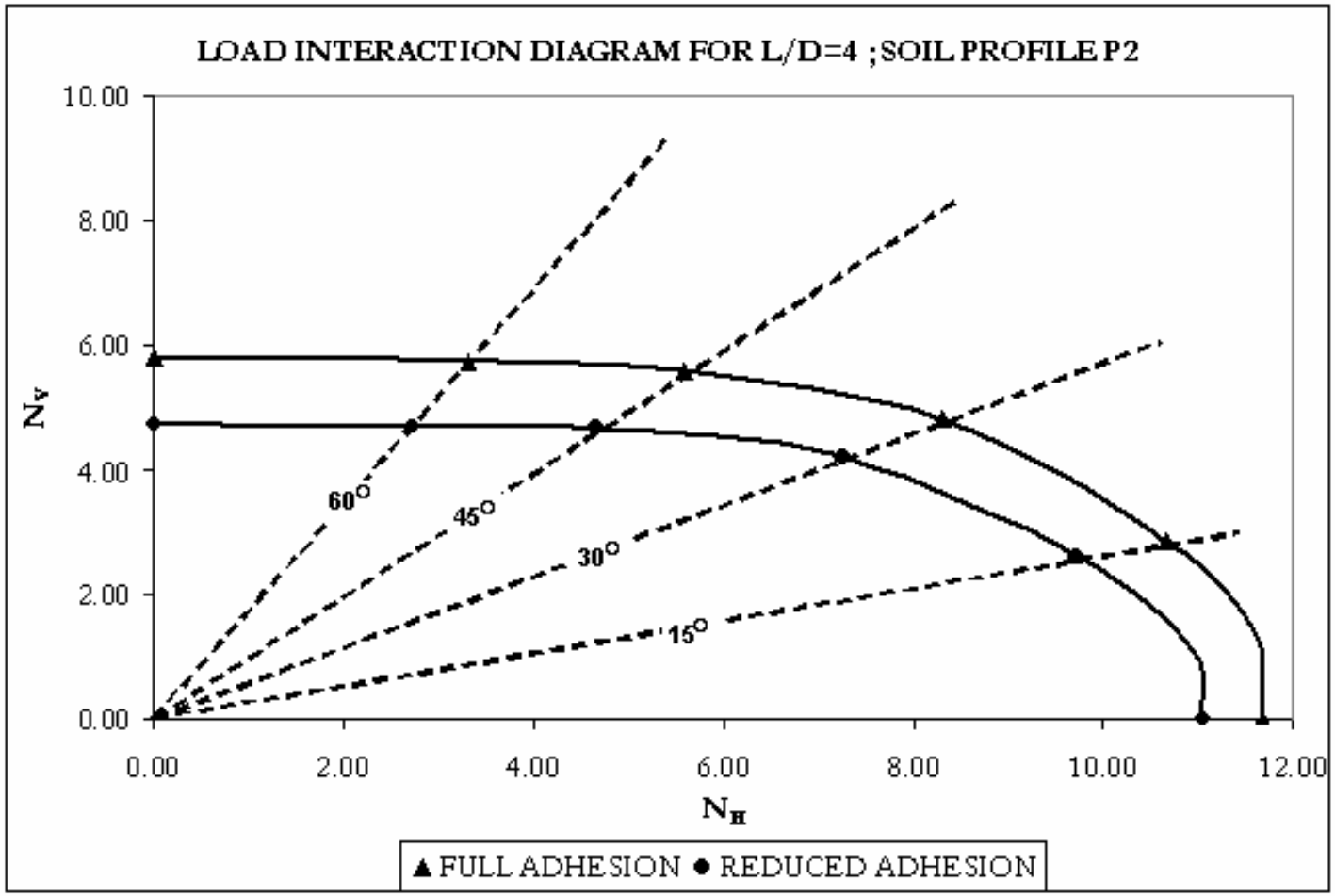

Figure B.6 Load interaction diagram for L/D=4; soil profile P2

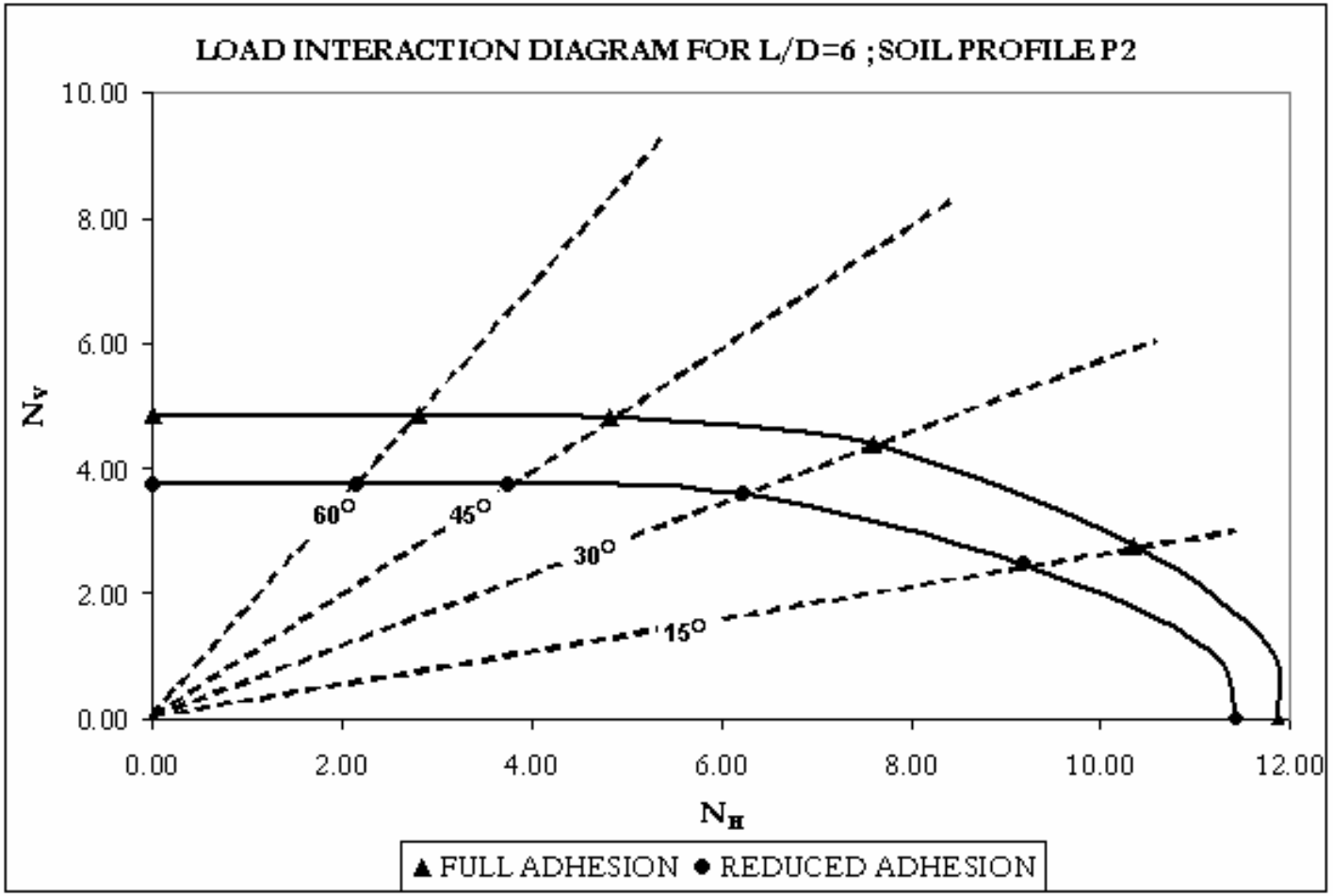

Figure B.7 Load interaction diagram for L/D=6; soil profile P2

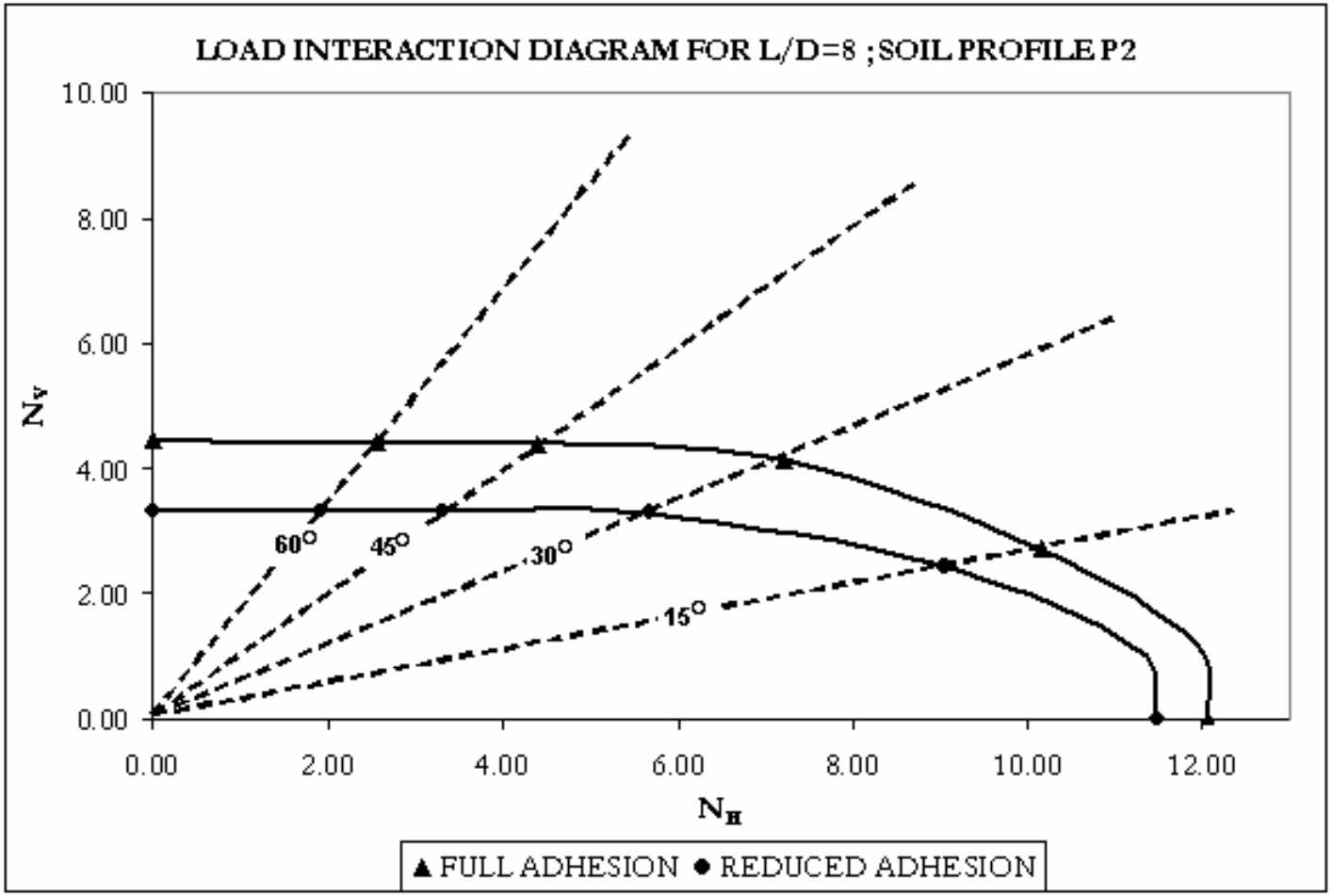

Figure B.8 Load interaction diagram for L/D=8; soil profile P2

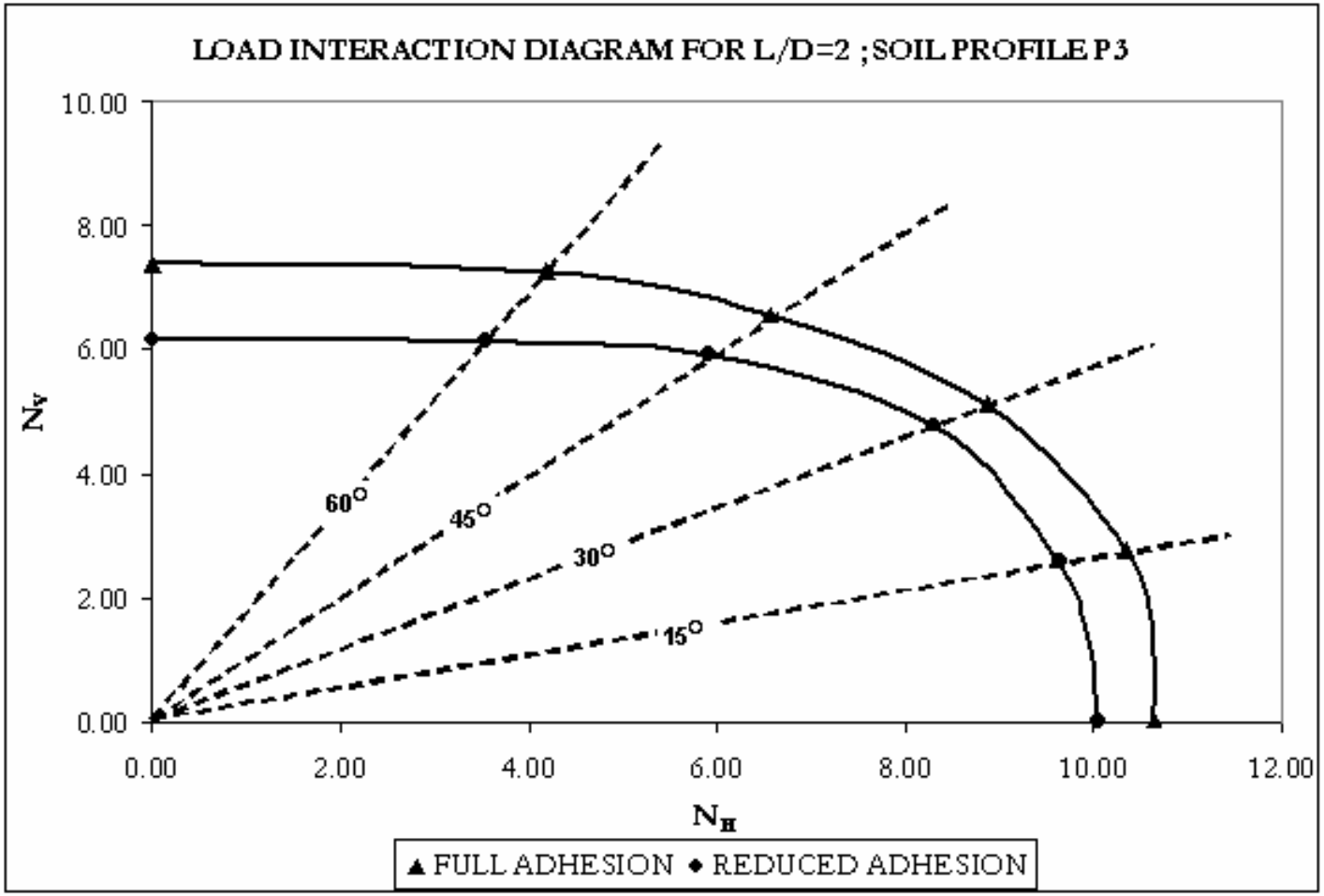

Figure B.9 Load interaction diagram for L/D=2; soil profile P3

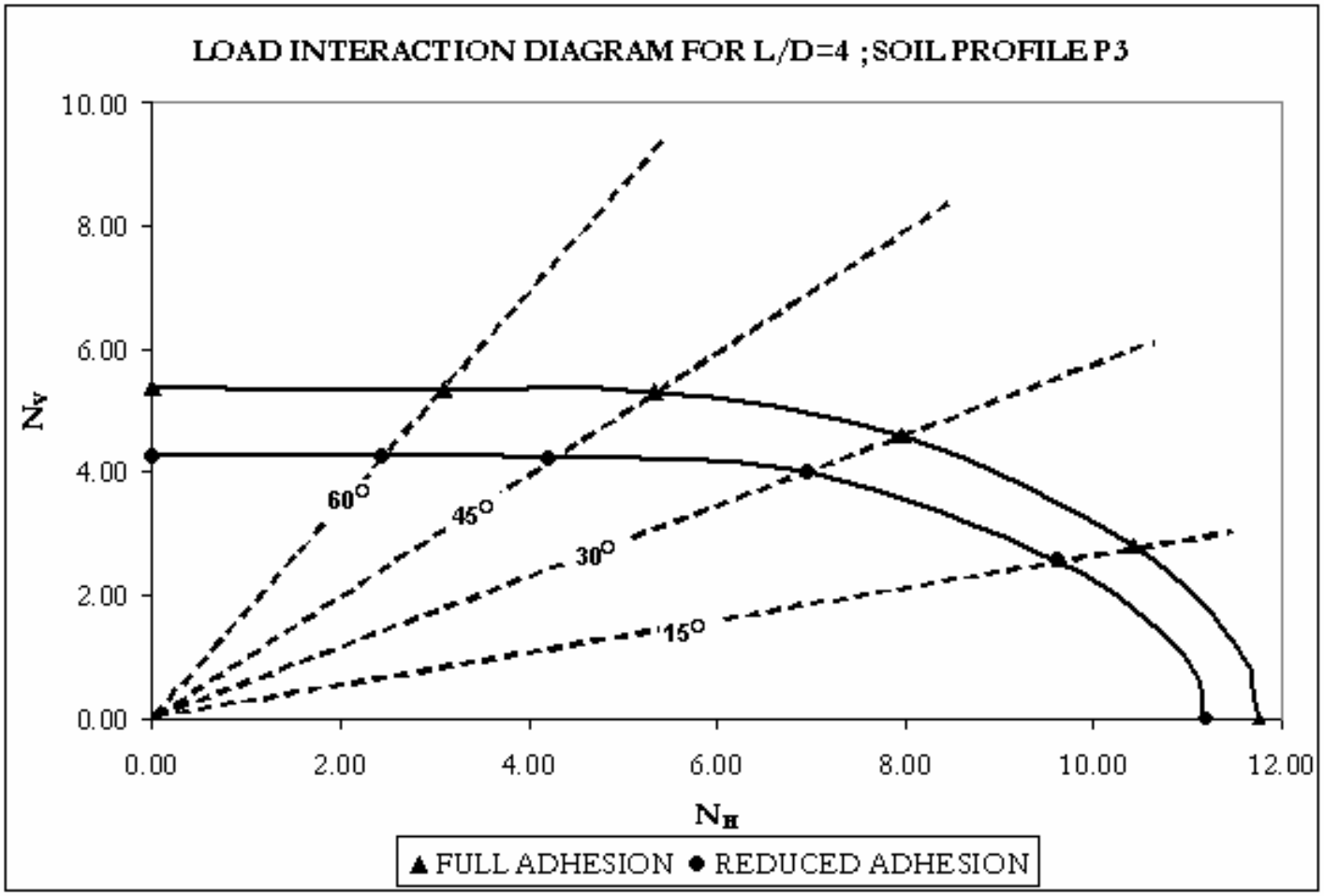

Figure B.10 Load interaction diagram for L/D=4; soil profile P3

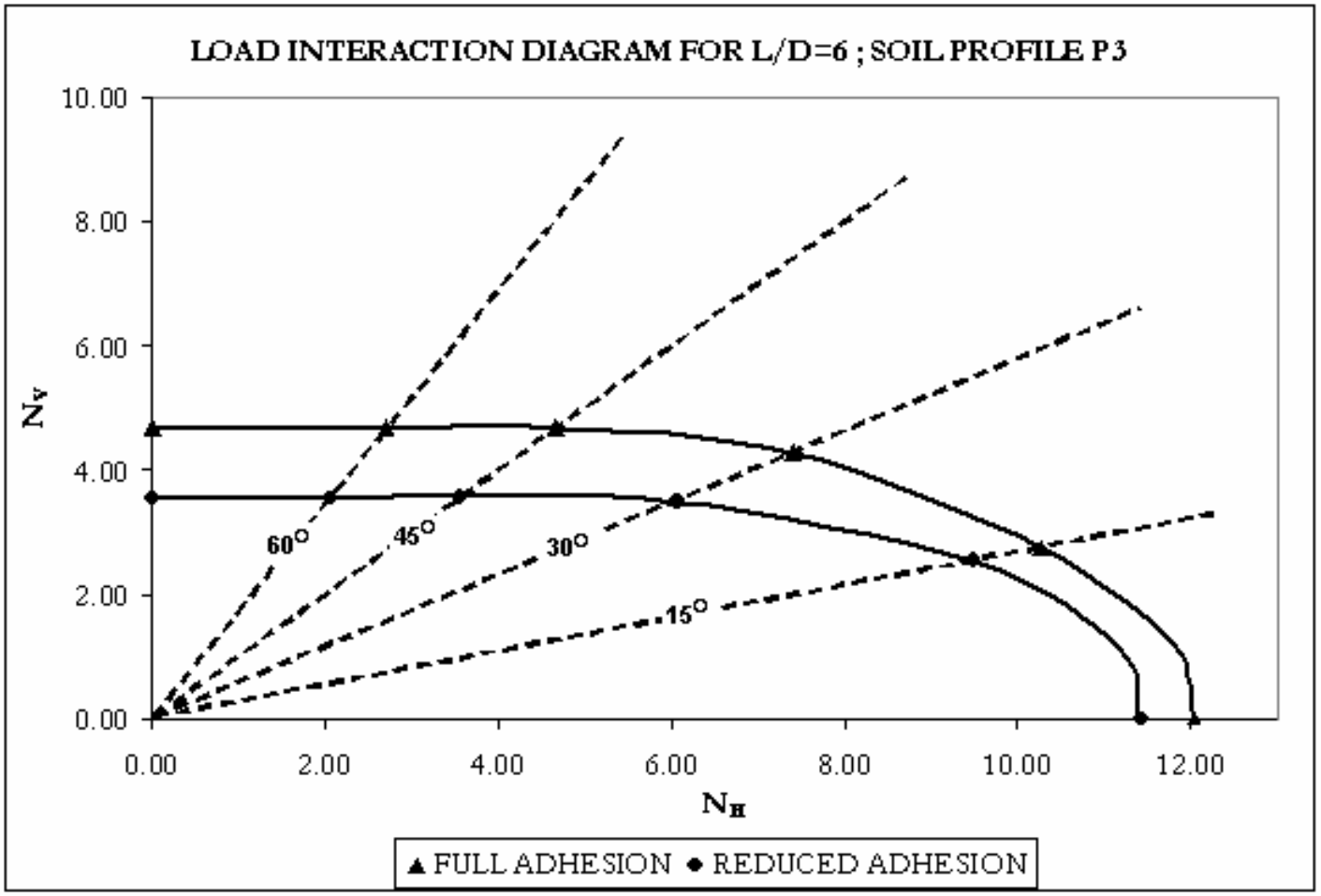

Figure B.11 Load interaction diagram for L/D=6; soil profile P3

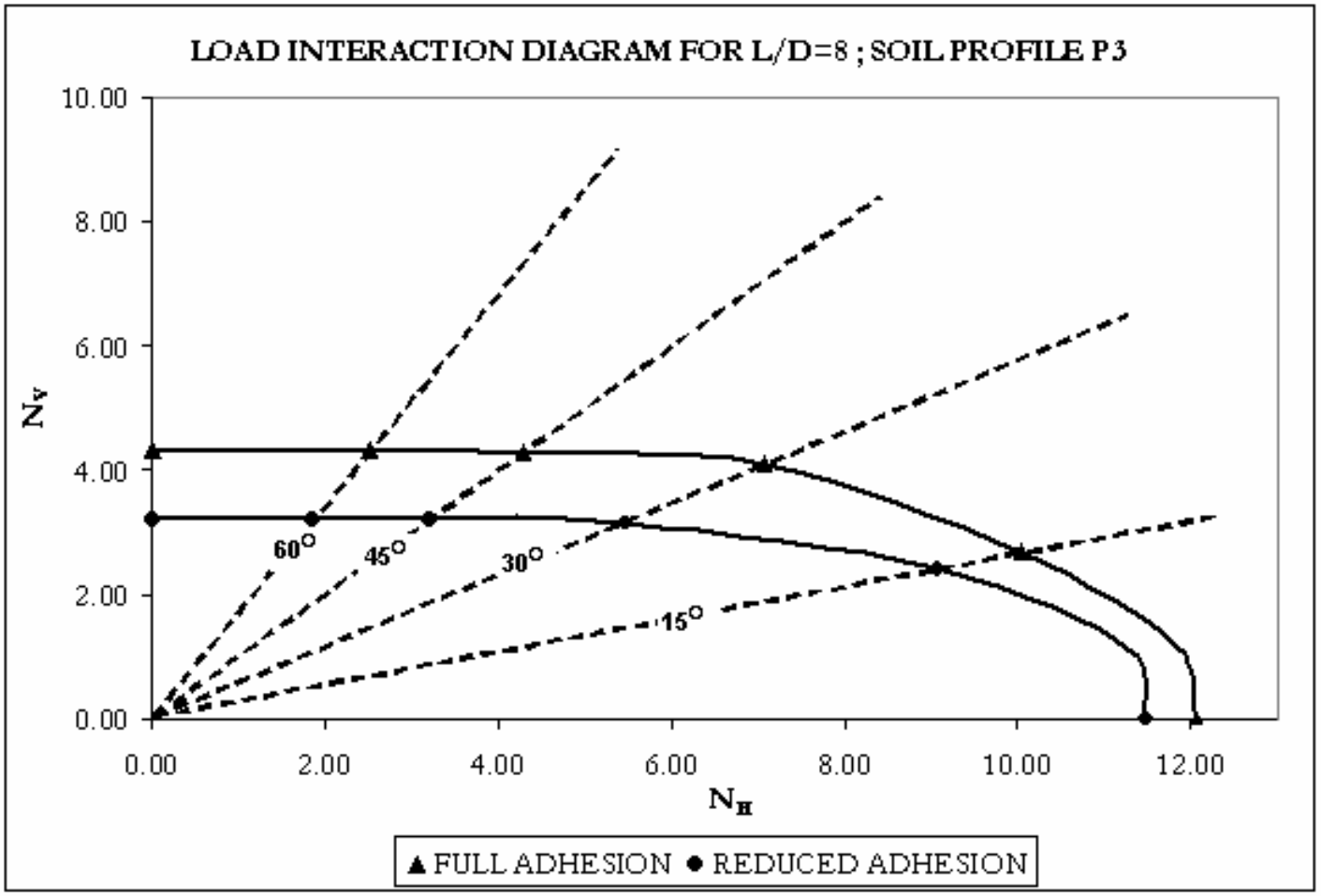

Figure B.12 Load interaction diagram for L/D=8; soil profile P3

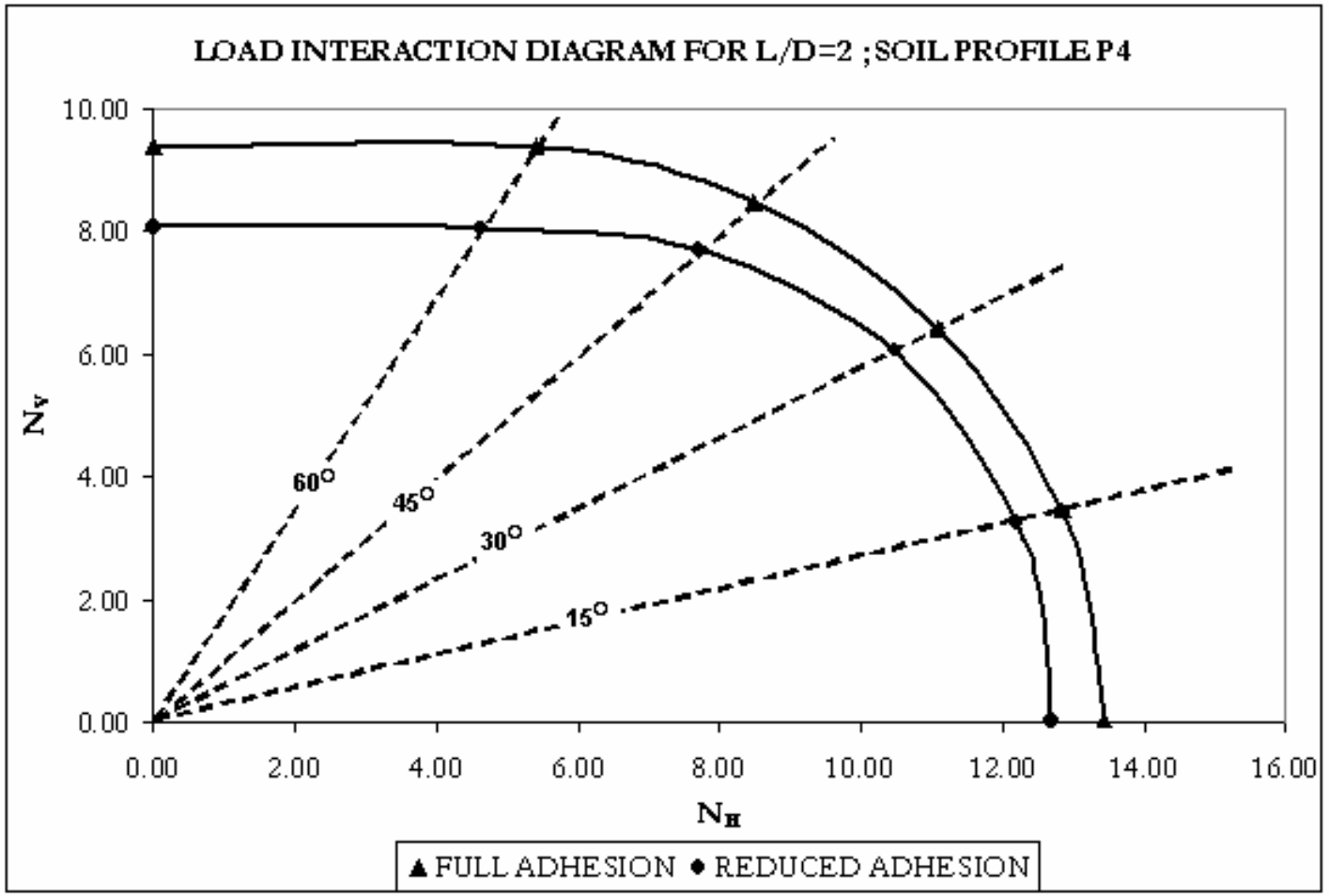

Figure B.13 Load interaction diagram for L/D=2; soil profile P4

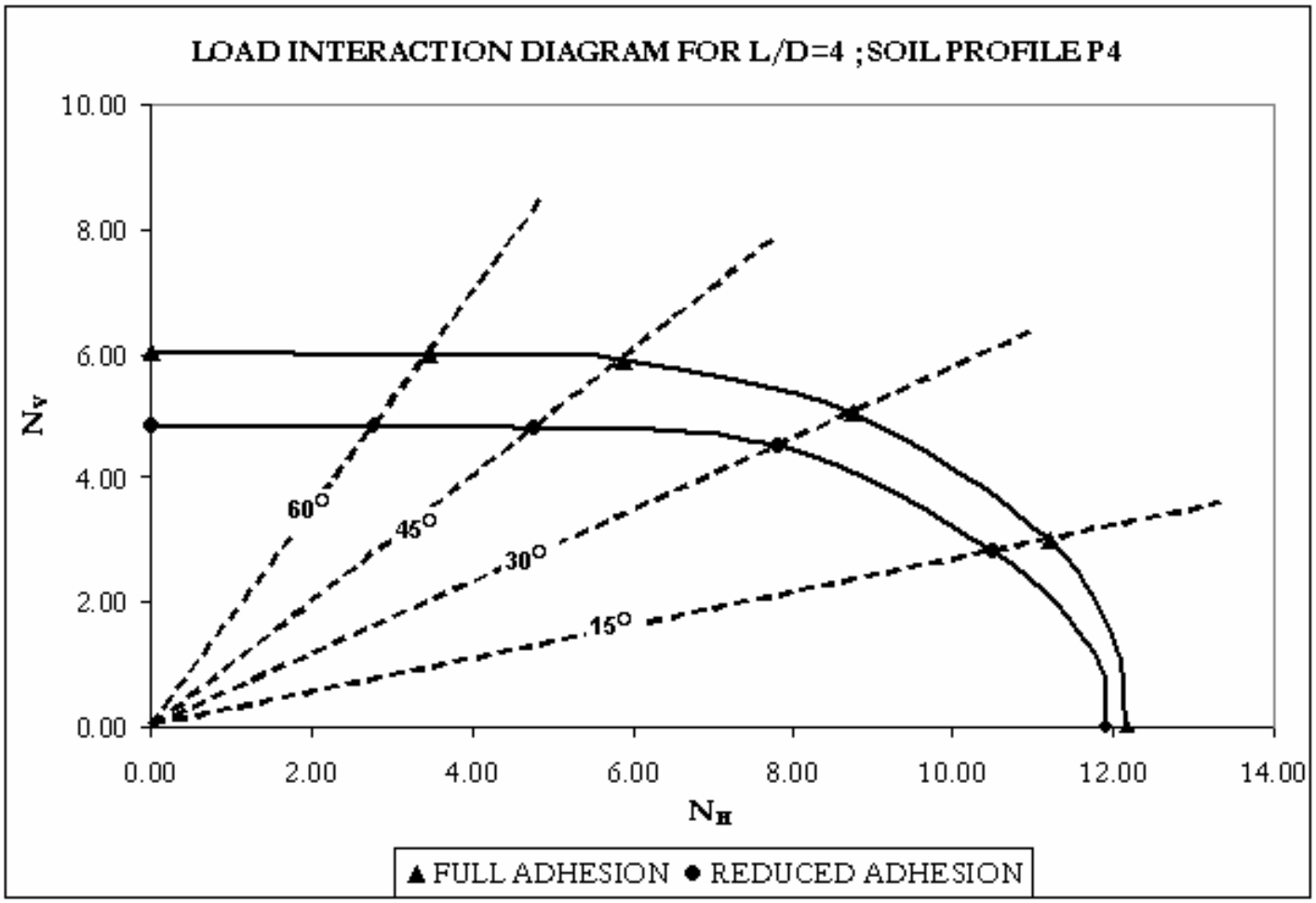

Figure B.14 Load interaction diagram for L/D=4; soil profile P4

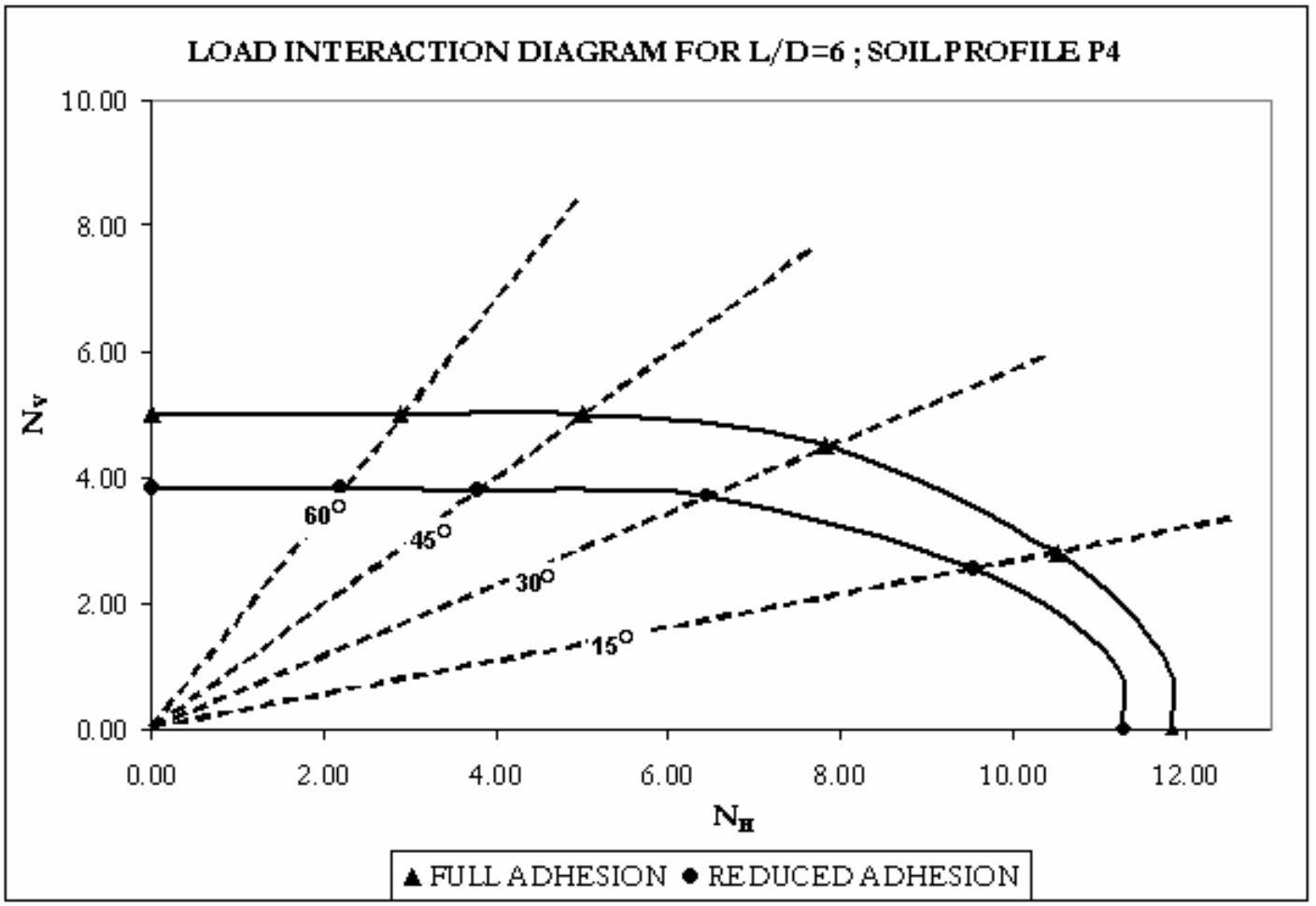

Figure B.15 Load interaction diagram for L/D=6; soil profile P4

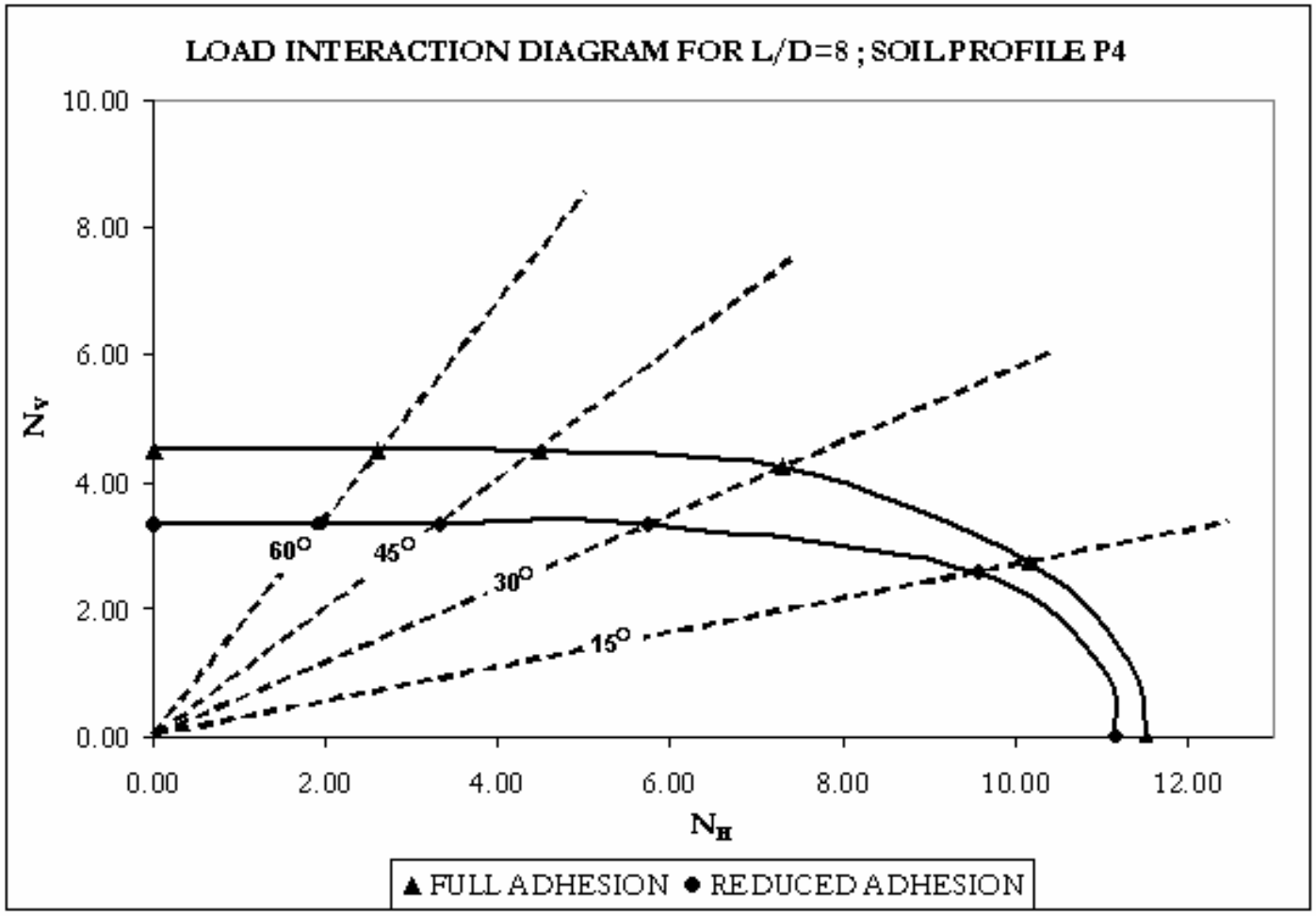

Figure B.16 Load interaction diagram for L/D=8; soil profileP4

APPENDIX C

LOAD INTERACTION TABLES

Table C.1 Ultimate capacity of caisson with L/D=2 in profile P1 with full adhesion

PROFILE	L (m)	D (m)	α	δ (deg)	H (kN)	V (kN)	RM (kN-m)	S_{u_AVG} (kPa)	N_H	N_V	Li/L
P1	10	5	1.00	0	5.194E+02	0.000E+00	2.910E+03	1.00	10.39	0.00	0.56
P1	10	5	1.00	15	4.818E+02	1.292E+02	2.670E+03	1.00	9.64	2.58	0.55
P1	10	5	1.00	30	3.888E+02	2.244E+02	2.182E+03	1.00	7.78	4.49	0.56
P1	10	5	1.00	45	2.666E+02	2.666E+02	1.518E+03	1.00	5.33	5.33	0.57
P1	10	5	1.00	60	1.598E+02	2.768E+02	8.944E+02	1.00	3.20	5.54	0.56
P1	10	5	1.00	90	0.000E+00	2.775E+02	0.000E+00	1.00	0.00	5.55	-NA-

Table C.2 Ultimate capacity of caisson with L/D=2 in profile P1 with reduced adhesion

PROFILE	L (m)	D (m)	α	δ (deg)	H (kN)	V (kN)	RM (kN-m)	$S_{u\ AVG}$ (kPa)	N_H	N_V	Li/L
P1	10	5	0.65	0	4.988E+02	0.000E+00	2.864E+03	1.00	9.98	0.00	0.57
P1	10	5	0.65	15	4.546E+02	1.218E+02	2.570E+03	1.00	9.09	2.44	0.57
P1	10	5	0.65	30	3.530E+02	2.038E+02	2.030E+03	1.00	7.06	4.08	0.58
P1	10	5	0.65	45	2.182E+02	2.182E+02	1.209E+03	1.00	4.36	4.36	0.55
P1	10	5	0.65	60	1.264E+02	2.190E+02	7.048E+02	1.00	2.53	4.38	0.56
P1	10	5	0.65	90	0.000E+00	2.210E+02	0.000E+00	1.00	0.00	4.42	-NA-

Table C.3 Ultimate capacity of caisson with L/D=4 in profile P1 with full adhesion

PROFILE	L (m)	D (m)	α	δ (deg)	H (kN)	V (kN)	RM (kN-m)	S_{u_AVG} (kPa)	N_H	N_V	Li/L
P1	20	5	1.00	0	1.112E+03	0.000E+00	1.229E+04	1.00	11.12	0.00	0.55
P1	20	5	1.00	15	9.638E+02	2.582E+02	1.053E+04	1.00	9.64	2.58	0.55
P1	20	5	1.00	30	6.896E+02	3.982E+02	7.598E+03	1.00	6.90	3.98	0.55
P1	20	5	1.00	45	4.332E+02	4.332E+02	4.786E+03	1.00	4.33	4.33	0.55
P1	20	5	1.00	60	2.518E+02	4.360E+02	2.760E+03	1.00	2.52	4.36	0.55
P1	20	5	1.00	90	0.000E+00	4.372E+02	0.000E+00	1.00	0.00	4.37	-NA-

Table C.4 Ultimate capacity of caisson with L/D=4 in profile P1 with reduced adhesion

PROFILE	L (m)	D (m)	α	δ (deg)	H (kN)	V (kN)	RM (kN-m)	$S_{u\ AVG}$ (kPa)	N_H	N_V	Li/L
P1	20	5	0.65	0	1.055E+03	0.000E+00	1.173E+04	1.00	10.55	0.00	0.56
P1	20	5	0.65	15	8.852E+02	2.372E+02	9.742E+03	1.00	8.85	2.37	0.55
P1	20	5	0.65	30	5.598E+02	3.232E+02	6.088E+03	1.00	5.60	3.23	0.54
P1	20	5	0.65	45	3.305E+02	3.305E+02	3.592E+03	1.00	3.30	3.30	0.54
P1	20	5	0.65	60	1.906E+02	3.302E+02	2.093E+03	1.00	1.91	3.30	0.55
P1	20	5	0.65	90	0.000E+00	3.309E+02	0.000E+00	1.00	0.00	3.31	-NA-

Table C.5 Ultimate capacity of caisson with L/D=6 in profile P1 with full adhesion

PROFILE	L (m)	D (m)	α	δ (deg)	H (kN)	V (kN)	RM (kN-m)	S_{u_AVG} (kPa)	N_H	N_V	Li/L
P1	30	5	1.00	0	1.706E+03	0.000E+00	2.774E+04	1.00	11.38	0.00	0.54
P1	30	5	1.00	15	1.446E+03	3.874E+02	2.335E+04	1.00	9.64	2.58	0.54
P1	30	5	1.00	30	9.968E+02	5.756E+02	1.625E+04	1.00	6.65	3.84	0.54
P1	30	5	1.00	45	5.970E+02	5.970E+02	9.730E+03	1.00	3.98	3.98	0.54
P1	30	5	1.00	60	3.455E+02	5.984E+02	5.634E+03	1.00	2.30	3.99	0.54
P1	30	5	1.00	90	0.000E+00	5.984E+02	0.000E+00	1.00	0.00	3.99	-NA-

Table C.6 Ultimate capacity of caisson with L/D=6 in profile P1 with reduced adhesion

PROFILE	L (m)	D (m)	α	δ (deg)	H (kN)	V (kN)	RM (kN-m)	$S_{u\ AVG}$ (kPa)	N_H	N_V	Li/L
P1	30	5	0.65	0	1.634E+03	0.000E+00	2.662E+04	1.00	10.89	0.00	0.54
P1	30	5	0.65	15	1.300E+03	3.482E+02	2.109E+04	1.00	8.67	2.32	0.54
P1	30	5	0.65	30	7.404E+02	4.276E+02	1.193E+04	1.00	4.94	2.85	0.54
P1	30	5	0.65	45	4.287E+02	4.287E+02	6.967E+03	1.00	2.86	2.86	0.54
P1	30	5	0.65	60	2.483E+02	4.301E+02	4.054E+03	1.00	1.66	2.87	0.54
P1	30	5	0.65	90	0.000E+00	4.298E+02	0.000E+00	1.00	0.00	2.87	-NA-

Table C.7 Ultimate capacity of caisson with L/D=8 in profile P1 with full adhesion

PROFILE	L (m)	D (m)	α	δ (deg)	H (kN)	V (kN)	RM (kN-m)	S_{u_AVG} (kPa)	N_H	N_V	Li/L
P1	40	5	1.00	0	2.316E+03	0.000E+00	4.955E+04	1.00	11.58	0.00	0.53
P1	40	5	1.00	15	1.959E+03	5.248E+02	4.179E+04	1.00	9.79	2.62	0.53
P1	40	5	1.00	30	1.282E+03	7.404E+02	2.758E+04	1.00	6.41	3.70	0.54
P1	40	5	1.00	45	7.572E+02	7.572E+02	1.632E+04	1.00	3.79	3.79	0.54
P1	40	5	1.00	60	4.372E+02	7.572E+02	9.447E+03	1.00	2.19	3.79	0.54
P1	40	5	1.00	90	0.000E+00	7.578E+02	0.000E+00	1.00	0.00	3.79	-NA-

Table C.8 Ultimate capacity of caisson with L/D=8 in profile P1 with reduced adhesion

PROFILE	L (m)	D (m)	α	δ (deg)	H (kN)	V (kN)	RM (kN-m)	$S_{u\ AVG}$ (kPa)	N_H	N_V	Li/L
P1	40	5	0.65	0	2.212E+03	0.000E+00	4.723E+04	1.00	11.06	0.00	0.53
P1	40	5	0.65	15	1.697E+03	4.546E+02	3.631E+04	1.00	8.48	2.27	0.54
P1	40	5	0.65	30	9.254E+02	5.343E+02	1.981E+04	1.00	4.63	2.67	0.54
P1	40	5	0.65	45	5.363E+02	5.363E+02	1.158E+04	1.00	2.68	2.68	0.54
P1	40	5	0.65	60	3.105E+02	5.375E+02	6.736E+03	1.00	1.55	2.69	0.54
P1	40	5	0.65	90	0.000E+00	5.377E+02	0.000E+00	1.00	0.00	2.69	-NA-

Table C.9 Ultimate capacity of caisson with L/D=2 in profile P2 with full adhesion

PROFILE	L (m)	D (m)	α	δ (deg)	H (kN)	V (kN)	RM (kN-m)	S_{u_AVG} (kPa)	N_H	N_V	Li/L
P2	10	5	1.00	0	3.256E+03	0.000E+00	2.276E+04	6.25	10.42	0.00	0.70
P2	10	5	1.00	15	3.210E+03	8.601E+02	2.246E+04	6.25	10.27	2.75	0.70
P2	10	5	1.00	30	2.917E+03	1.684E+03	2.045E+04	6.25	9.33	5.39	0.70
P2	10	5	1.00	45	2.396E+03	2.396E+03	1.692E+04	6.25	7.67	7.67	0.71
P2	10	5	1.00	60	1.552E+03	2.689E+03	1.103E+04	6.25	4.97	8.60	0.71
P2	10	5	1.00	90	0.000E+00	2.740E+03	0.000E+00	6.25	0.00	8.77	-NA-

Table C.10 Ultimate capacity of caisson with L/D=2 in profile P2 with reduced adhesion

PROFILE	L (m)	D (m)	α	δ (deg)	H (kN)	V (kN)	RM (kN-m)	$S_{u\ AVG}$ (kPa)	N_H	N_V	Li/L
P2	10	5	0.65	0	3.064E+03	0.000E+00	2.195E+04	6.25	9.80	0.00	0.72
P2	10	5	0.65	15	3.014E+03	8.078E+02	2.152E+04	6.25	9.64	2.58	0.71
P2	10	5	0.65	30	2.710E+03	1.564E+03	1.936E+04	6.25	8.67	5.01	0.71
P2	10	5	0.65	45	2.154E+03	2.154E+03	1.557E+04	6.25	6.89	6.89	0.72
P2	10	5	0.65	60	1.348E+03	2.334E+03	9.480E+03	6.25	4.31	7.47	0.70
P2	10	5	0.65	90	0.000E+00	2.362E+03	0.000E+00	6.25	0.00	7.56	-NA-

Table C.11 Ultimate capacity of caisson with L/D=4 in profile P2 with full adhesion

PROFILE	L (m)	D (m)	α	δ (deg)	H (kN)	V (kN)	RM (kN-m)	S_{u_AVG} (kPa)	N_H	N_V	Li/L
P2	20	5	1.00	0	1.459E+04	0.000E+00	2.066E+05	12.50	11.67	0.00	0.71
P2	20	5	1.00	15	1.333E+04	3.572E+03	1.860E+05	12.50	10.66	2.86	0.70
P2	20	5	1.00	30	1.040E+04	6.002E+03	1.462E+05	12.50	8.32	4.80	0.70
P2	20	5	1.00	45	6.980E+03	6.980E+03	9.851E+04	12.50	5.58	5.58	0.71
P2	20	5	1.00	60	4.138E+03	7.168E+03	5.799E+04	12.50	3.31	5.73	0.70
P2	20	5	1.00	90	0.000E+00	7.238E+03	0.000E+00	12.50	0.00	5.79	-NA-

Table C.12 Ultimate capacity of caisson with L/D=4 in profile P2 with reduced adhesion

PROFILE	L (m)	D (m)	α	δ (deg)	H (kN)	V (kN)	RM (kN-m)	$S_{u\ AVG}$ (kPa)	N_H	N_V	Li/L
P2	20	5	0.65	0	13822.00	0.00	197462.00	12.50	11.06	0.00	0.71
P2	20	5	0.65	15	12140.20	3252.20	170835.44	12.50	9.71	2.60	0.70
P2	20	5	0.65	30	9086.00	5246.00	128664.00	12.50	7.27	4.20	0.71
P2	20	5	0.65	45	5832.00	5832.00	81134.00	12.50	4.67	4.67	0.70
P2	20	5	0.65	60	3396.94	5883.36	47864.10	12.50	2.72	4.71	0.70
P2	20	5	0.65	90	0.00	5916.00	0.00	12.50	0.00	4.73	-NA-

Table C.13 Ultimate capacity of caisson with L/D=6 in profile P2 with full adhesion

PROFILE	L (m)	D (m)	α	δ (deg)	H (kN)	V (kN)	RM (kN-m)	S_{u_AVG} (kPa)	N_H	N_V	Li/L
P2	30	5	1.00	0	33430.00	0.00	700540.00	18.75	11.89	0.00	0.70
P2	30	5	1.00	15	29102.64	7798.92	604860.00	18.75	10.35	2.77	0.69
P2	30	5	1.00	30	21374.00	12340.00	447140.00	18.75	7.60	4.39	0.70
P2	30	5	1.00	45	13554.00	13554.00	283140.00	18.75	4.82	4.82	0.70
P2	30	5	1.00	60	7893.30	13671.45	165319.57	18.75	2.81	4.86	0.70
P2	30	5	1.00	90	0.00	13666.00	0.00	18.75	0.00	4.86	-NA-

Table C.14 Ultimate capacity of caisson with L/D=6 in profile P2 with reduced adhesion

PROFILE	L (m)	D (m)	α	δ (deg)	H (kN)	V (kN)	RM (kN-m)	$S_{u\ AVG}$ (kPa)	N_H	N_V	Li/L
P2	30	5	0.65	0	32138.00	0.00	676940.00	18.75	11.43	0.00	0.70
P2	30	5	0.65	15	25856.00	6928.00	539920.00	18.75	9.19	2.46	0.70
P2	30	5	0.65	30	17530.00	10122.00	365880.00	18.75	6.23	3.60	0.70
P2	30	5	0.65	45	10552.92	10552.92	220666.80	18.75	3.75	3.75	0.70
P2	30	5	0.65	60	6086.45	10543.15	128182.40	18.75	2.16	3.75	0.70
P2	30	5	0.65	90	0.00	10558.00	0.00	18.75	0.00	3.75	-NA-

Table C.15 Ultimate capacity of caisson with L/D=8 in profile P2 with full adhesion

PROFILE	L (m)	D (m)	α	δ (deg)	H (kN)	V (kN)	RM (kN-m)	S_{u_AVG} (kPa)	N_H	N_V	Li/L
P2	40	5	1.00	0	60272.00	0.00	1668860.00	25.00	12.05	0.00	0.69
P2	40	5	1.00	15	50834.76	13621.08	1399990.80	25.00	10.17	2.72	0.69
P2	40	5	1.00	30	36002.00	20786.00	996740.00	25.00	7.20	4.16	0.69
P2	40	5	1.00	45	22002.00	22002.00	608740.00	25.00	4.40	4.40	0.69
P2	40	5	1.00	60	12766.67	22112.79	354986.10	25.00	2.55	4.42	0.70
P2	40	5	1.00	90	0.00	22180.00	0.00	25.00	0.00	4.44	-NA-

Table C.16 Ultimate capacity of caisson with L/D=8 in profile P2 with reduced adhesion

PROFILE	L (m)	D (m)	α	δ (deg)	H (kN)	V (kN)	RM (kN-m)	$S_{u\ AVG}$ (kPa)	N_H	N_V	Li/L
P2	40	5	0.65	0	57452.00	0.00	1593720.00	25.00	11.49	0.00	0.69
P2	40	5	0.65	15	45236.00	12122.00	1250580.00	25.00	9.05	2.42	0.69
P2	40	5	0.65	30	28450.00	16426.00	783380.00	25.00	5.69	3.29	0.69
P2	40	5	0.65	45	16584.20	16584.20	459550.00	25.00	3.32	3.32	0.69
P2	40	5	0.65	60	9575.51	16587.13	266660.80	25.00	1.92	3.32	0.70
P2	40	5	0.65	90	0.00	16588.00	0.00	25.00	0.00	3.32	-NA-

Table C.17 Ultimate capacity of caisson with L/D=2 in profile P3 with full adhesion

PROFILE	L (m)	D (m)	α	δ (deg)	H (kN)	V (kN)	RM (kN-m)	S_{u_AVG} (kPa)	N_H	N_V	Li/L
P3	10	5	1.00	0	5984.00	0.00	38238.00	11.25	10.64	0.00	0.64
P3	10	5	1.00	15	5822.91	1560.37	37003.32	11.25	10.35	2.77	0.64
P3	10	5	1.00	30	4984.00	2878.00	31846.00	11.25	8.86	5.12	0.64
P3	10	5	1.00	45	3692.00	3692.00	24032.00	11.25	6.56	6.56	0.65
P3	10	5	1.00	60	2356.00	4082.00	15168.00	11.25	4.19	7.26	0.64
P3	10	5	1.00	90	0.00	4158.00	0.00	11.25	0.00	7.39	-NA-

Table C.18 Ultimate capacity of caisson with L/D=2 in profile P3 with reduced adhesion

PROFILE	L (m)	D (m)	α	δ (deg)	H (kN)	V (kN)	RM (kN-m)	$S_{u\ AVG}$ (kPa)	N_H	N_V	Li/L
P3	10	5	0.65	0	5644.00	0.00	36978.00	11.25	10.03	0.00	0.66
P3	10	5	0.65	15	5421.92	1452.51	35104.46	11.25	9.64	2.58	0.65
P3	10	5	0.65	30	4668.00	2694.00	30460.00	11.25	8.30	4.79	0.65
P3	10	5	0.65	45	3326.00	3326.00	21662.00	11.25	5.91	5.91	0.65
P3	10	5	0.65	60	1992.60	3452.00	12680.00	11.25	3.54	6.14	0.64
P3	10	5	0.65	90	0.00	3472.00	0.00	11.25	0.00	6.17	-NA-

Table C.19 Ultimate capacity of caisson with L/D=4 in profile P3 with full adhesion

PROFILE	L (m)	D (m)	α	δ (deg)	H (kN)	V (kN)	RM (kN-m)	S_{u_AVG} (kPa)	N_H	N_V	Li/L
P3	20	5	1.00	0	20582.00	0.00	273760.00	17.50	11.76	0.00	0.67
P3	20	5	1.00	15	18243.36	4888.38	238815.80	17.50	10.42	2.79	0.65
P3	20	5	1.00	30	13932.00	8044.00	183900.00	17.50	7.96	4.60	0.66
P3	20	5	1.00	45	9316.00	9316.00	122996.00	17.50	5.32	5.32	0.66
P3	20	5	1.00	60	5396.85	9348.51	71170.08	17.50	3.08	5.34	0.66
P3	20	5	1.00	90	0.00	9384.00	0.00	17.50	0.00	5.36	-NA-

Table C.20 Ultimate capacity of caisson with L/D=4 in profile P3 with reduced adhesion

PROFILE	L (m)	D (m)	α	δ (deg)	H (kN)	V (kN)	RM (kN-m)	$S_{u\ AVG}$ (kPa)	N_H	N_V	Li/L
P3	20	5	0.65	0	19596.00	0.00	262940.00	17.50	11.20	0.00	0.67
P3	20	5	0.65	15	16830.64	4508.64	222159.60	17.50	9.62	2.58	0.66
P3	20	5	0.65	30	12196.00	7040.00	161346.00	17.50	6.97	4.02	0.66
P3	20	5	0.65	45	7382.00	7382.00	96682.00	17.50	4.22	4.22	0.65
P3	20	5	0.65	60	4289.39	7429.80	56773.01	17.50	2.45	4.25	0.66
P3	20	5	0.65	90	0.00	7442.00	0.00	17.50	0.00	4.25	-NA-

Table C.21 Ultimate capacity of caisson with L/D=6 in profile P3 with full adhesion

PROFILE	L (m)	D (m)	α	δ (deg)	H (kN)	V (kN)	RM (kN-m)	S_{u_AVG} (kPa)	N_H	N_V	Li/L
P3	30	5	1.00	0	42876.00	0.00	856780.00	23.75	12.04	0.00	0.67
P3	30	5	1.00	15	36519.68	9785.00	722689.20	23.75	10.25	2.75	0.66
P3	30	5	1.00	30	26382.00	15232.00	525800.00	23.75	7.41	4.28	0.66
P3	30	5	1.00	45	16622.00	16622.00	330640.00	23.75	4.67	4.67	0.66
P3	30	5	1.00	60	9611.98	16647.40	192053.31	23.75	2.70	4.67	0.67
P3	30	5	1.00	90	0.00	16640.00	0.00	23.75	0.00	4.67	-NA-

Table C.22 Ultimate capacity of caisson with L/D=6 in profile P3 with reduced adhesion

PROFILE	L (m)	D (m)	α	δ (deg)	H (kN)	V (kN)	RM (kN-m)	$S_{u\ AVG}$ (kPa)	N_H	N_V	Li/L
P3	30	5	0.65	0	40670.00	0.00	815260.00	23.75	11.42	0.00	0.67
P3	30	5	0.65	15	33766.00	9048.00	672200.00	23.75	9.48	2.54	0.66
P3	30	5	0.65	30	21560.00	12448.00	427360.00	23.75	6.05	3.49	0.66
P3	30	5	0.65	45	12693.15	12693.15	252255.00	23.75	3.56	3.56	0.66
P3	30	5	0.65	60	7326.27	12689.53	146819.75	23.75	2.06	3.56	0.67
P3	30	5	0.65	90	0.00	12680.00	0.00	23.75	0.00	3.56	-NA-

Table C.23 Ultimate capacity of caisson with L/D=8 in profile P3 with full adhesion

PROFILE	L (m)	D (m)	α	δ (deg)	H (kN)	V (kN)	RM (kN-m)	S_{u_AVG} (kPa)	N_H	N_V	Li/L
P3	40	5	1.00	0	72294.00	0.00	1924100.00	30.00	12.05	0.00	0.67
P3	40	5	1.00	15	60232.00	16140.00	1595280.00	30.00	10.04	2.69	0.66
P3	40	5	1.00	30	42430.00	24496.00	1129780.00	30.00	7.07	4.08	0.67
P3	40	5	1.00	45	25756.00	25756.00	686100.00	30.00	4.29	4.29	0.67
P3	40	5	1.00	60	14976.51	25941.06	399648.30	30.00	2.50	4.32	0.67
P3	40	5	1.00	90	0.00	25956.00	0.00	30.00	0.00	4.33	-NA-

Table C.24 Ultimate capacity of caisson with L/D=8 in profile P3 with reduced adhesion

PROFILE	L (m)	D (m)	α	δ (deg)	H (kN)	V (kN)	RM (kN-m)	$S_{u\ AVG}$ (kPa)	N_H	N_V	Li/L
P3	40	5	0.65	0	68958.00	0.00	1837880.00	30.00	11.49	0.00	0.67
P3	40	5	0.65	15	54376.00	14570.00	1445700.00	30.00	9.06	2.43	0.66
P3	40	5	0.65	30	32868.00	18976.00	871600.00	30.00	5.48	3.16	0.66
P3	40	5	0.65	45	19254.82	19254.82	513475.20	30.00	3.21	3.21	0.67
P3	40	5	0.65	60	11106.13	19236.28	297841.60	30.00	1.85	3.21	0.67
P3	40	5	0.65	90	0.00	19242.00	0.00	30.00	0.00	3.21	-NA-

Table C.25 Ultimate capacity of caisson with L/D=2 in profile P4 with full adhesion

PROFILE	L (m)	D (m)	α	δ (deg)	H (kN)	V (kN)	RM (kN-m)	S_{u_AVG} (kPa)	N_H	N_V	Li/L
P4	10	5	1.00	0	6720.00	0.00	41658.00	10.00	13.44	0.00	0.62
P4	10	5	1.00	15	6426.00	1721.76	39555.60	10.00	12.85	3.44	0.62
P4	10	5	1.00	30	5554.00	3206.00	34390.00	10.00	11.11	6.41	0.62
P4	10	5	1.00	45	4246.00	4246.00	26642.00	10.00	8.49	8.49	0.63
P4	10	5	1.00	60	2704.00	4684.00	16882.00	10.00	5.41	9.37	0.62
P4	10	5	1.00	90	0.00	4690.44	0.00	10.00	0.00	9.38	-NA-

Table C.26 Ultimate capacity of caisson with L/D=2 in profile P4 with reduced adhesion

PROFILE	L (m)	D (m)	α	δ (deg)	H (kN)	V (kN)	RM (kN-m)	$S_{u\ AVG}$ (kPa)	N_H	N_V	Li/L
P4	10	5	0.65	0	6338.00	0.00	40298.00	10.00	12.68	0.00	0.64
P4	10	5	0.65	15	6098.00	1633.80	38338.00	10.00	12.20	3.27	0.63
P4	10	5	0.65	30	5242.00	3026.00	33104.00	10.00	10.48	6.05	0.63
P4	10	5	0.65	45	3852.00	3852.00	24267.60	10.00	7.70	7.70	0.63
P4	10	5	0.65	60	2322.00	4024.00	14268.00	10.00	4.64	8.05	0.61
P4	10	5	0.65	90	0.00	4043.78	0.00	10.00	0.00	8.09	-NA-

Table C.27 Ultimate capacity of caisson with L/D=4 in profile P4 with full adhesion

PROFILE	L (m)	D (m)	α	δ (deg)	H (kN)	V (kN)	RM (kN-m)	S_{u_AVG} (kPa)	N_H	N_V	Li/L
P4	20	5	1.00	0	24086.00	0.00	323620.00	19.81	12.16	0.00	0.67
P4	20	5	1.00	15	22181.12	5942.56	295505.60	19.81	11.20	3.00	0.67
P4	20	5	1.00	30	17336.00	10010.00	232780.00	19.81	8.75	5.05	0.67
P4	20	5	1.00	45	11666.00	11666.00	157224.00	19.81	5.89	5.89	0.67
P4	20	5	1.00	60	6860.00	11880.00	92110.00	19.81	3.46	6.00	0.67
P4	20	5	1.00	90	0.00	11921.76	0.00	19.81	0.00	6.02	-NA-

Table C.28 Ultimate capacity of caisson with L/D=4 in profile P4 with reduced adhesion

PROFILE	L (m)	D (m)	α	δ (deg)	H (kN)	V (kN)	RM (kN-m)	$S_{u\ AVG}$ (kPa)	N_H	N_V	Li/L
P4	20	5	0.65	0	23564.00	0.00	321300.00	19.81	11.90	0.00	0.68
P4	20	5	0.65	15	20795.70	5572.30	279397.80	19.81	10.50	2.81	0.67
P4	20	5	0.65	30	15496.00	8946.00	209180.00	19.81	7.82	4.52	0.67
P4	20	5	0.65	45	9484.00	9484.00	126626.00	19.81	4.79	4.79	0.67
P4	20	5	0.65	60	5516.16	9553.32	74533.44	19.81	2.78	4.82	0.68
P4	20	5	0.65	90	0.00	9549.24	0.00	19.81	0.00	4.82	-NA-

Table C.29 Ultimate capacity of caisson with L/D=6 in profile P4 with full adhesion

PROFILE	L (m)	D (m)	α	δ (deg)	H (kN)	V (kN)	RM (kN-m)	S_{u_AVG} (kPa)	N_H	N_V	Li/L
P4	30	5	1.00	0	53092.00	0.00	1082200.00	29.84	11.86	0.00	0.68
P4	30	5	1.00	15	47034.00	12602.00	955220.00	29.84	10.51	2.82	0.68
P4	30	5	1.00	30	35000.00	20206.00	715260.00	29.84	7.82	4.51	0.68
P4	30	5	1.00	45	22404.00	22404.00	456420.00	29.84	5.01	5.01	0.68
P4	30	5	1.00	60	12946.28	22423.20	265582.52	29.84	2.89	5.01	0.68
P4	30	5	1.00	90	0.00	22407.09	0.00	29.84	0.00	5.01	-NA-

Table C.30 Ultimate capacity of caisson with L/D=6 in profile P4 with reduced adhesion

PROFILE	L (m)	D (m)	α	δ (deg)	H (kN)	V (kN)	RM (kN-m)	$S_{u\ AVG}$ (kPa)	N_H	N_V	Li/L
P4	30	5	0.65	0	50474.00	0.00	1033740.00	29.84	11.28	0.00	0.68
P4	30	5	0.65	15	42698.00	11442.00	871460.00	29.84	9.54	2.56	0.68
P4	30	5	0.65	30	28778.00	16616.00	586480.00	29.84	6.43	3.71	0.68
P4	30	5	0.65	45	17006.00	17006.00	346920.00	29.84	3.80	3.80	0.68
P4	30	5	0.65	60	9847.53	17054.03	202632.57	29.84	2.20	3.81	0.69
P4	30	5	0.65	90	0.00	17056.02	0.00	29.84	0.00	3.81	-NA-

Table C.31 Ultimate capacity of caisson with L/D=8 in profile P4 with full adhesion

PROFILE	L (m)	D (m)	α	δ (deg)	H (kN)	V (kN)	RM (kN-m)	S_{u_AVG} (kPa)	N_H	N_V	Li/L
P4	40	5	1.00	0	91856.00	0.00	2497000.00	39.87	11.52	0.00	0.68
P4	40	5	1.00	15	80972.00	21696.00	2199200.00	39.87	10.15	2.72	0.68
P4	40	5	1.00	30	58278.00	33646.00	1590980.00	39.87	7.31	4.22	0.68
P4	40	5	1.00	45	35772.00	35772.00	975820.00	39.87	4.49	4.49	0.68
P4	40	5	1.00	60	20680.39	35818.70	565713.84	39.87	2.59	4.49	0.68
P4	40	5	1.00	90	0.00	35833.56	0.00	39.87	0.00	4.49	-NA-

Table C.32 Ultimate capacity of caisson with L/D=8 in profile P4 with reduced adhesion

PROFILE	L (m)	D (m)	α	δ (deg)	H (kN)	V (kN)	RM (kN-m)	$S_{u\ AVG}$ (kPa)	N_H	N_V	Li/L
P4	40	5	0.65	0	89158.00	0.00	2433400.00	39.87	11.18	0.00	0.68
P4	40	5	0.65	15	76504.00	20500.00	2087000.00	39.87	9.59	2.57	0.68
P4	40	5	0.65	30	45868.00	26482.00	1246540.00	39.87	5.75	3.32	0.68
P4	40	5	0.65	45	26524.00	26524.00	725300.00	39.87	3.33	3.33	0.68
P4	40	5	0.65	60	15340.32	26570.19	421396.50	39.87	1.92	3.33	0.69
P4	40	5	0.65	90	0.00	26544.82	0.00	39.87	0.00	3.33	-NA-

VITA

Partha Pratim Sharma was born on May 30, 1976 in the north east part of India. He is the eldest of two sons of Mr. Indreswar Sharma and Mrs. Nayan Sharma. His father is a consultant civil engineer and mother is a superintendent engineer of building division of Public Work Dept, Assam, India. Partha obtained his Bachelor's degree in 1999 from VNIT (Visvesvaraya National Institute of Technology), Nagpur, India. After completion of his bachelor's degree, he worked with Siemens Power Engineering Ltd, a German multinational company as a design engineer for one and a half years and then he joined his father's company ESS Foundation Pvt Ltd as a geotechnical engineer for one year. He entered Texas A&M University in Fall 2002. He worked as a graduate research assistant under the supervision of Dr. Charles Aubeny and Dr. James D. Murff. Partha performed research on the finite element analysis on the capacity of suction caissons. He is interested in finite element method, numerical analyses and offshore engineering. Partha plans to continue his research at Texas A&M University as a Ph.D student.

His permanent mailing address is:

ESS Foundation Pvt Ltd

Barthakur Mill Road

Ulubari, Guwahati -781007

Assam, India.